

An antioxidant metabolon at the red blood cell membrane

Bing Li

A Thesis

in

The Department

of

Chemistry and Biochemistry

Presented in Partial Fulfillment of the Requirements  
For the Degree of Master of Science (Chemistry) at  
Concordia University  
Montreal, Quebec, Canada

July 2009

© Bing Li, 2009



Library and Archives  
Canada

Bibliothèque et  
Archives Canada

Published Heritage  
Branch

Direction du  
Patrimoine de l'édition

395 Wellington Street  
Ottawa ONK1A0N4  
Canada

395, rue Wellington  
Ottawa ONK1A0N4  
Canada

*Your file Votre référence*  
ISBN: 978-0-494-63204-8  
*Our file Notre référence*  
ISBN: 978-0-494-63204-8

**NOTICE:**

The author has granted a non-exclusive license allowing Library and Archives Canada to reproduce, publish, archive, preserve, conserve, communicate to the public by telecommunication or on the Internet, loan, distribute and sell theses worldwide, for commercial or non-commercial purposes, in microform, paper, electronic and/or any other formats.

The author retains copyright ownership and moral rights in this thesis. Neither the thesis nor substantial extracts from it may be printed or otherwise reproduced without the author's permission.

In compliance with the Canadian Privacy Act some supporting forms may have been removed from this thesis.

While these forms may be included in the document page count, their removal does not represent any loss of content from the thesis.

**AVIS:**

L'auteur a accordé une licence non exclusive permettant à la Bibliothèque et Archives Canada de reproduire, publier, archiver, sauvegarder, conserver, transmettre au public par télécommunication ou par l'Internet, prêter, distribuer et vendre des thèses partout dans le monde, à des fins commerciales ou autres, sur support microforme, papier, électronique et/ou autres formats.

L'auteur conserve la propriété du droit d'auteur et des droits moraux qui protègent cette thèse. Ni la thèse ni des extraits substantiels de celle-ci ne doivent être imprimés ou autrement reproduits sans son autorisation.

Conformément à la loi canadienne sur la protection de la vie privée, quelques formulaires secondaires ont été enlevés de cette thèse.

Bien que ces formulaires aient inclus dans la pagination, il n'y aura aucun contenu manquant.

1\*1

**Canada**

**CONCORDIA UNIVERSITY**  
**SCHOOL OF GRADUATE STUDIES**

This is to certify that the thesis prepared

By: **Bing Li**

Entitled: **An antioxidant metabolon at the red blood cell membrane**

and submitted in partial fulfillment of the requirements for the degree of

**Master of Science (Chemistry)**

complies with the regulations of the University and meets the accepted standards with respect to originality and quality.

Signed by the final examining committee:

\_\_\_\_\_Chair  
Dr.

\_\_\_\_\_Examiner  
**~D7**

\_\_\_\_\_Examiner  
Dr.

\_\_\_\_\_Supervisor  
Dr.

Approved by

Chair of Department or Graduate Program Director

July 27<sup>th</sup>

2009

\_\_\_\_\_  
Dean of Faculty

## Abstract

An antioxidant metabolon at the red blood cell membrane

Bing Li

Red blood cells (RBCs) transport oxygen and carbon dioxide as their main function and repeatedly circulate through the lung and capillaries during their 120 day life spans. RBCs concentrate large amounts of oxygen and are exposed continuously to intracellular reactive oxygen species (ROS) derived from autoxidation of oxyhemoglobin (oxyHb).

Limiting the potential damage caused by these ROS is important in the RBC. Therefore, the antioxidant enzymes, CuZn-superoxide dismutase (CuZnSOD), catalase, glutathione peroxidase (GPx), and its substrate glutathione (GSH) are found in red blood cells. The localization of these antioxidants under physiological and oxidative stress conditions was examined. Our results showed that most CuZnSOD and catalase were concentrated at the RBC membrane and less in the cytosol, while GPx localized at the membrane under physiological conditions. After prolonged exposure of RBCs to air (1 h), CuZnSOD and catalase migrated to the membrane and they both associated with the cytoplasmic domain of band 3 (CDB3). No association at the membrane of the three proteins was observed when RBCs were deaerated. Small amount of catalase and GPx localized to the membrane while CuZnSOD and GSH remained evenly distributed in the cytosol under two types (H<sub>2</sub>O<sub>2</sub> and O<sub>2</sub><sup>•-</sup>) of ROS stress. In summary, CuZnSOD and catalase form a complex with CDB3 at the membrane, and the association of these proteins is mediated by the oxygenation state of the RBC. It is speculated that GPx

cooperates with catalase to protect the whole RBC (membrane and cytoplasm) from ROS damage.

## **Acknowledgments**

During my MSc studies, I got help from many people. Now I would like to take the opportunity to express my gratitude to these people.

First, I would like to express my sincere thanks to my research supervisor, Dr. Ann M. English, for giving me this wonderful opportunity to be a member of her group. During my graduate studies with Dr. English, I have further developed my knowledge and skills in biochemistry. Her great passion for science and insightful thoughts on science and technology have left a permanent imprint on my future as a researcher. Her advice and helpful discussions guided me through my MSc research.

I would also like to thank Dr. Joanne L. Turnbull and Dr. Paul Joyce for being members of my research committee, for taking the time to evaluate my project, and for giving me precious and useful suggestions and comments.

I want to thank all the members of my group for sharing the literature, especially group members, Mr. Biao Shen, Ms. Stella Muthuri, Ms. Mengwei Ye, and Ms. Juliana Garcia. I will not forget the time we spent doing confocal microscopy and their practical and invaluable assistance. I also thank them for their friendship and their strong support in difficult times, and for making my time in the laboratory enjoyable.

Finally, I wish to express my love and gratitude to my beloved family for their understanding and endless love during my studies. I want to thank my husband and my lovely daughter who have been so patient and supportive throughout this long journey. Without their support, this work could not have been completed.

*Dedication*

*To my father Mr. S. Z. Li and my mother Mrs. J. X. Wang*

*Without them I could never have made it this far in life*

## Table of contents

List of Figures.....	x
List of tables.....	xii
List of abbreviation.....	xiii
Chapter 1: Introduction.....	1
1.1 Environment and function of RBCs.....	1
1.2 Oxidative stress.....	2
1.3 Effects of oxidative stress on RBCs.....	3
1.4 Importance of antioxidant function and antioxidant defense systems in RBCs.....	6
1.5 Copper, zinc-superoxide dismutase (CuZnSOD).....	8
1.5.1 Properties of human CuZnSOD (SOD1).....	8
1.5.2 Superoxide dismutase (SOD) activity of CuZnSOD.....	11
1.5.3 Antioxidant role and physiological importance of CuZnSOD.....	11
1.6 Catalase.....	12
1.6.1 Properties of catalase.....	13
1.6.2 Catalysis of H <sub>2</sub> O <sub>2</sub> decomposition.....	16
1.6.3 Antioxidant role and physiological importance of catalases.....	17
1.7 GSH and glutathione peroxidase (GPx).....	17
1.7.1 Properties of RBC GPx.....	19
1.7.2 Catalysis of H <sub>2</sub> O <sub>2</sub> decomposition.....	20
1.7.3 Antioxidant role and physiological importance of GPx.....	21
1.8 Immunofluorescence.....	22
1.9 Confocal microscopy.....	23
1.10 Outline and scope of thesis.....	25
Chapter 2: Materials and methods.....	27

2.1	Materials	<b>27</b>
2.2	Methods.....	28
2.2.1	Preparation of RBCs.....	28
2.2.2	Fixing and permeabilizing RBCs.....	28
2.2.3	Staining of RBCs.....	29
2.2.3.1	Staining of RBCs for a specific protein.....	29
2.2.3.2	Double staining.....	29
2.2.3.3	Competitive binding of antibodies.....	30
2.2.4	Confocal microscopy of labelled RBCs.....	31
2.2.5	Deaeration of RBCs.....	31
2.2.6	Aeration of RBCs.....	33
2.2.7	Steady-state H <sub>2</sub> O <sub>2</sub> production.....	33
2.2.8	Monitoring O <sub>2</sub> production by phenazine methosulfate (PMS).....	34
2.2.9	Effects of H <sub>2</sub> O <sub>2</sub> and O <sub>2</sub> <sup>-</sup> on RBCs.....	36
2.2.10	Cu and Fe concentrations of human RBCs.....	36
Chapter 3: Results.....		39
3.1	Localization of Hb and CDB3 in fixed human RBCs.....	39
3.2	Localization of CuZnSOD, catalase, and GPx in fixed human RBCs.....	41
3.3	Localization of CuZnSOD, catalase, and GPx in fixed RBCs following deaeration.....	41
3.4	Localization of CuZnSOD, catalase, and GPx, in fixed aerated human RBCs.....	43
3.5	Colocalization of CuZnSOD, catalase, and CDB3.....	46
3.6	Competition between anti-CuZnSOD and anti-CDB3.....	49
3.7	Steady-state generation of H <sub>2</sub> O <sub>2</sub> and superoxide.....	55
3.7.1	H <sub>2</sub> O <sub>2</sub> .....	55
3.7.2	Superoxide generation.....	58
3.8	Localization of CuZnSOD, catalase, GPx, and GSH in fixed human RBCs under an exogenous H <sub>2</sub> O <sub>2</sub> flux.....	61

3.9	Localization of CuZnSOD, catalase, GPx, and GSH in fixed human RBCs under intracellular $O_2^-$ generation.....	62
3.10	ICP-MS determination of RBC Cu and Fe concentrations.....	66
	Chapter 4: Discussion.....	70
4.1	Evaluation of methods.....	70
4.2	RBC response to changes in oxygenation.....	77
4.3	RBC response to $H_2O_2$ and $O_2^-$ .....	84
	Chapter 5: Conclusions and future studies.....	90
	References.....	93
	Appendix: List of images and Z-stacks of images on DVD submitted with this thesis..!	11

## List of Figures

Figure 1.1. A red blood cell.....	1
Figure 1.2. Structure of MDA.....	5
Figure 1.3. Structure of human CuZnSOD dimer.....	10
Figure 1.4. Oxidized and reduced metal-binding sites of bovine CuZnSOD.....	10
Figure 1.5. Structure of human catalase.....	15
Figure 1.6. Active-site channel of human catalase.....	16
Figure 1.7. Structure of bovine GPx-1.....	20
Figure 1.8. The direct method of immunofluorescent staining.....	23
Figure 1.9. The indirect method of immunofluorescent staining.....	23
Figure 1.10. Ray path in a confocal LSM.....	25
Figure 2.1. Excitation (blue) and emission (red) spectra of the different dyes.....	32
Figure 3.1. Structure of acrolein.....	39
Figure 3.2. Confocal immunofluorescence images of Hb and CDB3 in fixed intact human RBCs.....	40
Figure 3.3. Confocal immunofluorescence images of CuZnSOD, catalase, and GPx in fixed intact human RBCs.....	42
Figure 3.4. Confocal immunofluorescence and corresponding bright field images of CDB3, CuZnSOD, catalase, and GPx in fixed intact deaerated human RBCs.....	44
Figure 3.5. Confocal immunofluorescence and corresponding bright field images of CuZnSOD, catalase, and GPx in fixed intact aerated human RBCs.....	47
Figure 3.6. Colocalization of CuZnSOD, catalase, and CDB3 in fixed intact aerated human RBCs.....	50

Figure 3.7. Competition between anti-CuZnSOD and anti-CDB3 in fixed intact aerated human RBCs.....	54
Figure 3.8. HRP-catalyzed ABTS oxidation by H <sub>2</sub> O <sub>2</sub> .....	56
Figure 3.9. H <sub>2</sub> O <sub>2</sub> calibration plot.....	56
Figure 3.10. H <sub>2</sub> O <sub>2</sub> generation by GOx-catalyzed oxidation of glucose.....	57
Figure 3.11. H <sub>2</sub> O <sub>2</sub> production by GOx/glucose vs time.....	58
Figure 3.12. PMS-catalyzed superoxide generation.....	59
Figure 3.13. Initial rates of superoxide generation by PMS/NADPH in 2 mL of PBS in an open 1-cm cuvette at room temperature.....	60
Figure 3.14. NADPH concentration dependence of superoxide generation.....	60
Figure 3.15. CuZnSOD inhibits superoxide generated by NADPH/PMS.....	61
Figure 3.16. Confocal immunofluorescence images of CuZnSOD, catalase, GPx, and GSH in fixed intact human RBCs under H <sub>2</sub> O <sub>2</sub> flux.....	63
Figure 3.17. Confocal immunofluorescence images of CuZnSOD, catalase, GPx, and GSH in fixed intact human RBCs under intracellular O <sub>2</sub> generation.....	67
Figure 4.1. Structures of the dyes used in this work.....	76
Figure 4.2. Normalized emission spectra of Cy2, FITC, and Alexa 488.....	77

## **List of tables**

Table 2.1: Competitive staining with anti-CuZnSOD and anti-CDB3.....	30
Table 2.2: ICP-MS settings for multielement analysis in He gas mode.....	37
Table 2.3: ICP-MS tuning parameters.....	38
Table 3.1: ICP-MS analysis of Cu and Fe concentrations in human RBCs_	66

## List of abbreviation

ABTS	2,2'-azino-di-3-ethylbenzthiazoline-6-sulphonic acid
AE 1	Anion exchanger 1
CAII	Carbonic anhydrase isoform II
CAD	Coronary artery disease
CDB3	Cytoplasm domain of band 3
Cpdl	Compound I
CuZnSOD	CuZn-superoxide dismutase
fALS	Familial amyotrophic lateral sclerosis
GAPDH	Glyceraldehyde-3- phosphate dehydrogenase
GOx	Glucose oxidase
GPx	Glutathione peroxidase
G-PBS	Glucose phosphate buffered saline
GSH	Glutathione
Hb	Hemoglobin
HRP	Horseradish peroxidase
Ht	Hematocrit
ICP-MS	Inductively coupled plasma mass spectrometry
IS	Internal standard
LSM	Laser scanning microscopy
MetHb	Methemoglobin
MDA	Malondialdehyde
NABs	Naturally occurring antibodies

NBT	Nitroblue tetrazolium salt
OxyHb	Oxyhemoglobin
PAM	Programmable array microscopes
PBS	Phosphate buffered saline
PMS	Phenazine methosulfate
Prx2	Peroxiredoxin 2
RBC	Red blood cell
ROS	Reactive oxygen species
Se	Selenium
SeCys	Selocysteine

# Chapter 1: Introduction

## 1.1 Environment and function of RBCs

Blood is critical for nutrient and oxygen delivery to and waste clearance from tissue. Blood is composed of cells and a liquid (plasma). More than 99% (by number) of blood cells are erythrocytes or red blood cells (RBCs). The major function of RBCs is to carry O<sub>2</sub> from the lungs to tissues, and CO<sub>2</sub> from tissues to the lungs. RBCs contain a large amount of hemoglobin (Hb) which reversibly binds O<sub>2</sub>. The red color of blood comes from oxygenated Hb in RBCs.

RBCs are small biconcave discs thicker at the edges than in the middle (Figure 1.1). Their high surface-to-volume ratio ensures that O<sub>2</sub> and CO<sub>2</sub> can diffuse rapidly to and from the interior of the cell. In order to travel through microcapillaries (5-10  $\mu\text{m}$  in diameter), RBCs are flexible and can change their shape.

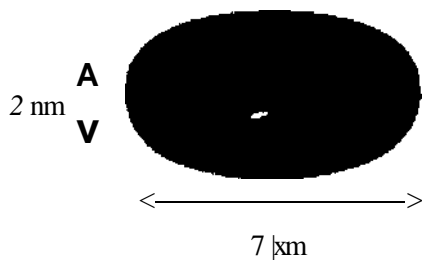


**Figure 1.1. A red blood cell.** The RBC is  $< 2 \mu\text{m}$  thick and has a diameter of  $\sim 7 \mu\text{m}$ , and a biconcave disk shape. Adapted from <http://services.epnet.com/GetImage.aspx/getImage.aspx?ImageIID=7297>

In humans, RBCs are produced in the bone marrow. With differentiation, they ultimately lose their nuclei and organelles to become mature RBCs that leave the bone marrow and enter the blood. Because RBCs have no nuclei and organelles, they can not divide nor maintain their normal structure for very long. The average life span of a RBC is 120 days (/).

RBCs are suspended in the plasma which constitutes -55% of whole blood and acts as a buffer to maintain human arterial blood pH at 7.35-7.45. The plasma is essentially an aqueous solution containing -92% water, 8% plasma proteins, and trace amounts of other materials.

## 12 Oxidative stress

Oxygen plays both deleterious and beneficial roles in living organisms. Its poisonous property is attributed to its partially reduced forms, which are collectively called reactive oxygen species (ROS) (2). ROS include oxygen-centered radicals (3), such as the superoxide anion ( $O_2^-$ ), the hydroxyl radical (HO) and nitric oxide ( $NO^\cdot$ ), but also non-radical species, hydrogen peroxide ( $H_2O_2$ ).

ROS can be produced from both endogenous and exogenous sources. Endogenous sources include mitochondria, cytochrome P450 metabolism, peroxisomes, and inflammatory cell activation (4). Exogenous sources include environmental agents such as non-genotoxic carcinogens, which can directly generate or indirectly induce ROS in cells. ROS are also observed following exposure to chlorinated compounds, metal ions, radiation, and barbiturates (4).

Since ROS are products of normal cellular metabolism, living organisms have not only adapted to coexistence with ROS but have developed mechanisms for the advantageous use of ROS in various physiological functions. The beneficial effects of ROS occur at low and moderate concentrations. ROS play a physiological role in the intracellular killing of bacteria by neutrophil granulocytes and in cell signalling. A further beneficial example of ROS function is the induction of the mitogenic response (5).

ROS are highly reactive which explains their participation in unwanted side reactions resulting in cell damage. Disturbance of the ROS balance can damage all cell components, including DNA, lipids and proteins, and could also lead to many human pathologies. For example, the hydroxyl radical could react with the DNA double-helix at both purine and pyrimidine bases and at the deoxyribose backbone (6). Permanent modification of the genetic material as a result of oxidative damage is the cause of mutagenesis, carcinogenesis, and aging. ROS can attack not only DNA, but also lipids, in particular the polyunsaturated fatty acid residues of phospholipids (4). The side chains of amino acid residues of proteins, in particular cysteine and methionine, are also susceptible to oxidation by the action of ROS (7). Oxidation of cysteine residues may lead to the formation of a reversible disulfide bond between two thiol groups. The harmful effects of ROS causing potential biological damage are collectively termed oxidative stress. Oxidative stress results from ROS overproduction or from the weakening of the antioxidant defense system. In humans, oxidative stress is involved in many pathological conditions, including cardiovascular disease, cancer, neurological disorders, diabetes, ischemia, and aging (5).

### 1.3 Effects of oxidative stress on RBCs

In most cells, the major source of ROS is the mitochondrion (S). In the RBC, the major source of ROS is the oxygen carrier protein hemoglobin (Hb), which has two forms (oxyHb and deoxyHb). The mature RBC continuously produces ROS due to its physiologic role of transporting oxygen and its abundant heme iron content. OxyHb undergoes slow autoxidation to produce superoxide and metHb, which can not transport oxygen. This results in loss of the most important task of RBCs (9). During autoxidation

an electron is lost from the heme Fe<sup>2+</sup> to give Fe<sup>3+</sup>. This superoxide, either generated spontaneously or due to the effect of an exogenous source such as certain drugs (10), is capable of attacking the RBC membrane directly and causing structural alterations in lipids and proteins (77). Furthermore, dismutation of superoxide readily generates a second ROS, F<sup>•</sup>C<sup>•</sup>Eq 1.1) (70), which adds to the extracellular flux of H<sub>2</sub>O<sub>2</sub> that enters the RBC (9).



Human RBCs undergo various modifications including formation of oxidized lipids, crosslinking of membrane proteins to membrane lipids, altering protein function by modifying sulfhydryl groups, and denaturing Hb when exposed to oxidative stress. (9). H<sub>2</sub>O<sub>2</sub> can easily damage polyunsaturated fatty acids within the membrane (77) leading to altered phospholipid fluidity, loss of membrane integrity and loss of cellular homeostasis, which may cause cell death (72). Malondialdehyde (MDA) (Fig. 1.2), a highly reactive bifunctional molecule, is an end product of membrane lipid peroxidation (9) and has been shown to crosslink RBC phospholipids and proteins. This may result in the impairment of membrane-related functions that could ultimately diminish survival. MDA accumulation can affect the anion transport of band 3 (AE1) as well as the function of its associated enzymes, such as glyceraldehyde-3-phosphate dehydrogenase and phosphofructokinase (73). Band 3 is an important structural component of the RBC membrane with molecular weight of -93 kDa. Band 3 is an integral, assymmetrically disposed, transmembrane glycoprotein. It consists of transmembrane and cytoplasmic domains. Its transmembrane segment is 55 kDa and has been identified with the anion transport property (transports Cl<sup>-</sup> and HCO<sub>3</sub><sup>-</sup>). The 41 kDa cytoplasmic domain of band

3 (CDB3) is also its amino terminus and specifically binds RBC cytoskeleton proteins, ankyrin (band 2.1) and band 4.2, and at least four different cytoplasmic proteins (14).

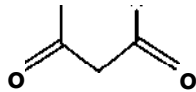


Figure 1.2. Structure of MDA

Among the membrane proteins that are possible targets for oxidants, the calcium ATPase may be of crucial importance for the survival of RBCs. Ca-ATPase contains one or more reactive sulfhydryl groups that are susceptible to oxidation with resultant loss of enzyme activity. Because this enzyme is critical in maintaining the very steep gradient between extracellular and intracellular calcium, loss of activity is associated with decreased RBC deformability and premature destruction (15).

Like RBC membrane proteins, cytosolic proteins, such as Hb, are also susceptible to peroxidation. OxyHb oxidative modifications as a result of H<sub>2</sub>O<sub>2</sub> exposure have been proposed to act as selective signals for proteolysis in RBCs (16). In addition to the modification of Hb by H<sub>2</sub>O<sub>2</sub>, peroxidation may result in Hb crosslinking to membrane proteins, such as spectrin and band 3, and also the aggregation of band 3 (17, 18). Synder *et al.* demonstrated that H<sub>2</sub>O<sub>2</sub> induces a complex formation between spectrin and Hb, as well as alteration of phospholipid organization, cell shape, membrane deformability, and cell surface characteristics (19). The crosslinking of spectrin and Hb and the aggregation of band 3 can trigger the phagocytosis of altered RBCs (20, 21). The formation of crosslinked spectrin and Hb results in the RBC membrane becoming rigid, less deformable and less adaptable (19, 22). Decreased membrane deformability, which is one of the factors that influences blood flow/shear rate, makes the blood more viscous and

results in vascular abnormalities such as thrombotic events, atherosclerosis, and coronary artery disease (CAD).

#### 1.4 Importance of antioxidant function and antioxidant defense systems in RBCs

During its lifetime, a RBC circulates through the body about 75,000 times (23), and is loaded with  $\text{O}_2$  on each cycle. As a consequence of their physiological role, RBCs are exposed to continuous oxidative stress. In addition, cells are exposed to high shear rates in laminar and turbulent flow, and must pass through narrow capillaries.

Since the RBC concentration of oxyHb is high (5 mM), even a low rate of autoxidation can produce substantial levels of  $\text{O}_2^-$ . Superoxide crosses membranes only via transmembrane anion channels such as band 3, but  $\text{H}_2\text{O}_2$ , its dismutation product (Eq 1.1) can cross the cell membrane almost as readily as water (24).  $\text{H}_2\text{O}_2$  is not especially toxic to macromolecules within cells, but it can pass through membranes and this feature is potentially important because the extracellular environment possesses few antioxidant defense mechanisms (24). Thus, not only does oxidative stress damage the RBC itself, but the exit of large quantities of ROS from the RBC could damage other components of the circulation (25). To fulfill their physiological requirements, the cell membrane and cytosol must remain in an active state, despite the fact that the human RBC demonstrates limited resynthesis processes (26). Furthermore, the mobility of the RBC makes it an ideal oxidant scavenger throughout the circulation.

Aerobic organisms need a continuous flow of oxygen to their tissues, while simultaneously protecting themselves from the inherent toxicity of  $\text{O}_2$ . Oxygen-carrying proteins provide the required  $\text{O}_2$ , and oxidant defense systems protect against its toxicity

(27). The antioxidant system in human RBCs consists of non-enzymatic and enzymatic pathways.

Endogenous non-enzymatic low-mass antioxidants are divided into lipophilic (vitamin E, carotenoids, ubiquinone, melatonin, etc.) and hydrophilic (vitamin C, glutathione, uric acid, etc.) compounds. Three vitamins, A, C, and E, protect RBCs against oxidative damage. Vitamin C acts in the aqueous phase, and is chemically known as ascorbic acid. As a reducing and antioxidant agent, it directly reacts with  $O_2^-$  and  $OH^-$ , and it also recycles vitamin E (12, 28). Vitamin E is chemically referred to as *D-α*-tocopherol and it acts in the lipid phase as a chain-breaking antioxidant (9). Vitamin E is the most widely distributed antioxidant in nature. When vitamin E donates an electron to a lipid peroxy radical, its radical form is stabilized by resonance (9). Vitamin A, a potent radical scavenger, is also a lipophilic antioxidant (12). Carotenoids can exert antioxidant effects as the precursors of vitamin A (29). In all cell types, GSH is the most important non-enzymatic regulator of intracellular redox homeostasis (30). It assumes a vital role in keeping vitamin E and vitamin C in their reduced states (57). Uric acid is an end product of purine metabolism in mammals. Its antioxidant properties were confirmed by its protection against oxidative damage (37).

A group of enzymatic antioxidants is additionally found in cells. In RBCs, the best characterized members of this group include catalase, glutathione peroxidase-1 (GPx-1), methHb reductase, and CuZnSOD. Catalase, GPx-1 and CuZnSOD have long been considered to possess central antioxidant functions in RBCs (9).

## 1.5 Copper, zinc-superoxide dismutase (CuZnSOD)

SOD enzymes were previously considered as metalloproteins with unknown function. For example, CuZnSOD was known as erythrocuprein because of its high concentration (1.8  $\mu\text{M}$ ) in RBCs (32, 33). The SOD function (Eq 1.1) of the protein was proposed by McCord and Fridovich in 1969 as a result of various observations on the reduction of cytochrome C by the superoxide radical generated from the xanthine/xanthine oxidase reaction. (34). The SOD family of enzymes is comprised of three major classes depending on the metal cofactor: CuZn (which binds both copper and zinc), Fe and Mn (which bind either iron or manganese), and Ni, which binds nickel. The best known function of SODs is the protection of cells from ROS, particularly  $\text{O}_2^-$ . In humans, three forms of SOD are present. SOD1 is located in the cytosol, SOD2 in the mitochondrion and SOD3 is extracellular. Both SOD1 and SOD3 contain CuZn, while SOD2 has Mn at its active centre.

### 1.5.1 Properties of human CuZnSOD (SOD 1)

Human RBCs contain only CuZnSOD, a homodimer with a molecular weight of 32 kDa. The two subunits are held together primarily by hydrophobic interactions and each subunit contains one active site. The distance between the two active sites in the homodimer is over 30 Å. Each monomer consists primarily of an eight-stranded  $\beta$ -barrel with two large loops - an 'electrostatic loop' and a 'metal binding' loop. The metal-binding region is fully contained within each monomer and consists of one Cu- and one Zn-binding site. The two metal binding sites share an imidazolate ligand, His63, indicating their close proximity. This structure around the metal-binding sites is further

stabilized and linked to functionally important portions of the protein by a hydrogen-bond network (35).

The Cu and Zn ions play structural and catalytic roles in CuZnSOD. The Cu<sup>II</sup> is bound by His46, 48, 63, and 120 in a distorted tetrahedral geometry. There is a fifth ligand, H<sub>2</sub>O, for Cu<sup>II</sup> (36). Cu<sup>I</sup> is also bound by His46, 48, and 120 in a distorted trigonal planar geometry (37). The Zn ion, bound by His63, 71, 80, and Asp83, is thought to play a structural role and act as a positively-charged sink (Fig. 1.3). The positively charged active site makes up approximately 11% of the total exposed surface (38). The rest of the surface is negatively charged, and the charge gradient contributes to substrate binding by electrostatic steering (39).

The crystal structure of the Cu<sup>I</sup> form of the enzyme is only slightly changed from that of the Cu<sup>II</sup> enzyme, except in one aspect: the Cu<sup>I</sup> undergoes a 1.3-Å shift, moving away from the His63 nitrogen to which it is bound in the Cu<sup>II</sup> form of the enzyme. Besides releasing His63, the Cu<sup>I</sup> ion also releases the water ligand upon reduction. This causes it to alter its irregular five-coordinate geometry to a trigonal planar three-coordinate configuration. At the same time, His63 gets protonated and exclusively binds to the Zn ion (35, 39) (Fig. 1.4). CuZnSOD is a very stable protein because dimerization reduces the surface area of the protein and makes it less solvent accessible (40). When fully loaded with metals, the protein melts at 85 - 95°C depending on the buffer (41), and is enzymatically active in 8 M urea or 4 M guanidine-HCl (42).



**Figure 1.3. Structure of human CuZnSOD dimer** (pdb 1SPD) (adopted from (39)). The left subunit is shown in the stick representation for detail. Copper is colored blue, zinc is colored lavender, and the metal bridging His63 is shown in red. The secondary H-bond bridge includes His46 (yellow), Asp 124 (magenta), and His71 (yellow). The remaining metal binding histidines are shown in cyan. The right subunit is shown as a ribbon cartoon to illustrate the overall architecture of the CuZnSOD subunit. The p-barrel is shown in gray, the metal binding loop in green, and the electrostatic loop in blue.

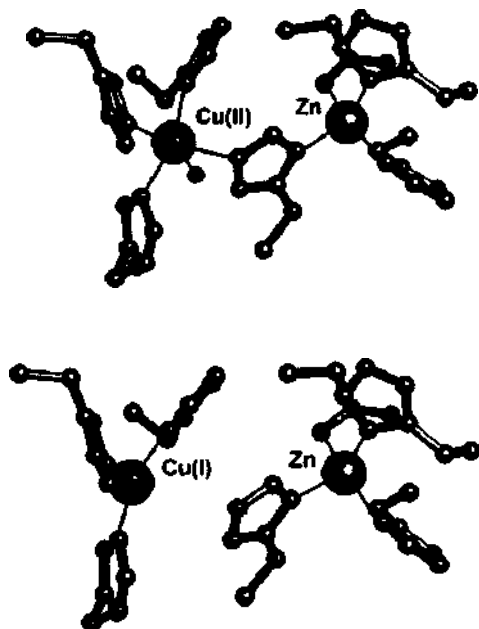
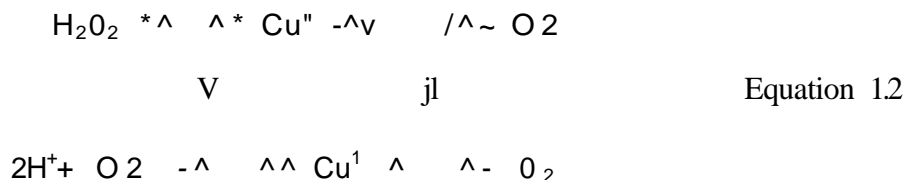


**Figure 1.4. Oxidized and reduced metal-binding sites of bovine CuZnSOD** (adopted from (35)). The  $\text{Cu}^{\text{II}}$  form of the enzyme (top; from pdb ICBJ) possesses an intact imidazolate bridge between  $\text{Cu}^{\text{II}}$  and  $\text{Zn}^{\text{II}}$ .  $\text{Cu}^{\text{II}}$  is five-coordinate bonded to four histidyl side chains and one water molecule. In the  $\text{Cu}^{\text{I}}$  form of the enzyme (bottom; from pdb IQOE) the imidazolate bridge is broken between the bridging histidine (His63) and the  $\text{Cu}^{\text{I}}$ , which becomes three-coordinate, bonded to only three histidyl side chains.

### 1.5.2 Superoxide dismutase (SOD) activity of CuZnSOD

The copper site is where the dismutation of two molecules of superoxide to O<sub>2</sub> and H<sub>2</sub>O<sub>2</sub> takes place (Eq 1.1). This catalysis is a two-step process, involving copper reduction and re-oxidation: One molecule of O<sub>2</sub><sup>-</sup> is first oxidized by Cu<sup>II</sup> to form O<sub>2</sub> (Eq 1.2) and then a second molecule of O<sub>2</sub><sup>-</sup> is reduced by Cu<sup>I</sup> to form H<sub>2</sub>O<sub>2</sub>. The enzyme's catalytic cycle is described as a ping-pong mechanism (39):



CuZnSOD is a very efficient catalyst and the activity is nearly independent of pH over the range of 5.0 to 9.5 (35). Under nonsaturating conditions, the rate-limiting step in the dismutation catalyzed by CuZnSOD is the diffusion of O<sub>2</sub><sup>-</sup> toward the active-site cavity. Based on the estimated diffusion rates of O<sub>2</sub><sup>-</sup> and CuZnSOD, the catalytic rate constant of 2x 10<sup>9</sup> M<sup>-1</sup> s<sup>-1</sup> corresponds to that of a diffusion-controlled reaction (43).

### 1.5.3 Antioxidant role and physiological importance of CuZnSOD

In biological systems, O<sub>2</sub><sup>-</sup> reacts with itself (dismutation) or with another radical such as NO to form peroxynitrite. Although O<sub>2</sub><sup>-</sup> spontaneously dismutates to O<sub>2</sub> and H<sub>2</sub>O<sub>2</sub> quite rapidly (~10<sup>5</sup> M<sup>-1</sup> s<sup>-1</sup> at pH 7), the half-life of O<sub>2</sub><sup>-</sup> is actually quite long at low concentrations (e.g., 14 h at 0.1 nM O<sub>2</sub><sup>-</sup>). SODs are biologically necessary to outcompete the damaging reactions of O<sub>2</sub><sup>-</sup>, thus protecting the cell from O<sub>2</sub><sup>-</sup> toxicity.

The CuZnSOD concentration in aerobic cells is normally  $10^5$  M, which maintains the steady-state superoxide concentration at  $10^{10}$  M (44, 45). For a given  $O^{\cdot -}$  molecule, the probability of meeting a molecule of CuZnSOD is much higher than meeting another  $O_2^{\cdot -}$  molecule. Taking these concentrations into account, CuZnSOD in the cellular environment shortens the lifetime of  $O_2^{\cdot -}$  by a factor of  $10^{10}$  (46). Since superoxide is one of the main ROS in the cell, CuZnSOD is believed to play a major role in front-line antioxidant defense.

The physiological importance of SODs is illustrated by the severe pathologies evident in mice genetically engineered to lack these enzymes. Mice lacking SOD1 develop a wide range of pathologies, including hepatocellular carcinoma, an acceleration of age-related muscle mass loss, an earlier incidence of cataracts, and a reduced lifespan (47, 48). Mutations in gene coding for SOD1 can cause familial amyotrophic lateral sclerosis (FALS), a form of motor neuron disease (35).

## 1.6 Catalase

Catalase is found in most organisms that are exposed to oxygen. It catalyzes the decomposition of  $H_2O_2$  to water and oxygen. Catalase was first reported in 1811 by Thenard who discovered  $H_2O_2$  in living tissue and proposed that its breakdown is caused by a specific molecule (49). In 1900, Loew named this  $H_2O_2$ -degrading enzyme 'catalase' (50). In 1937, the first crystal of catalase from beef liver was obtained by Sumner and Dounce (49), and its molecular weight was determined in 1938 (51). In 1969, the amino acid sequence of bovine liver catalase was determined by Schroeder (52), and more than 300 catalase sequences are now available (53).

Catalases can be organized into four main groups (54). The most widespread class in nature is composed of the monofunctional, heme-containing enzymes, which are subdivided based on subunit size ( $> 75$  kDa or  $< 60$  kDa) (53). The second group is composed of the bifunctional, heme-containing catalase-peroxidases. The third class includes the nonheme or Mn-containing catalases. Miscellaneous proteins with minor catalytic activities are grouped in the fourth class (54).

### 1.6.1 Properties of catalase

Human catalase is a homotetramer of 60-kDa subunits (Fig. 1.5c) and it belongs to the first group of monofunctional catalases. Each subunit contains a heme group (ferriprotoporphylin IX) at the active site, which is internally located and approachable by a passageway that becomes narrow at the heme (55). Each subunit can be divided into four domains (Fig. 1.5a). The first domain, the hydrophobic core of each subunit, is generated by an eight-stranded antiparallel P-barrel. The P-barrel loops and nine helices (the second and third domains, respectively) cap the hydrophobic core on both sides. The N-terminal threading arm is the fourth domain. It connects two subunits by interacting with the wrapping loop on another subunit to form a dimer (Fig. 1.5b). The two dimers assemble to form the tetramer, which is roughly square with overall dimensions of 100 Å x 100 Å x 70Å (Fig. 1.5c) (56). Tetramerization forces the threading arms from the arm-exchanged dimer to cover the heme active sites in the other dimer (56). Tetramerization could be critical for sequestering the active sites. This allows the enzyme to complete the reaction cycle rather than allowing generation of hydroxyl radicals from exposed hemes.

The heme active site is at the bottom of a 25-Å channel extending from the enzyme's surface. A 3-Å-wide hydrophobic constriction, lined by the side chains of

Val74, Val 16, Phe153, Phe154, and Trp186 (Fig. 1.6), is located directly above the active site. It allows only H<sub>2</sub>O, H<sub>2</sub>O<sub>2</sub> or other small molecules to reach the heme. Throughout the catalase structure, H<sub>2</sub>O fills packing defects between the four domains of each subunit, and between subunits within the tetramer. At either end of the hydrophobic constriction, well-ordered H<sub>2</sub>O molecules form hydrogen bonds to the protein, which promotes the selection of H<sub>2</sub>O<sub>2</sub> as substrate (56).

In addition to heme, human catalase has another cofactor, NADPH. This binds in a cleft between the helical and the p-barrel domains on the surface of the enzyme. The redox-active nicotinamide C4 atom of NADPH is 19 Å from the nearest heme iron (Fig. 1.5a) (56).

Catalase is a very stable enzyme and is resistant to treatment with ethanol and chloroform mixtures (53). When the solution pH falls outside the range of 3.5-11, the heme completely dissociates from the active site and catalase completely loses its enzymatic activity (57). Catalase exhibits strong absorbance in the Soret region ( $\epsilon_{405\text{nm}} = 3.24 \times 10^5 \text{ M}^{-1} \text{ cm}^{-1}$ ) (49, 58). RBC catalase possesses one of the highest known enzymatic rates with a turnover number of  $2.25 \times 10^7 \text{ s}^{-1}$  (59) at its pH optimum of ~7 (60). Human catalase works at an optimum temperature of 37°C (61), which is approximately the temperature of the human body.

helical domain  
 threading, 4- ^ ^ f e  
 " ^ am . ^ - T w f f e l a  
  
 P-barrel O | ^ ^ J ? - \*\*  
 wrapping ^ r ^  
 loop —> f ~ ~ \*

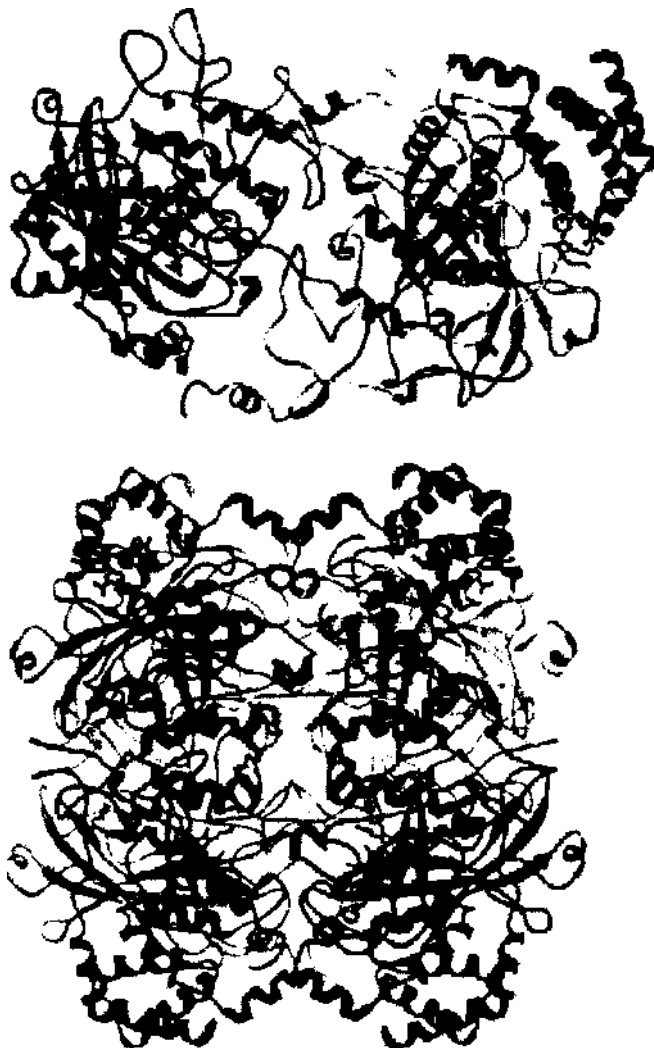


**Figure 1.5. Structure of human catalase** (adopted from (56)). (a) Stereo view of an individual subunit with the central P-barrel in yellow, surrounding helices in blue, and active-site heme in red. The heme is surrounded by the P-barrel,  $\alpha$ -helix and loops with one open face. The NADPH in dark green is on the far side of the molecule in this view, (b) Stereo view of an arm-exchanged dimer of the yellow and blue subunit and a second purple subunit. (c) Stereo view of the catalase tetramer with the addition of a second arm-exchanged dimer of orange and green subunits. Formation of the tetramer buries the heme active sites from solvent.

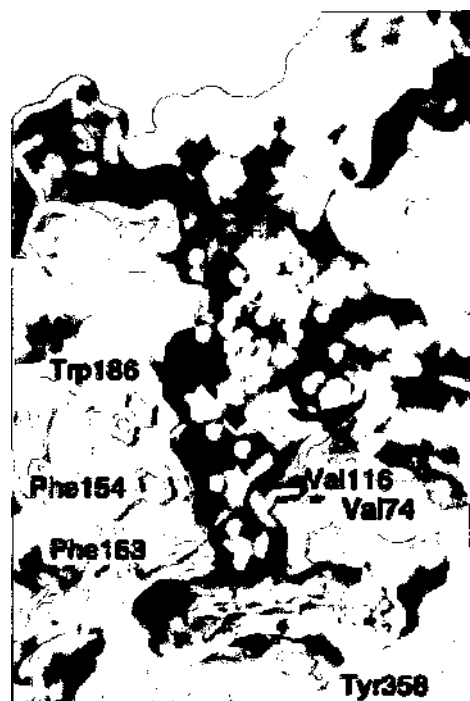


**Figure 1.6. Active-site channel of human catalase** (adopted from (56)). A 25-Å channel leads from the enzyme's surface to the heme active site and forms a hydrophobic constriction 2-3-Å wide immediately above the heme. This is critical for the 'molecular ruler recognition' mechanism for H<sub>2</sub>O<sub>2</sub> (56). Side chains making up the hydrophobic channel and the Tyr358 ligand are displayed in green. The backbone is shown in white, water in red, and the heme in dark red.

## 1.6.2 Catalysis of H<sub>2</sub>O<sub>2</sub> decomposition

The 'catalytic' reaction is very simple on paper,  $2\text{H}_2\text{O}_2 \rightarrow 2\text{H}_2\text{O} + \text{O}_2$ , with two distinct stages in the reaction pathway. The first stage involves oxidation of the heme iron using H<sub>2</sub>O<sub>2</sub> to form compound I (Cpd I), an oxyferryl group with a cationic porphyrin radical (Eq 1.3). In the second stage, reduction of Cpd I regenerates the resting-state enzyme (Enz) by involving a second molecule of H<sub>2</sub>O<sub>2</sub> as an electron donor (Eq 1.4).



### 1.6.3 Antioxidant role and physiological importance of catalases

As stated above, catalase is present in both mammalian and nonmammalian aerobic cells. The major defined role of catalase is the destruction of H<sub>2</sub>O<sub>2</sub> by the catalatic reaction (Eq 1.3 and Eq 1.4). In RBCs, catalase functions alongside other systems (GPx and metHb reductase) to prevent the accumulation of methemoglobin (metHb), either by preventing the oxidation of Hb by H<sub>2</sub>O<sub>2</sub> (catalase, GPx) or by reducing the metHb (metHb reductase) at a comparable rate as it is being formed. The amount of metHb generated in RBCs by exposing them to H<sub>2</sub>O<sub>2</sub> has been found to be inversely proportional to their catalase content (57), suggesting that catalase is a critical enzyme in the defense against oxidative damage and inactivation of Hb in RBCs (56).

However, the true biological significance of catalase is not easy to assess because genetically engineered mice that lack catalase are phenotypically normal (62) and humans with low levels of catalase (acatalasia) show few ill effects (63). However, catalase has been implicated as an important factor in inflammation, mutagenesis, prevention of apoptosis, and in the stimulation of a wide spectrum of tumors. Loss of catalase leads to the human genetic disease known as acatalasemia, or Takahara's disease (57).

### 1.7 GSH and glutathione peroxidase (GPx)

GPx was discovered in 1957 by Mills as a RBC enzyme that protects Hb from oxidative breakdown (64). In 1973, Rotruck (65) in the United States and Flohe (66) in Germany independently found that selenium was a component of GPx. GPx is the general name of an enzyme family with peroxidase activity. There are several isozymes encoded by different genes, which vary in location and substrate specificity. Four distinct GPx

isoforms have been identified so far in mammals, each containing one Se in the form of selenocysteine (SeCys) per subunit (67, 68). GPx-1 is the most abundant isoform. It is found in the cytosol of nearly all mammalian tissues and has also been called cytosolic or cellular GPx. A second form of GPx (GPx-2) is an intestinal enzyme, which is also located in the cytosol. It has approximately 65% amino acid sequence identity and 60% nucleotide identity to GPx-1 (67). Both GPx-1 and GPx-2 have similar substrate specificities because they reduce H<sub>2</sub>O<sub>2</sub> or fatty acid hydroperoxides rapidly but not phospholipid hydroperoxides (67). GPx-3 is found in the extracellular space. It is especially abundant in plasma with distinct properties from GPx-1 (67). Phospholipid hydroperoxide GPx (GPx-4) is the fourth GPx that has been characterized. GPx-4 has a high preference for phospholipid hydroperoxide as a substrate. It is expressed in most mammalian cells but at much lower levels than GPx-1. The sequence similarity between GPx-1 and GPx-4 is between 30% and 40% (67). There are many differences between GPx-4 and the other GPxs, the main one being that GPx-4 is a monomer in contrast to the tetrameric structure of the other GPxs. It also has a wider range of substrates than the tetrameric GPxs (67).

Glutathione (GSH) is the most abundant intracellular thiol, reaching high (mM) concentrations in most cell types. GSH is involved in antioxidant defense via direct interaction with ROS or as a substrate of detoxification enzymes like GPx. Importantly, GSH plays an essential role in maintaining a constant redox environment inside the cell that is critical for the function of cellular proteins. GSH is a tripeptide of glycine, glutamate, and cysteine. Cysteine, a sulfur-containing amino acid, is the "rate-limiting" amino acid for the production of GSH (69).

GSH has reduced and oxidized forms. Cellular GSH is predominantly present in the reduced form (70). Under oxidizing conditions, oxidation of GSH to its disulfide, GSSG, results in a decreased GSH-to-GSSG ratio.

### 1.7.1 Properties of RBC GPx

Two GPx forms have been identified in blood: cellular (GPx-1 present in RBCs), and extracellular (GPx-3 present in plasma). GPx-1 is a tetramer with four identical subunits each with a molecular weight of 23 kDa. Each subunit contains one active-site SeCys, in which the cysteine sulfur atom has been replaced by a selenium atom. In general, GPx proteins consist of 201 amino acid residues and the SeCys residue is located 47 residues from the N-terminal end of the protein (71). Bovine RBC GPx-1 has been crystallized (72). It consists of four spherical subunits, each with a diameter of 3.8 nm, arranged in a square-planar configuration (71). Each subunit contains four  $\alpha$ -helices, four  $\beta$ -sheets, and connecting loops involved in subunit contact. The active centres of GPx-1 are readily accessible for the solvent via channels in the crystals. The x-ray structure reveals that the catalytically active SeCys is located at the end of an  $\alpha$ -helix associated with two adjacent parallel  $\beta$ -strands in a PaP structure (Fig. 1.7). This arrangement is important for catalysis and substrate binding (72). The Se atoms are no closer than 20 Å, which strongly suggests that each Se functions independently (71).

With GSH as an electron donor, the specific activity of GPx-1 is 193.6 nmol/min per mg of protein. The  $K_m$  values for GSH and H<sub>2</sub>O<sub>2</sub> are 3.7 mM and 0.24 mM, respectively (73).

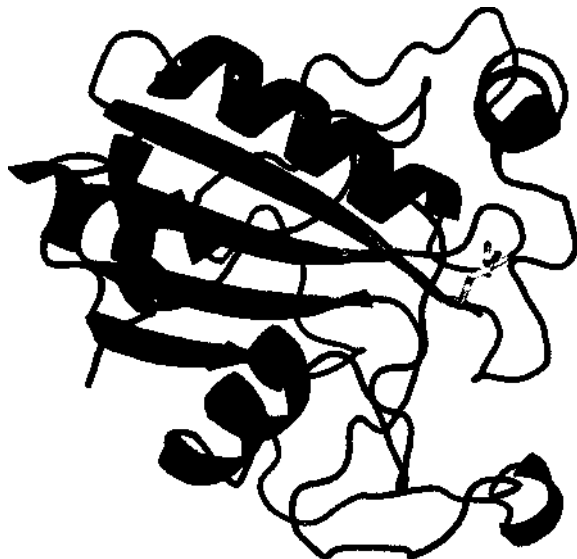
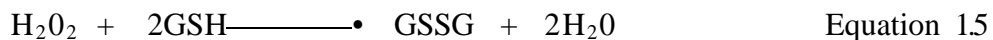


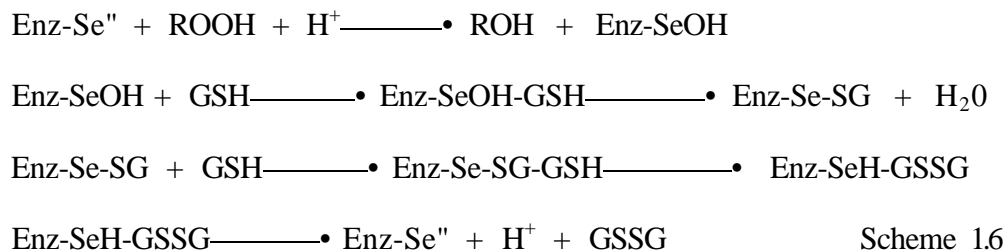
**Figure 1.7. Structure of bovine GPx-1 (dimer).** Each subunit consists of 4  $\alpha$ -helices, 4  $\beta$ -sheets and connection loops, arranged in an almost flat configuration. The active centres of GPx-1 are in flat depressions on the molecular surface. The catalytically active SeCys residues are the multicolored sticks and each is located at the end of an  $\alpha$ -helix associated with two adjacent parallel  $\beta$  strands in a pap (72).

### 1.7.2 Catalysis of $H_2O_2$ decomposition

GPx-1 removes  $H_2O_2$  by coupling its reduction to  $H_2O$  with oxidation of reduced GSH. GPx-1 also reduces fatty acid hydroperoxides (74).



During the catalytic cycle of GPx, the ionized selenol ( $Enz-Se^-$ ) reacts with  $H_2O_2$  to give a selenenic acid ( $Enz-SeOH$ ), which is trapped by a GSH molecule to form  $Enz-Se-SG$  and  $H_2O$ . The  $Enz-Se-SG$  is reduced back to  $Enz-Se^-$  by another GSH molecule and GSSG is released as a by-product (Scheme 1.6) (6).



### 1.7.3 Antioxidant role and physiological importance of GPx

GPx is another major enzyme that protects against the oxidative stress caused by H<sub>2</sub>O<sub>2</sub>. The physiological role of this enzyme is difficult to evaluate because both GPx and catalase decompose H<sub>2</sub>O<sub>2</sub>. Although GPx shares its substrate, H<sub>2</sub>O<sub>2</sub>, with catalase, GPx alone can react effectively with lipid and other organic hydroperoxides. The physiological importance of GPx has been demonstrated by using animals on a selenium-deficient diet (75). A dramatic decrease of GPx activity has been implicated in causing a number of diseases found in selenium-deficient animals (75). More experiments further underline that the physiological relevance of GPx is difficult to evaluate. A transgenic mouse model deficient in cellular GPx-1 was generated (75). Mice deficient in this enzyme were healthy and fertile and showed no increased sensitivity to hyperoxia. Their tissues exhibited neither a retarded rate of extracellular H<sub>2</sub>O<sub>2</sub> consumption nor an increased content of protein carbonyl groups or lipid peroxidation compared with those of wild-type mice (75). These results suggest that the contribution of GPx-1 to cellular antioxidant defense under normal animal development and physiological conditions and to pulmonary defense against hyperoxic insult is very limited (75). Thus, the potential antioxidant role of this enzyme in protecting cells and animals against the pathogenic effect of ROS remains to be defined (75).

## 1.8 Immunofluorescence

Immunofluorescence requires the labelling of antibodies or antigens with fluorescent dyes. The purpose of immunofluorescence is to detect the subcellular distribution and relative abundance of a protein of interest. Since antibodies are small and can not be visualized directly, a fluorescent dye covalently attached to the antibody is used. When the dye is illuminated, it absorbs the light and emits a light of different color which is visible to the investigator and which can be photographed (76).

There are two strategies used for the immunofluorescence detection of antigens in cells, the direct method (Fig. 1.8) and the indirect method (Fig. 1.9). The former is a one-step staining method where a labelled antibody reacts directly with the protein of interest. The indirect method involves an unlabeled primary antibody and a labelled secondary antibody. The primary antibody reacts with protein of interest, and then the secondary antibody is introduced to recognize the primary antibody. Usually immunofluorescence uses the indirect method as it is more sensitive due to the researcher's ability to amplify the signal. The amplification is accomplished through the reaction of several secondary antibody molecules with different antigenic sites on the primary antibody (77). Immunofluorescent-labelled cells, tissue sections or cultures are studied using a fluorescence or confocal microscope.

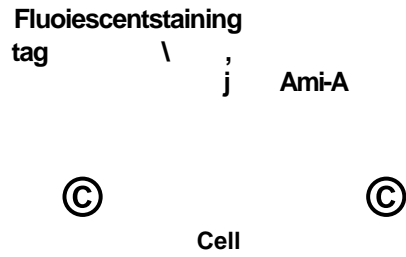


**Figure 1.8. The direct method of immunofluorescent staining.** The green triangle is the protein A of interest. The fluorescent or staining-tag-conjugated antibody (anti-A) binds directly to protein A. Adopted from <http://en.wikipedia.org/wiki/Immunohistochemistry>.

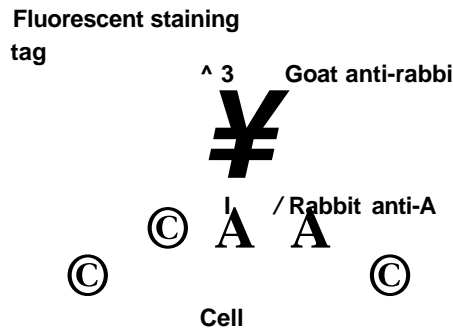


**Figure 1.9. The indirect method of immunofluorescent staining.** This method uses one antibody (rabbit anti-A) against the protein A, and a second, labelled, antibody (goat anti-rabbit) against the first. Adopted from <http://en.wikipedia.org/wiki/Immunohistochemistry>.

## 1.9 Confocal microscopy

Confocal microscopy is an imaging technique that allows the researcher to view images more clearly than possible with a conventional light microscope. In a conventional light microscope, object-to-image transformation takes place simultaneously for all object points. All parts of the specimen are excited at the same time and fluorescence is sensed by a photodetector. In conventional fluorescence

microscopy, the in-focus image from the object plane of interest is mixed with the out-of-focus image from planes outside of the focal plane, which reduces image contrast.

The specimen in a confocal microscope is irradiated in a point-like fashion. The laser beam used in confocal microscopy is focused to a spot which illuminates only a single point of the object at a time. Furthermore, in a confocal microscope the pinhole eliminates out-of-focus information. The pinhole diameter is variable; ideally, it is infinitely small, and thus the detector looks at a point. The image quality of confocal microscopy is much better than that of images from conventional light microscopy (78, 79).

While the light microscope requires cutting through a specific cross-section, the confocal microscope allows viewing of 3D images by combining images from different cross-sections. There is no need to cut through the cross-section that is about to be viewed because the confocal microscope is a depth-discriminating optical system. The confocal microscope can image a thin optical slice in a thick specimen, a method known as optical sectioning. Under suitable conditions, the thickness of such a segment may be less than 500 nm.

In addition to the possibility of observing a single plane of a thick specimen in good contrast, optical sectioning allows a large number of slices from different planes to be recorded. As the specimen is moved along the optical axis ( $Z$ ) in small increments, the resulting  $Z$ -scan provides information about the 3D structure of the object. Also, the spatial rearrangement of living specimens can be recorded by confocal microscopy (79).

Three types of confocal microscopes are commercially available: confocal laser scanning microscopes (LSM), spinning-disk confocal microscopes, and programmable

array microscopes (PAM) (80). The LSM yields better image quality than the other two (80).

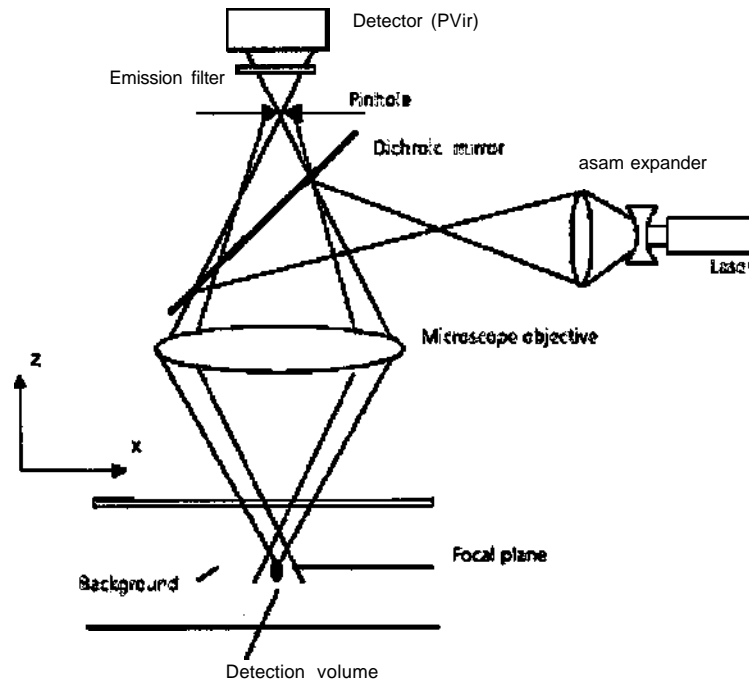


**Figure 1.10. Ray path in a confocal LSM** (from (79)). A microscope objective is used to focus a laser beam onto the specimen, where it excites fluorescence. The fluorescent radiation is collected by the object and efficiently directed onto the detector via a dichroic beam splitter. The interesting wavelength range of the fluorescence spectrum is selected by an emission filter, which also acts as a barrier blocking the excitation laser line. The pinhole is arranged in front of the detector, on a plane conjugate to the focal plane of the objective. Light coming from planes above or below the focal plane is out of focus when it hits the pinhole (broken line), so most of it cannot pass the pinhole and therefore it does not contribute to the image.

### 1.10 Outline and scope of thesis

This thesis describes antioxidant function in human RBCs using immunofluorescence to localize the antioxidant enzymes, CuZnSOD, catalase, GPx, and its substrate GSH. RBCs have a strong antioxidant defense system that not only protects the cells themselves from oxidative damage, but also RBCs function as a ROS sink to

protect other cells and tissues (81). Understanding the properties and specific roles of these antioxidant enzymes in RBCs is of critical importance to fundamental cell biology as well as biomedicine.

Chapter 1 introduces the properties of human RBCs, ROS, and the effects of ROS on RBCs. Next, basic information is provided about the antioxidant defense in RBCs, especially the antioxidant enzymes, followed by a description of the main technique used in the project.

Chapter 2 describes the experimental procedures including the materials and methods for preparing, fixing, permeabilizing, and staining RBCs, as well as the confocal settings for RBC visualization. The treatment of cells for different studies as well the methods used for  $H_2O_2$  and  $O_2^-$  generation are also outlined.

Chapter 3 summarizes the results, and the functional relevance of antioxidant enzymes under different experimental conditions is discussed in Chapter 4. The final conclusions and future studies are discussed in Chapter 5.

All the immunofluorescence images in Chapter 3 are provided in electronic format in the DVD submitted with the thesis. Also, additional images and Z-stacks are provided in the DVD as listed in the Appendix.

## Chapter 2: Materials and methods

### 2.1 Materials

Phosphate-buffered saline (PBS) tablets (one tablet was dissolved in 200 mL of deionized water to give 137 mM NaCl, 2.7 mM KCl, 8.1 mM  $K_2HPO_4$ , 1.5 mM  $KH_2PO_4$  at pH7.4), Triton X-100, fish skin gelatin, sodium azide, poly-lysine, ABTS, acrolein, PMS, NBT, glucose oxidase (GOx), catalase, and CuZnSOD were from Sigma. Glucose was from EMD. Glycine was from Bioshop. Aqua-mount was from Lerner Laboratories. Formaldehyde was from Pierce (now Thermo Scientific). HRP and NADPH were from Boehringer Mannheim (now Roche). EDTA and 30% ammonia solution were from BDH Inc. Butan-1-ol was from Fisher Scientific. All the chemicals were analytical grade.

Rabbit polyclonal anti-human CuZnSOD (SOD-100, affinity purified) was from Stressgen, mouse monoclonal anti-human CDB3 (abl 1012, Ascites), and rabbit polyclonal anti-human GSH (ab9443, whole antiserum), sheep polyclonal anti-human antibodies for Hb (ab35306, IgG fraction), catalase (ab8954, IgG fraction), and glutathione peroxidase-1 (GPx-1, ab8850, IgG fraction) were from Abcam. The secondary antibodies, Cy2-(711-226-152), Cy3-(711-166-152), and Cy5-(711-176-152) conjugated donkey anti-rabbit, FITC-(713-096-147), Cy3-(713-166-147), and Cy5-(713-176-147) conjugated donkey anti-sheep, and Cy3-(715-166-150) and Cy2-(715-226-150) conjugated donkey anti-mouse were from Jackson ImmunoResearch. Alexa 488-conjugated donkey anti-sheep (A-11015) was from Invitrogen. All the secondary antibodies were supplied as affinity purified.

## 2.2 Methods

### 2.2.1 Preparation of RBCs

All procedures involving the collection of human blood samples from healthy female volunteers 25-35 years old were approved by Concordia's Human Research Ethics Committee. All blood donors provided their informed consent. Blood was drawn into heparin-coated blood collection tubes from the antecubital area of the arm and gently mixed by reversing the vial several times. The collected blood was maintained at 4°C and processed within 2 h. The whole blood was transferred to 2.0-mL Eppendorf tubes and centrifuged at 1000xg for 10 min at room temperature. After removal of the upper layer (plasma and buffy coat) by pipette, the RBC pellet was washed three times in glucose-PBS (G-PBS) (137 mM NaCl, 2.7 mM KCl, 8.1 mM K<sub>2</sub>HPO<sub>4</sub>, 1.5 mM KH<sub>2</sub>PO<sub>4</sub>, pH7.4 containing 5 mM glucose) and resuspended in this buffer at 10% hematocrit (Ht). Cells were examined using a light microscope (40x objective) to ensure their viability before fixing and staining.

### 2.2.2 Fixing and permeabilizing RBCs

A 50- $\mu$ L aliquot of cells at 10% Ht in G-PBS was centrifuged at 1000xg for 5 min at room temperature. The RBC pellet was resuspended in 1 mL of 0.5% acrolein in PBS, gently mixed for 5 min at room temperature, centrifuged at 650xg for 1 min and the supernatant was removed. The RBC pellet was rinsed 3x with rinsing buffer (PBS containing 0.1 M glycine), the cells were permeabilized in 1 mL of rinsing buffer plus 0.1% Triton X-100 for 5 min, and rinsed 3x in rinsing buffer. To ensure complete neutralization of unreacted acrolein, the cells were incubated in rinsing buffer at room

temperature for 30 min. Acrolein reacts with the free amino group of glycine in the rinsing buffer.

### 2.2.3 Staining of RBCs

#### 2.2.3.1 Staining of RBCs for a specific protein

Fixed, permeabilized RBCs were next processed for immunofluorescence microscopy. After incubation in rinsing buffer for 30 min, the RBCs were pelleted by centrifugation at 650xg for 1 min. To prevent nonspecific antibody binding, the pellet was resuspended (0.5% Ht) and incubated in blocking buffer (PBS containing 0.05 mM glycine, 0.2% fish skin gelatin, and 0.05% sodium azide) for a minimum of 60 min. Staining of the fixed, permeabilized RBCs (5% Ht) was performed by incubating with the primary antibody at 1% dilution in blocking buffer overnight at 4°C with gentle shaking. The RBCs were rinsed 3x in rinsing buffer, and incubated with secondary antibodies at 2% dilution in blocking buffer with gentle shaking at room temperature for 2-3 h. After labelling, the RBCs were rinsed 2x in rinsing buffer and 1x in PBS, and resuspended in PBS. A 5- $\mu$ L aliquot of labelled RBCs was allowed to attach to a glass slide coated with 10% polylysine, and mounted using Aqua-Mount.

#### 2.2.3.2 Double staining

Double staining is used to reveal the localization of two different proteins in the same cell. The two primary antibodies used must be raised in different species. For the first antigen, fixed and permeabilized RBCs (Section 2.2.2) were resuspended (0.5% Ht) and incubated in blocking buffer (Section 2.2.2) for a minimum of 60 min. The cells were

incubated at 5% Ht with the primary antibody at 1 % dilution in blocking buffer overnight with gentle shaking at 4°C, rinsed 3x in rinsing buffer, and incubated with secondary antibody at 2% dilution in blocking buffer with gentle shaking at room temperature for 2-3 h. Before staining for the secondary antigen, the RBCs were incubated in blocking buffer again for 1 h. The next staining steps were the same as for the first antigen, and after double labelling, the RBCs were rinsed 2x in rinsing buffer, 1x in PBS, and resuspended in PBS. A 5-uL aliquot of labelled RBCs was allowed to attach to a glass slide coated with 10% polylysine, and mounted using Aqua-Mount.

### 2.2.3.3 Competitive binding of antibodies

The procedure was the same as that used for double staining, except that the order of staining with the two primary antibodies was reversed in two separate vials under the same experimental conditions. For example, the details for competitive staining of CuZnSOD and CDB3 are outlined in Table 2.1.

Table 2.1: Competitive staining with anti-CuZnSOD and anti-CDB3

Experiment 1 (vial 1)	Experiment 2 (vial 2)
Fixing and permeabilizing of RBCs	Fixing and permeabilizing of RBCs
Staining with rabbit anti-CuZnSOD	Staining with mouse anti-CDB3
Staining with anti-rabbit Cy2	Staining with anti-mouse Cy3
Blocking	Blocking
Staining with mouse anti-CDB3	Staining with rabbit anti-CuZnSOD
Staining with anti-mouse Cy3	Staining with anti-rabbit Cy2
Cell mounting and protein visualization	Cell mounting and protein visualization

## 2.2.4 Confocal microscopy of labelled RBCs

Stained RBCs were visualized using the 63X/1.32 optical object of a Leica TCS SP2 (CSFG, Concordia University) or a Zeiss LSM 510 (Imaging Facility, McGill University) laser confocal microscope. The laser lines used for the excitation of the dyes in the stained RBCs were the blue excitation (488 nm) of an Argon laser for Cy2, Alexa 488, and FITC; the green excitation (543 nm) of a GreNe laser for Cy3, and the red excitation (633 nm) of a HeNe laser for Cy5. The laser lines and emission filters were selected to ensure that the fluorescence from the samples did not include any laser light and that emission crosstalk was avoided in the double labelling experiments. The excitation and emission spectra of the dyes used for RBCs staining are shown in Figure 2.1. The pinhole size was 1 Airy unit, which produces the best signal-to-noise ratio. The laser power was adjusted according to the dye used. The power was set to ~ 10% for the Argon laser, -100% for the GreNe laser, and -50% for the HeNe laser of the Zeiss LSM 510 laser confocal microscope. The power was set to 100% for all the laser lines using the Leica TCS SP2 since the laser was old and its output was weak.

## 2.2.5 Deaeration of RBCs

After removal of the plasma and buffy coat and after washing (Section 2.2.1), RBCs were suspended at 10% Ht in 2 mL of G-PBS in a 2-mL sealed Eppendorf tube. Nitrogen gas at 15 *psi* was flushed gently above the RBC suspension for 2 min. To fix the cells, formaldehyde was then added to a final concentration of 1% to the sealed tube through the gas-inlet needle. Initial fixation of the cells with formaldehyde was necessary because acrolein cannot fix cells in the absence of O<sub>2</sub>. After 20 min at room temperature, an aliquot of formaldehyde-fixed cells was centrifuged at 650xg for 1 min, resuspended

in 1 mL of 0.5% acrolein in PBS, permeabilized, and stained as described in Section 2.2.2.

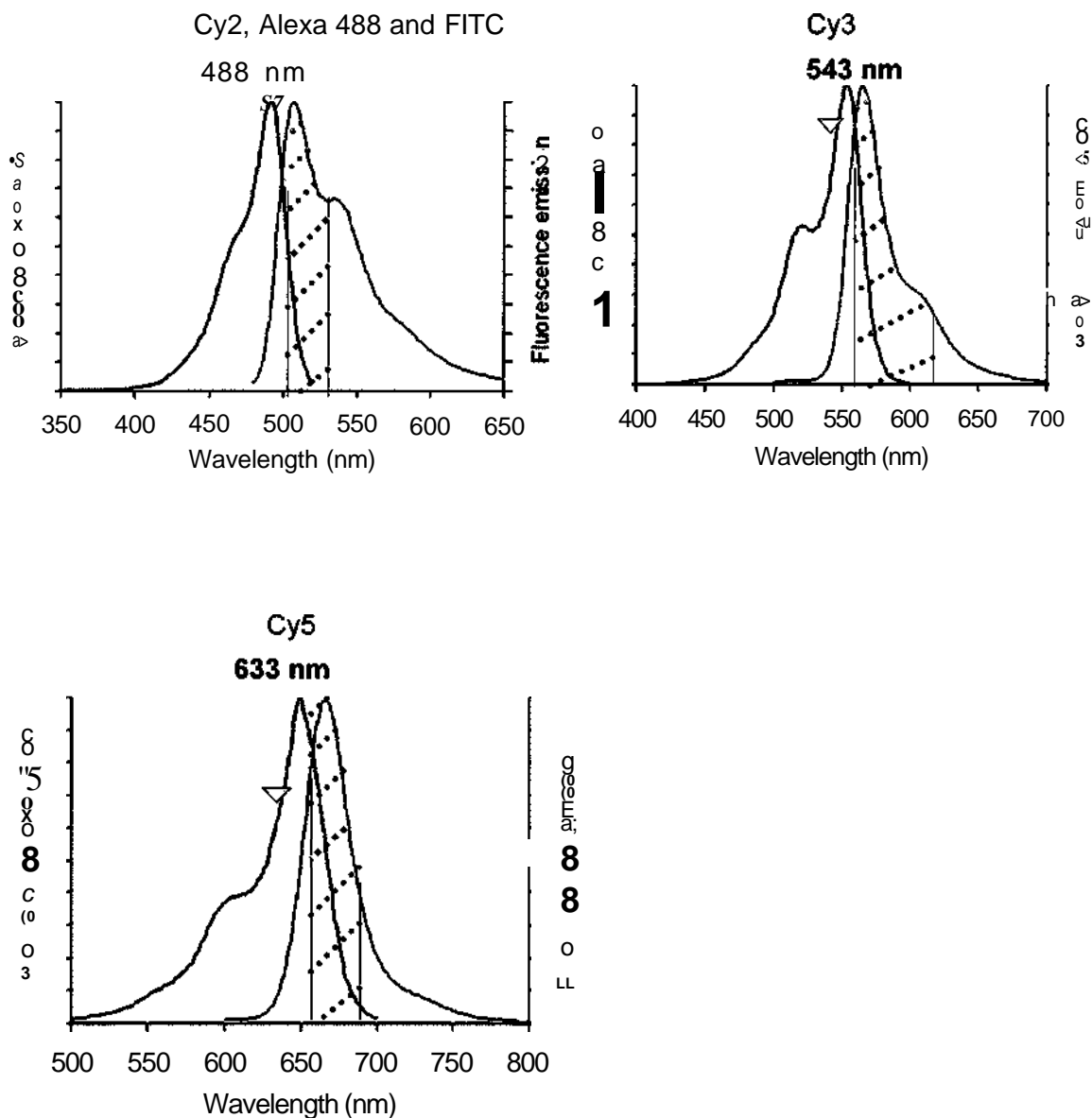


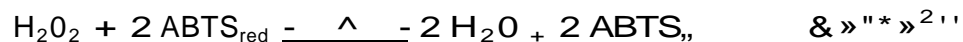
**Figure 2.1. Excitation (blue) and emission (red) spectra of the different dyes.** The wavelength used for excitation is marked by the green triangles, and the area under the pink broken lines is emission wavelength range detected by the confocal microscope. For Cy2, Alexa 488, and FITC, the excitation wavelength was 488 nm, and the emission wavelength range was 500-530 nm. For Cy3, the excitation wavelength was 543 nm, and the emission wavelength range was 560-620 nm. For Cy5, the excitation wavelength was 633 nm, and the emission wavelength range was 660-690 nm. Modified from <http://www.opentech.com/doc/image/cy3-2.gif>, [http://www.opentech.com/doc/image/cy5\\_2.gif](http://www.opentech.com/doc/image/cy5_2.gif)

### 2.2.6 Aeration of RBCs

Washed RBCs (Section 2.2.1) were suspended at 10% Ht in 2 mL of G-PBS in a 2-mL Eppendorf tube and exposed to air on the bench for ~ 1 h at ambient temperature with gentle reverse mixing for 15 s at 10-min interval. An aliquot of aerated RBCs was fixed, permeabilized, and stained as described in Sections 2.2.2 and 2.2.3.

### 2.2.7 Steady-state H<sub>2</sub>O<sub>2</sub> production

The generation of H<sub>2</sub>O<sub>2</sub> by glucose and GOx was monitored spectrophotometrically. The rate of horseradish peroxidase (HRP)-catalyzed 2,2'-azino-di-3-ethylbenzthiazoline-6-sulphonic acid (ABTS) oxidation depends on the H<sub>2</sub>O<sub>2</sub> concentration, so it can be used to quantify the peroxide:



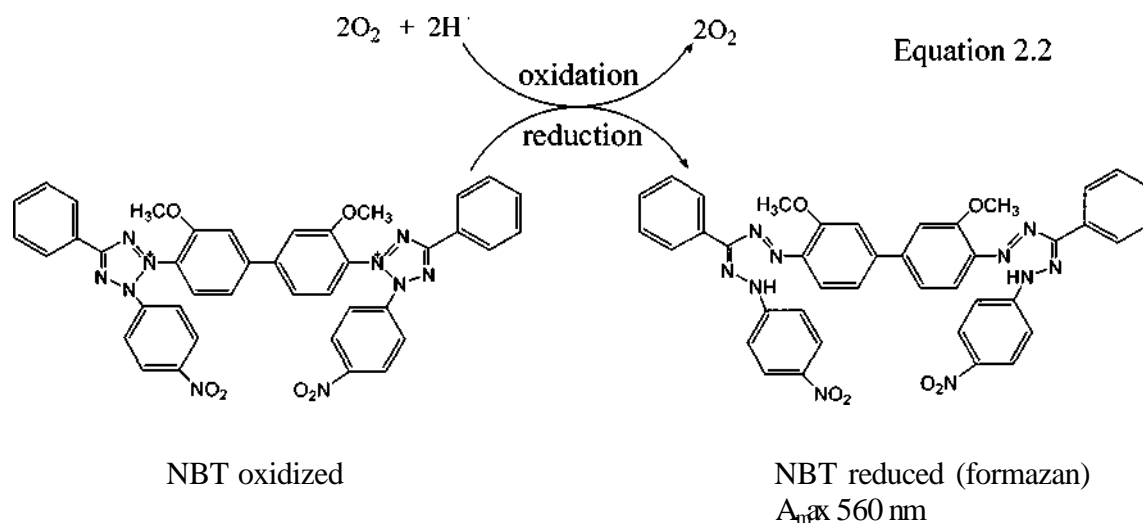
Stock solutions containing 9.15 nM HRP (concentration determined using the Soret band with  $S_{403\text{nm}}=100 \text{ mM}^{-1}\text{cm}^{-1}$ ) (82) in 50 mM sodium phosphate buffer (pH 7.0), 9.1 mM ABTS (concentration determined using  $S_{340\text{nm}}=366 \text{ mM}^{-1}\text{cm}^{-1}$ ) (85) in 100 mM sodium phosphate (pH 5.0), and 10 mM H<sub>2</sub>O<sub>2</sub> in water were prepared. For the standard assay, 10 uL of HRP stock was added to 550 uL of ABTS stock in a 1.5-mL quartz cuvette (1-cm pathlength), and the UV-vis spectrophotometer (Beckman DU 800) was blanked using this assay solution. After blanking, 50 uL of H<sub>2</sub>O<sub>2</sub> standard (10 uM to 120 uM; concentration determined using  $S_{240\text{nm}}=40 \text{ mM}^{-1}\text{cm}^{-1}$ ) (84) was added to the cuvette and the solution was mixed quickly. The final concentrations of HRP, ABTS, and H<sub>2</sub>O<sub>2</sub> in 610 uL of assay solution were 0.15 nM, 8.20 mM and 0.82-9.84 uM,

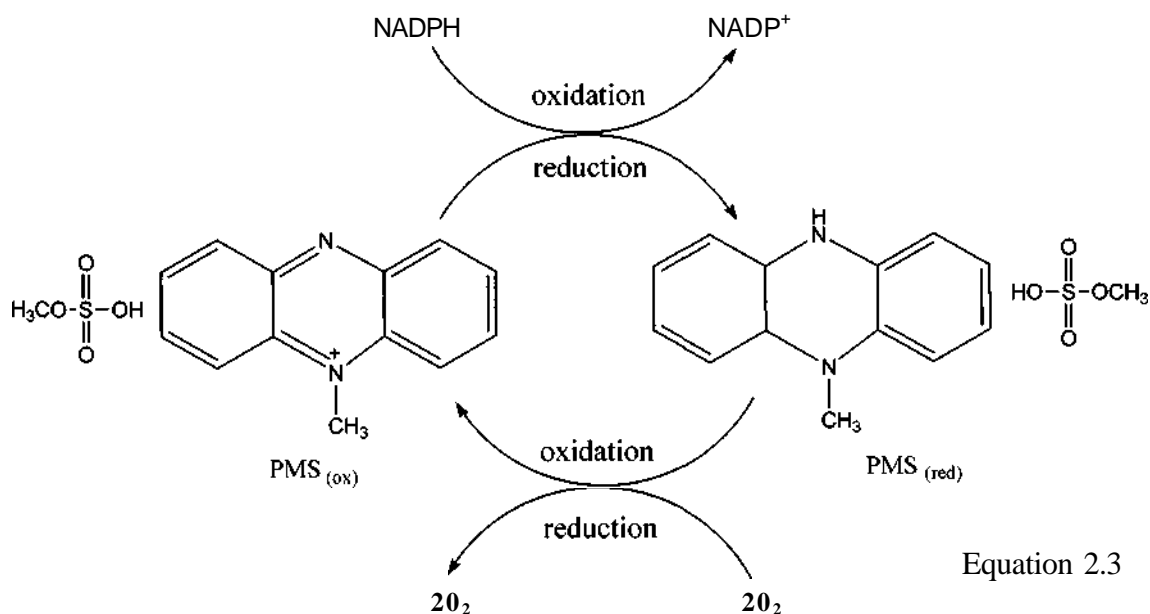
respectively. The absorbance was measured at 405 nm every 10 s over 90 s, and the slope of the initial absorption increase was measured.

To determine the efficiency of H<sub>2</sub>O<sub>2</sub> production, 0.915-2.135 units of GOx were added to 2 mL of G-PBS in a sealed 2-mL Eppendorf tube. The sample was incubated for 10 min with gentle reverse mixing for 15 s at 2-min intervals. A 50- $\mu$ L aliquot of each GOx solution was added to the HRP/ABTS assay solution and ABTS oxidation was followed as described above for the H<sub>2</sub>O<sub>2</sub> standards. The concentration of H<sub>2</sub>O<sub>2</sub> generated in samples was determined from the H<sub>2</sub>O<sub>2</sub> standard calibration plot.

### 2.2.8 Monitoring O<sub>2</sub> production by phenazine methosulfate (PMS)

Nitroblue tetrazolium salt (NBT) is stoichiometrically reduced by O<sub>2</sub> to a blue product (formazan) that absorbs light at 560 nm (Eq 2.2). Hence, the production of superoxide by PMS and NADPH (Eq 2.3) was quantified using the NBT reduction assay.





Stock solutions of 3.15 mM PMS ( $\epsilon_{387\text{nm}}=26.3 \text{ mM}^{-1}\text{cm}^{-1}$ ) (85) in deionized water, 605  $\mu\text{M}$  NBT ( $\epsilon_{257\text{nm}}=61.3 \text{ mM}^{-1}\text{cm}^{-1}$ ) (86) in PBS, and 9.26 mM NADPH ( $\epsilon_{340\text{nm}}=6.22 \text{ mM}^{-1}\text{cm}^{-1}$ ) (87) in PBS were prepared spectrophotometrically. For the assay, 5 to 18  $\mu\text{L}$  of NADPH stock was added to 1 mL of NBT stock in an open 3.0-mL cuvette (1-cm pathlength), and PBS was used to adjust the volume to 2.0 mL. The spectrophotometer (Beckman DU 800) was blanked using this solution, 10  $\mu\text{L}$  of PMS was added to the cuvette, the solution was mixed quickly, and the absorbance at 560 nm was determined every 30 s over 10 min. The final concentrations of PMS, NBT, and NADPH in the assay solution were 4.7  $\mu\text{M}$ , 302  $\mu\text{M}$  and 23-85  $\mu\text{M}$ , respectively. To establish the effect on superoxide production, a range of PMS concentrations (1.6-7.9  $\mu\text{M}$ ) was added to an assay solution containing 302  $\mu\text{M}$  NBT and 46.3  $\mu\text{M}$  NADPH.

### 2.2.9 Effects of H<sub>2</sub>O<sub>2</sub> and O<sub>2</sub> on RBCs

RBCs (Section 2.2.1) were resuspended at 10% Ht in 2 mL of G-PBS. To generate H<sub>2</sub>O<sub>2</sub> in the sample, 1.22 units of GOx were added. The 2-mL cell suspension was incubated in a sealed 2-mL Eppendorf tube at room temperature for 10 min with gentle reverse mixing for 15 s at 2-min intervals. A 400-uL aliquot was centrifuged at 1,000xg for 1 min, the supernatant was removed, the RBC pellet was fixed, permeabilized, and stained as described in Sections 2.2.2 and 2.2.3.

To examine the effect of O<sub>2</sub><sup>-</sup> generation, RBCs (Section 2.2.1) were resuspended at 10% Ht in 2 mL of G-PBS and 5 uM PMS was added. The 2-mL cell suspension was incubated in a sealed 2-mL Eppendorf tube at room temperature for 5 min, and processed as described above for the L<sup>AC</sup>-exposed cells.

### 2.2.10 Cu and Fe concentrations of human RBCs

Whole blood (1 mL) was centrifuged at 1,000xg for 10 min at room temperature in 2.0-mL Eppendorf tubes. After removal of the upper layer (plasma and buffy coat) by pipette, a 100-uL aliquot of the RBC pellet was diluted 20-fold using 1.9 mL of ICP-MS (inductively coupled plasma mass spectrometry) buffer containing ~0.7 mM ammonia, 0.01 mM EDTA, and 0.07% (v/v) Triton X-100. A 30-uL aliquot of butan-1-ol was added as a carbon source at 1.5% (v/v) to improve matrix matching between the standards and samples and thereby increase the accuracy of the measurements. The ICP-MS buffer was also used for pre- and post-analysis rinsing to keep the chemistry of the sample introduction system stable throughout the run. <sup>45</sup>Sc and <sup>72</sup>Ge were selected as internal standards (IS) for <sup>56</sup>Fe and <sup>63</sup>Cu, respectively, and their solutions were prepared the same way as the RBC samples. An Agilent 7500ce ICP-MS was used in helium-gas

mode. Quantitation was performed for each isotope by averaging the signals at the isotope mass (M, amu) and at M+0.05 and M-0.05. For example, the signal for  $^{63}\text{Cu}$  is average of the signals at 62.95, 63.00, and 63.05 amu. Triplicate measurements were performed on each sample. The standard calibration plots for  $^{56}\text{Fe}$  and  $^{63}\text{Cu}$  both exhibited an  $R^2$  value of 1.0000 (data not shown). The ICP-MS operating conditions, integration times, and gas mode (He) for the multielement determinations are summarized in Tables 2.2 and 2.3.

Table 2.2: ICP-MS settings for multielement analysis in He gas mode

Isotope	Mass, M (amu)	Detection Mode	Integration time (s/point)	Integration time (s/Mass)
$^{45}\text{Sc}$	45.00	Auto	0.30000	0.90000
$^{72}\text{Ge}$	72.00	Auto	0.30000	0.90000
$^{63}\text{Cu}$	63.00	Auto	0.30000	0.90000
$^{56}\text{Fe}$	56.00	Auto	0.30000	0.90000

Table 2.3: ICP-MS tuning parameters

Plasma conditions	Ion lenses	Octopole parameters	Q-pole parameters	Reaction cell
RF power: 1,500 W	Extract 1: OV	Octp bias: -18 V	QP bias: -14 V	Reaction mode: on
Carrier gas: 0.7 L/min	Extract 2: -110V			He gas: 5 mL/min
S/C temp: 2degC	Omega bias-ce: -22 V			
	Omega lens-ce: -0.6 V			
	Cell entrance: -30 V			
	QP focus: -11 V			
	Cell exit: -38 V			

RF power: radio frequency power

S/C temp: spray chamber temperature

## Chapter 3: Results

### 3.1 Localization of Hb and CDB3 in fixed human RBCs

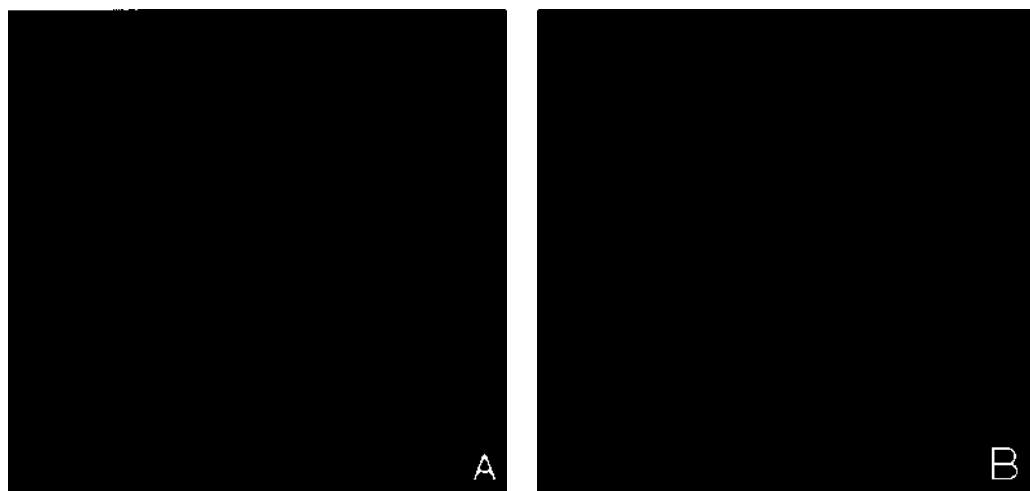
Cell fixing is a necessary step in immunohistochemistry before visualization (88). This is to preserve the structure of cells with minimum alteration from the living state and to protect cells against subsequent treatment including rinsing, permeabilizing and staining. Acrolein (Fig. 3.1), an aldehyde, was used for fixation since it reacts with many chemical groups. For example, the reaction between acrolein and proteins involves the intermolecular and intramolecular formation of crosslinks with cysteine, histidine, and lysine residues (89). Crosslinking may limit the access of antibodies to epitopes on the target proteins. Furthermore, aggressive fixation changes the spatial relationships of macromolecules (90). To characterize the localization of target proteins under physiologically relevant conditions, a method developed for RBCs by Low and coworkers (2004) (90) was used to rapidly fix freshly isolated human RBCs. The localization of antioxidant enzymes in the intact cells was then examined by confocal microscopy.



Figure 3.1. Structure of acrolein

It is known that band 3 is an important structural component of the RBC membrane. Each RBC contains approximately  $10^6$  copies of band 3 (91). Hb is the main protein in the RBC cytosol, being present at 5 mM or -270,000,000 copies (9). The working conditions for cell fixing and staining were established by examining the localization of Hb and CDB3, the cytoplasmic N-terminus of band 3 in intact human RBCs. Under the filter settings used, autofluorescence was negligible in treated and

untreated cells. Invariably, staining for CDB3 revealed that the protein was concentrated at the membrane and Hb staining revealed that this protein was evenly dispersed throughout the cytosol (Fig. 3.2). CDB3, which comprises the first 403 amino acid residues of band 3 (92), binds cytoplasmic proteins. The monoclonal anti-CDB3 antibody used in these studies specifically recognized an epitope within residues 1-136 of CDB3. Hence, the membrane pattern of CDB3 staining in intact RBCs (Fig. 3.2B) confirmed that its antibody had access to the cytoplasmic side of the membrane after cell fixing and permeabilizing. Also, the Hb distribution (Fig. 3.2A) demonstrated that the highly dense macromolecular network of crosslinked Hb expected after chemical fixation does not restrict access of the antibody to the cell interior. Therefore, the staining patterns observed for target proteins should reflect their actual localization (90).



**Figure 3.2. Confocal immunofluorescence images of Hb and CDB3 in fixed intact human RBCs.** A. Hb was stained by sheep polyclonal anti-human Hb and FITC anti-sheep IgG. B. CDB3 was stained by mouse monoclonal anti-human CDB3 and Cy2 anti-mouse IgG. Filter settings were as follows: excitation 488 nm; emission 500-530 nm. The RBC pellet was fixed and stained as described in Sections 2.2.2 and 2.2.3.1. Cells were exposed to air for < 5 min, and fixed within 2 h of drawing blood.

### 3.2 Localization of CuZnSOD, catalase, and GPx in fixed human RBCs

CuZnSOD, catalase, and GPx are antioxidant enzymes (Chapter 1). To establish the response of these enzymes to various oxidative-stress conditions, their localization under physiological conditions needs to be characterized. Freshly drawn human RBCs were fixed and stained immediately after washing. CuZnSOD, catalase, and GPx were stained as described in Section 2.2.3.1. Using the filter settings given in the figure legends, the confocal images reveal that CuZnSOD was more concentrated at the cell membrane with a punctate distribution, and less was distributed throughout the cytosol (Fig. 3.3A). Catalase was also partially distributed at the membrane and partially in the cytosol (Fig. 3.3B). GPx exhibited a definite membrane distribution with low detection in the cytosol (Fig. 3.3C). Notably, the punctate membrane staining of the antioxidant proteins is clearly different from the even membrane staining of CDB3 (Fig. 3.2B) in these intact human RBCs, which were exposed to air for < 5 min and fixed within 2 h of drawing blood.

### 3.3 Localization of CuZnSOD, catalase, and GPx in fixed RBCs following deaeration

Oxygen is essential for life, and cells have developed numerous adaptive responses to changes in O<sub>2</sub> levels. RBCs, the major supplier of O<sub>2</sub> to tissue, also serve as an O<sub>2</sub> sensor (93). In nucleated CD34(+) cells, hypoxia decreased the mRNA expression of both catalase and GPx but not of SOD. The cellular antioxidant enzyme activity under hypoxia was also affected in these cells (94). However, the RBC is an anucleated cell, so enzyme levels and activities can not be altered by protein synthesis. We examined

**Figure 3.3. Confocal immunofluorescence images of CuZnSOD, catalase, and GPx in fixed intact human RBCs.** A. CuZnSOD stained by rabbit polyclonal anti-human CuZnSOD and Cy2 conjugated anti-rabbit IgG. B. Catalase stained by sheep polyclonal anti-human catalase and Alexa 488 conjugated anti-sheep IgG. C. GPx stained by sheep anti-human GPx-1 and Alexa 488 conjugated anti-sheep IgG. Filter settings for both Alexa 488 and Cy2 were as follows: excitation 488 nm; emission 500-530 nm. The RBC pellet was fixed and stained as described in Sections 2.2.2 and 2.2.3.1. Cells were exposed to air for < 5 min, and fixed within 2 h of drawing blood.

whether the O<sub>2</sub> tension influenced the location of the key antioxidant enzymes to affect their local activity.

RBCs were deaerated under N<sub>2</sub> for 2 min, fixed, and stained as described in Sections 2.2.2, 2.2.3.2 and 2.2.5. CuZnSOD, catalase, and GPx were stained with the antibodies listed in the figure legends. As a control, CDB3 was stained at the same time by double labelling (Section 2.2.3.2) but CuZnSOD, catalase, and GPx were stained first. The confocal images showed that CuZnSOD (Fig. 3.4D), catalase (Fig. 3.4E), and GPx (Fig. 3.4F) were evenly distributed in the cytosol of deaerated RBCs. In contrast, CDB3 (Fig. 3.4G-I) showed membrane staining in all cells. The bright-field images revealed that the deaerated cells remain intact and exhibit biconcave shape. From Figure 3.4, it appears that relocalization of these antioxidant enzymes to the cytosol is the response of RBCs to 2 min of hypoxia.

### 3.4 Localization of CuZnSOD, catalase, and GPx, in fixed aerated human RBCs

Oxygen not only is transported by RBCs to meet the metabolic requirements of tissues, but also regulates the mechanical properties of the cells (95) including their membrane (96). Thus, Hb may act as a transducer regulating cellular function in an O<sub>2</sub>-dependent manner through its interaction with cytoskeletal proteins. Furthermore, the autoxidation of oxyHb is the main source of ROS in RBCs. To examine whether exposure of RBCs to room air for 1 h would change the localization of their antioxidant enzymes, aerated cells were fixed and stained as described in Sections 2.2.2 and 2.2.3.1.

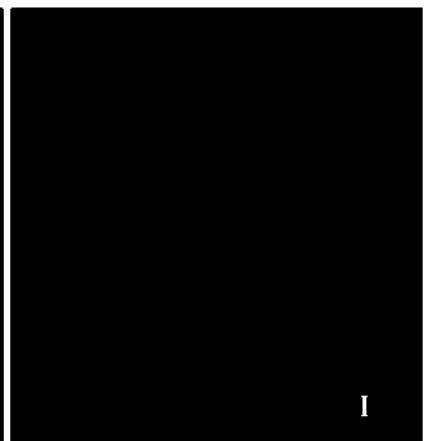
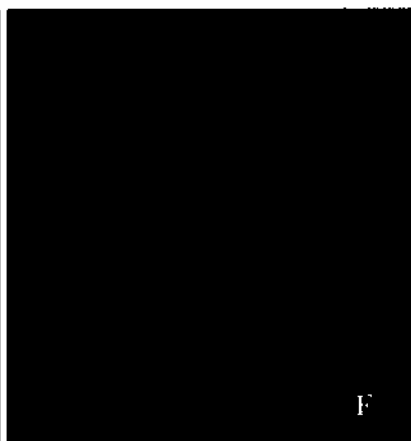
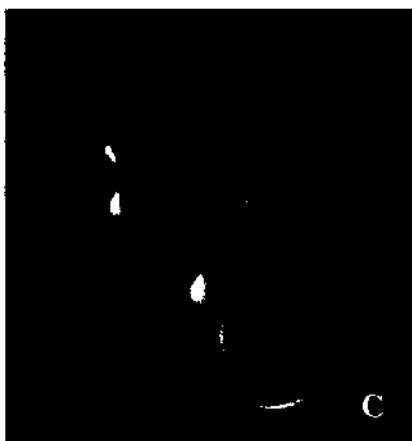
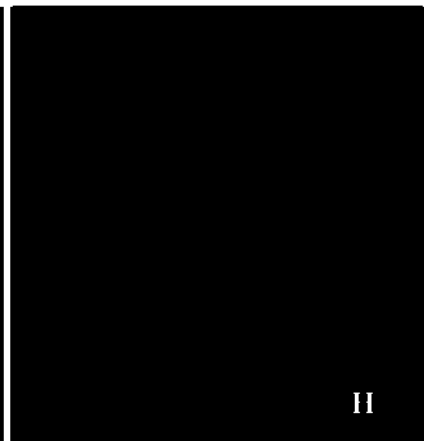
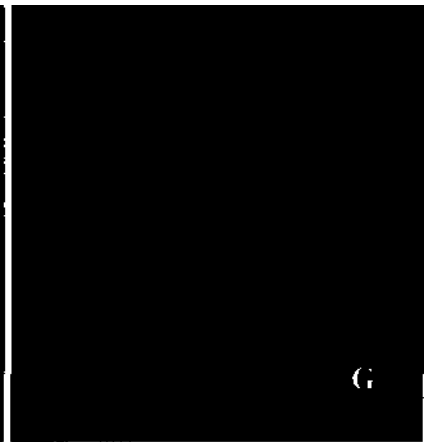
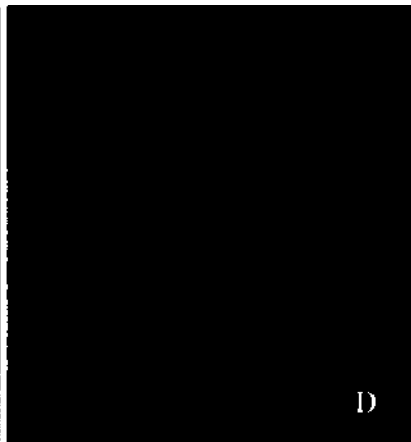
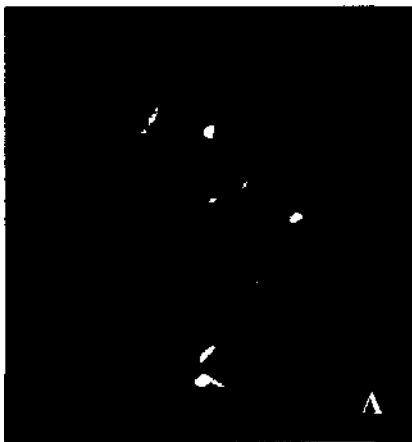
The confocal images show that prolonged aeration induced more CuZnSOD (Fig. 3.5A vs Fig. 3.3A) and catalase (Fig. 3.5B vs Fig. 3.3B) to localize at the membrane

**Figure 3.4. Confocal immunofluorescence and corresponding bright field images of CDB3, CuZnSOD, catalase, and GPx in fixed intact deaerated human RBCs.** A-C. Bright field image. D. CuZnSOD stained by rabbit polyclonal anti-human CuZnSOD and Cy5 conjugated anti-rabbit IgG. E. Catalase stained by sheep polyclonal anti-human catalase and Cy5 conjugated anti-sheep IgG. F. GPx stained by sheep anti-human GPx-1 and Cy5 conjugated anti-sheep IgG. G-I. CDB3 stained by mouse monoclonal anti-human CDB3 and Cy2 conjugated anti-mouse IgG. Filter settings were as follows: for Cy2, excitation 488 nm; emission 500-530 nm, and for Cy5, excitation 633 nm; emission 660-690 nm. Within 3 h of drawing blood, RBCs at 10% Ht in G-PBS buffer were deaerated under nitrogen gas at ambient temperature for 2 min then fixed as described in Section 2.2.5. Cells were stained for enzyme first and then for CDB3 as outlined in Section 2.2.3.2.

Bright field

Enzyme

Band 3

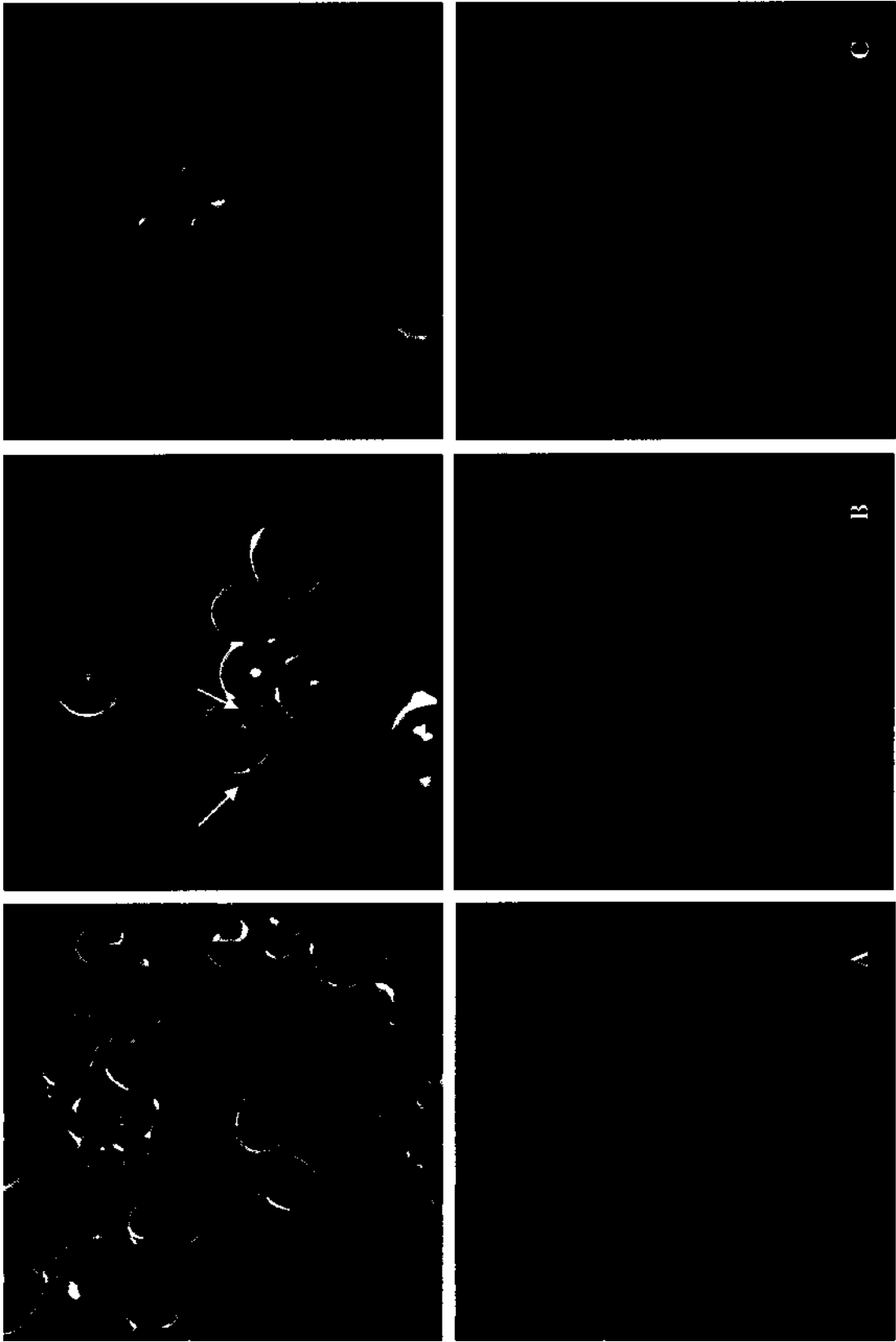


compared to their distribution in fresh RBCs exposed to air for < 5 min (Fig. 3.3). In contrast, GPx exhibited a similar amount of membrane staining under both conditions (Fig. 3.5C vs Fig. 3.3C). The cells retained their biconcave-disk shape after prolonged exposure to air as evidenced from their bright field images (Fig. 3.5, upper panels). Although both CuZnSOD and catalase exhibited increased membrane staining in aerated RBCs, their staining patterns are considerably different (Fig. 3.5A vs 3.5B). CuZnSOD immunofluorescence suggests that the protein aggregates around the center of the RBCs biconcave membrane whereas catalase staining shows a more even membrane distribution. Note the two bright spots at the membrane of a single RBC in the catalase image (Fig. 3.5B, lower panel). The bright field image revealed two small fragments attached to the cell at these sites (Fig. 3.5B, upper panel, at arrows). These fragments may correspond to autofluorescent particles such as dye-conjugated antibody bound to the cell surface.

### 3.5 Colocalization of CuZnSOD, catalase, and CDB3

An examination of their localization in aerated and deaerated RBCs revealed that CuZnSOD and catalase exhibited a similar response to O<sub>2</sub> variation (Fig. 3.3-3.5). For example, both enzymes showed membrane staining in aerated RBCs (Fig. 3.5). Thus, we next investigated colocalization of these proteins. Since CDB3 is considered to regulate several O<sub>2</sub>-dependent RBC functions by its interaction with cytoplasmic proteins (91, 97, 98), we tested whether CuZnSOD and catalase colocalize with CDB3. In a separate experiment from that in Figure 3.5, RBCs were exposed to room air for 1 h at ambient temperature, and then fixed and stained as described in Sections 2.2.2, 2.2.3.2 and 2.2.6. As seen before for aerated RBCs (Fig. 3.5), the images show that CuZnSOD aggregates

**Figure 3.5. Confocal immunofluorescence and corresponding bright field images of CuZnSOD, catalase, and GPx in fixed intact aerated human RBCs.** The bright field images are shown in the upper panels and the corresponding immunofluorescence images in the lower panels. A. CuZnSOD stained by rabbit polyclonal anti-human CuZnSOD and Cy2 conjugated anti-rabbit IgG. B. Catalase stained by sheep polyclonal anti-human catalase and Alexa conjugated anti-sheep IgG. C. GPx stained by sheep anti-human GPx-1 and Alexa 488 conjugated anti-sheep IgG. Filter settings for both Cy2 and Alexa 488 were as follows: excitation 488 nm; emission 500-530 nm. Within 3 h of drawing blood, RBCs at 10% Ht in G-PBS were exposed to room air for 1 h at ambient temperature. Cells were then stained as outlined in Section 2.2.3.1. The arrows on bright-field image B correspond to the two bright spots on the immunofluorescence image B.



CuZnSOD

Catalase

GPx-1

at the membrane, especially at the biconcave sites (Fig. 3.6A,I). Catalase exhibits punctate distribution at the membrane (Fig. 3.6E,J) while CDB3 is more evenly distributed (Fig. 3.6B,F). The overlay images in panel D reveals yellow spots at the cell surface implying colocalization of CuZnSOD and CDB3 at the membrane. The overlay images in panel H and L also reveal yellow spots at the membrane, indicating that catalase colocalized with both CDB3 and CuZnSOD. The bright-field images (Fig. 3.6C,G,K) confirmed that the aerated RBCs possessed normal shape as also seen in Figure 3.5.

### 3.6 Competition between anti-CuZnSOD and anti-CDB3

In Section 3.5, CuZnSOD and CDB 3 were shown to colocalize in aerated RBCs. If two proteins colocalize or their locations are very close, their antibodies would have to compete for binding within a limited space. Hence, antibody binding to one protein should hinder antibody binding to the second protein. Competition between anti-CuZnSOD and anti-CDB3 binding was performed to further confirm the results of the study in Section 3.5. RBCs were exposed to room air for 1 h, fixed and stained as described in Sections 2.2.2, 2.2.3.2, 2.2.3.3, and 2.2.6.

The images clearly reveal that the intensity of CuZnSOD staining is lower if anti-CDB3 was added first than when anti-CuZnSOD was added first (Fig. 3.7A vs 3.7B). In contrast, the intensity of CDB3 fluorescence is similar whether anti-CDB3 or anti-CuZnSOD were added first (Fig. 3.7C vs 3.7D). The decrease in CuZnSOD intensity upon first binding anti-CDB3 reveals that this antibody inhibits anti-CuZnSOD binding. However, the intensity of CDB3 is not noticeably affected due to the high

abundance of CDB3 relative to CuZnSOD. Thus, anti-CuZnSOD could only block a small fraction of anti-CDB3 binding.

**Figure 3.6. Colocalization of CuZnSOD, catalase, and CDB3 in fixed intact aerated human RBCs.** A. CuZnSOD stained by rabbit polyclonal anti-human CuZnSOD and Cy2 conjugated anti-rabbit IgG. B. CDB3 stained by mouse monoclonal anti-human CDB3 and Cy3 conjugated anti-mouse IgG. D. Overlay of image A and B (CuZnSOD and CDB3). E. Catalase stained by sheep polyclonal anti-human catalase and Cy3 conjugated anti-sheep IgG. F. CDB3 stained by mouse monoclonal anti-human CDB3 and Cy2 conjugated anti-mouse IgG. H. Overlay of image E and F (catalase and CDB3). I. CuZnSOD stained by rabbit polyclonal anti-human CuZnSOD and Cy2 conjugated anti-rabbit IgG. J. Catalase stained by sheep polyclonal anti-human catalase and Cy3 conjugated anti-sheep IgG. L. Overlay of image I and J (CuZnSOD and catalase). C,G,K. Bright-field images. Filter settings were as follows: for Cy2, excitation 488 nm; emission 500-530 nm; and for Cy3, excitation 543 nm; emission 560-620 nm. Within 3 h of drawing blood, RBCs at 10% Ht in G-PBS at ambient temperature were exposed to room air for 1 h. The cells were then stained as outlined in Section 2.2.3.2.

CuZnSOD Cy2

CDB3 Cy3

Bright field

Overlay of A & B

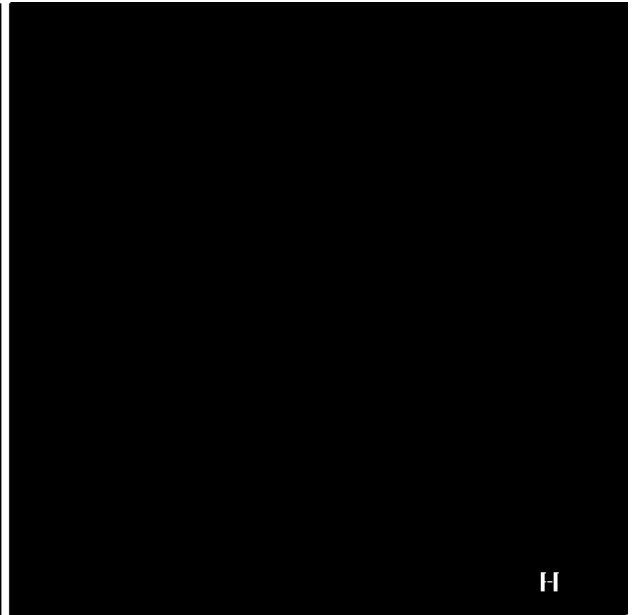


Catalase Cy3

CDB3 Cy2

Bright field

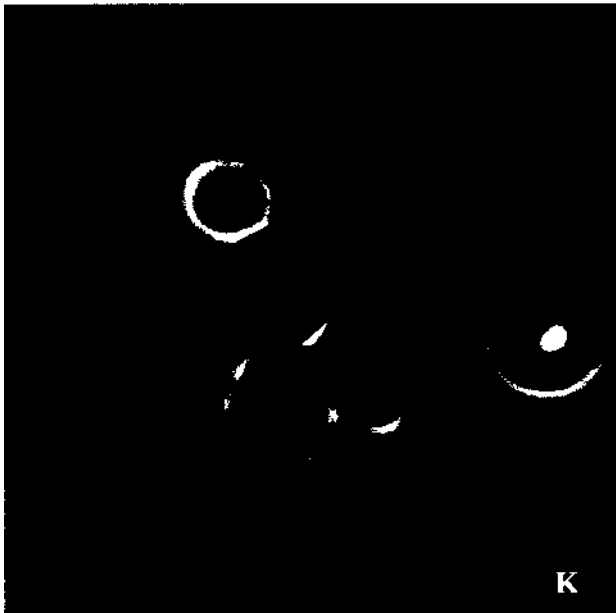
Overlay of E & F



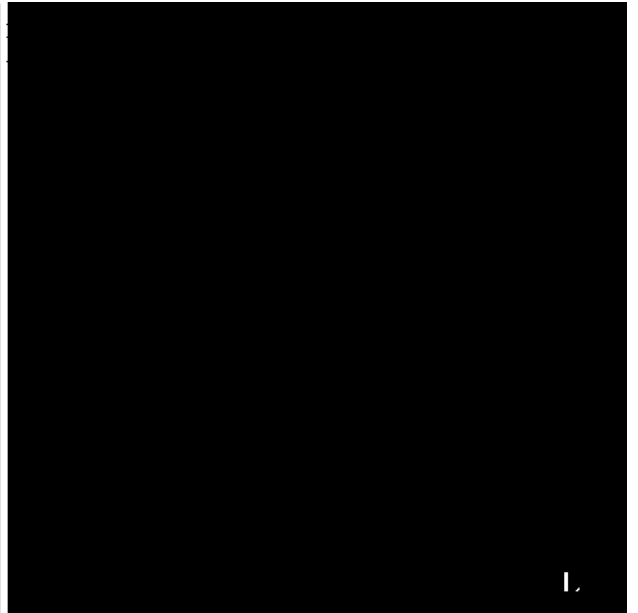
CuZnSOD Cy2

Catalase Cy3

Bright field



Overlay of I & J



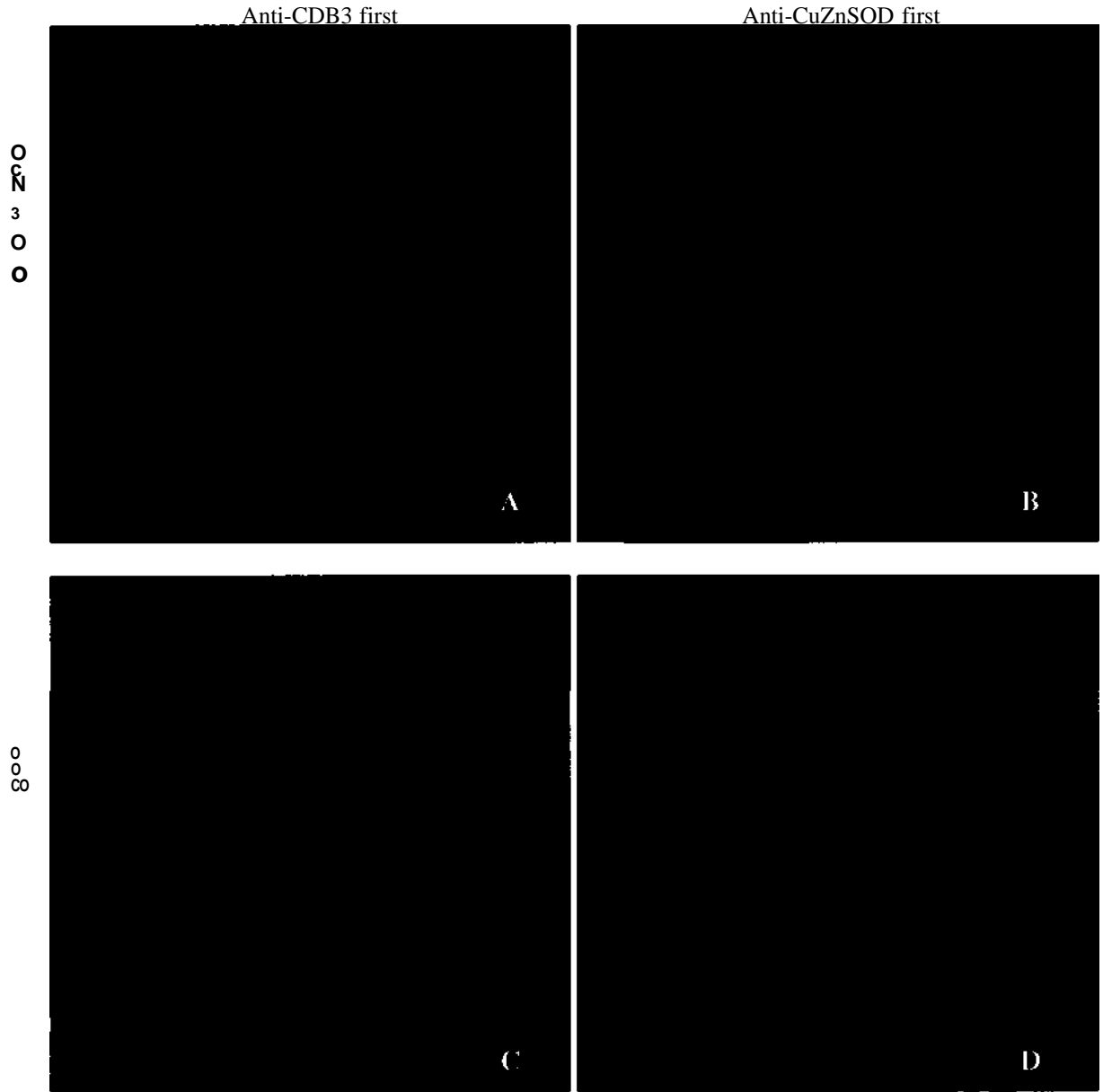


**Figure 3.7. Competition between anti-CuZnSOD and anti-CDB3 in fixed intact aerated human RBCs.** A,C. Anti-CDB3 was added first, then anti-CuZnSOD. B,D. Anti-CuZnSOD was added first, then anti-CDB3. A,B. CuZnSOD stained by rabbit polyclonal anti-human CuZnSOD and Cy2 conjugated anti-rabbit IgG. C,D. CDB3 stained by mouse monoclonal anti-human CDB3 and Cy2 conjugated anti-mouse IgG, Filter settings were as follows: for Cy2, excitation 488 nm; emission 500-530 nm, and for Cy3, excitation 543 nm; emission 560-620 nm. Within 3 h of drawing blood, RBCs at 10% Ht in G-PBS at ambient temperature were exposed to room air for 1 h. The cells were then stained as outlined in Section 2.2.3.2.



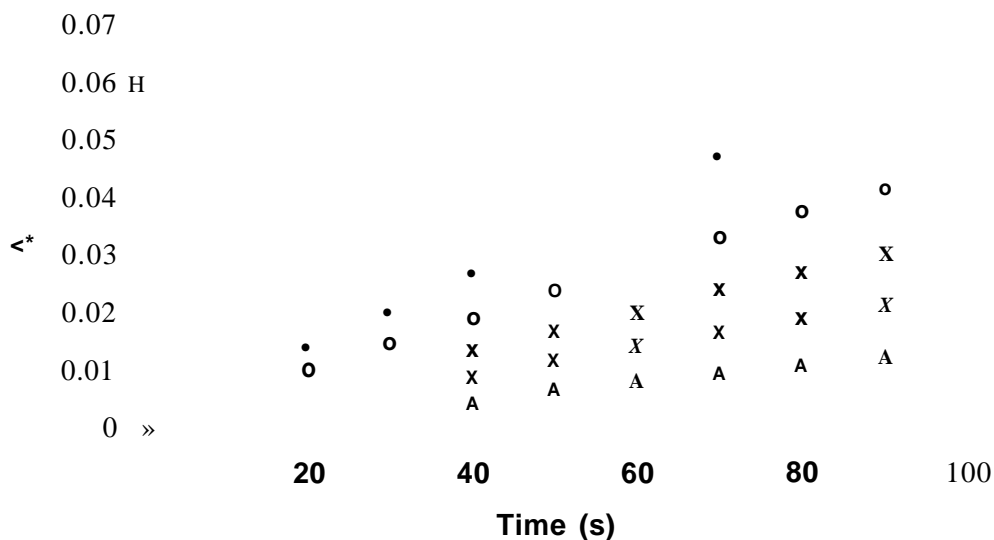


**Figure 3.8. HRP-catalyzed ARTS oxidation** by H<sub>2</sub>O<sub>2</sub>. The assay solution contained 0.15 nM HRP, 8.20 mM ABTS, and 0.82-9.84 uM H<sub>2</sub>O<sub>2</sub> in 1 mM sodium phosphate (pH 5.0) at ambient temperature. The reaction was initiated by the addition of H<sub>2</sub>O<sub>2</sub>, and ABTS oxidation was followed at 405 nm in a 1 -cm pathlength cuvette vs time. The data points correspond to the final [H<sub>2</sub>O<sub>2</sub>] as follows: A 0.82 uM, \* 2.05 uM, x 4.1 uM, o 6.56 uM, • 8.2 uM, • 9.84 uM.



**Figure 3.9. H<sub>2</sub>O<sub>2</sub> calibration plot.** Rates of ABTS oxidation (10<sup>4</sup>x AA<sub>405</sub>/s) observed in Figure 3.8 are plotted vs [H<sub>2</sub>O<sub>2</sub>]. See legend of Figure 3.8 for experimental details.  $y=5E-06x + 5E-05$ ,  $R^2=0.9966$ .

Rates of ABTS oxidation at different GOx concentrations were compared to the H<sub>2</sub>O<sub>2</sub> calibration plot (Fig. 3.9). To generate -10 uM H<sub>2</sub>O<sub>2</sub> per min (or -100 uM H<sub>2</sub>O<sub>2</sub> within 10 min) (Fig. 3.10), 1.22 units of GOx were required. To ensure that H<sub>2</sub>O<sub>2</sub> was generated at a constant rate over longer times, the H<sub>2</sub>O<sub>2</sub> concentration of the glucose/GOx solution was determined at different time points using the calibration plot in Figure 3.9. Figure 3.11 shows that H<sub>2</sub>O<sub>2</sub> was produced at a constant rate of 8 uM per min and reached a concentration of - 70 uM in 9 min. The effects of extracellular H<sub>2</sub>O<sub>2</sub> on protein localization within RBCs are discussed in Section 3.8.

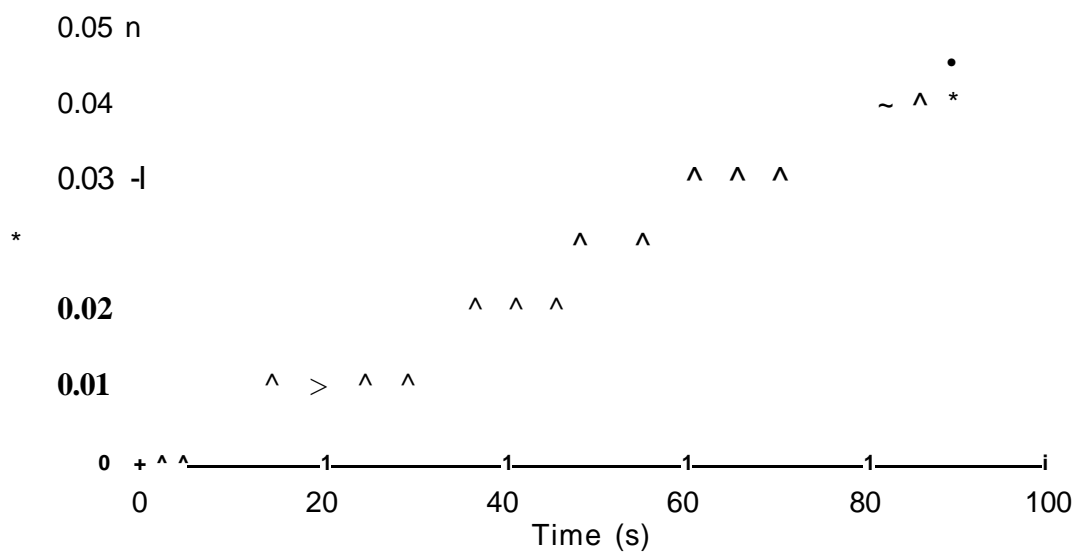


**Figure 3.10. H<sub>2</sub>O<sub>2</sub> generation by GOx-catalyzed oxidation of glucose.** GOx (1.22 units) in G-PBS (pH 7.4) containing 5 mM glucose at room temperature linearly generated H<sub>2</sub>O<sub>2</sub> ( $y= 5E-4x - 3E-4$ ,  $R_2=0.9977$ ) as determined by HRP (0.15 nM)-catalyzed ABTS (8.2 mM) oxidation by H<sub>2</sub>O<sub>2</sub>. GOx addition initiated the ABTS oxidation, which was followed spectrophotometrically at 405 nm in a 1-cm pathlength cuvette.

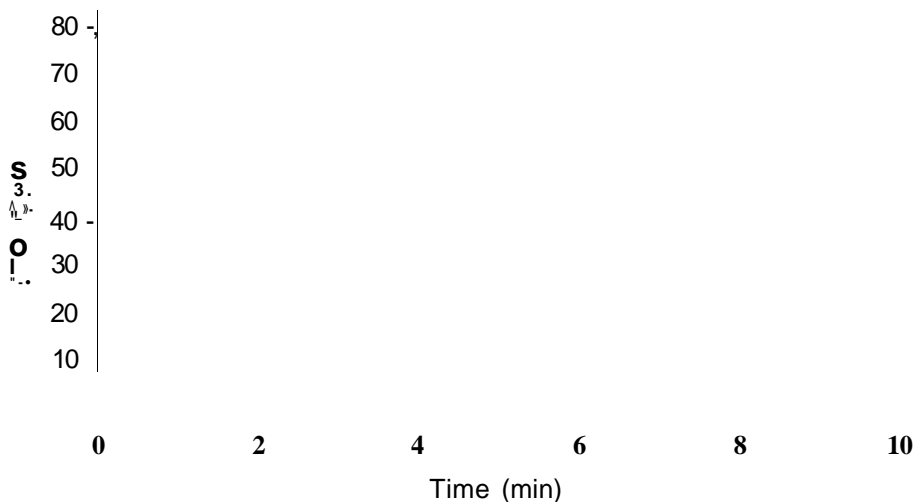


**Figure 3.11. H<sub>2</sub>O<sub>2</sub> production by GOx/glucose vs time.** The H<sub>2</sub>O<sub>2</sub> generated by 1.22 units GOx in 2 mL of G-PBS at room temperature over 9 min in a sealed 2-mL Eppendorf tube. Aliquots of 50  $\mu$ L GOx/glucose solution were added to the ABTS/H<sub>2</sub>O<sub>2</sub> assay buffer at 1.0, 3.5, 6.0, and 9.0 min. ABTS oxidation was followed at 405 nm in a 1-cm pathlength cuvette (See legend to Figure 3.8 for ABTS/H<sub>2</sub>O<sub>2</sub> assay conditions).

### 3.7.2 Superoxide generation

Both external generation of O<sub>2</sub><sup>-</sup> by activated leukocytes, and internal generation by Hb autoxidation can affect RBCs (P). Superoxide possesses a negative charge so it can not freely penetrate the RBC membrane (P). Since the goal in the current work is to mimic O<sub>2</sub><sup>-</sup> production by Hb autoxidation, PMS was used to generate O<sub>2</sub><sup>-</sup> within the RBC. PMS easily enters RBCs (100) where it catalyzes the direct transfer of an electron from NAD(P)H to O<sub>2</sub> to produce O<sub>2</sub><sup>-</sup> (Eq 2.3) (101). Generation of O<sub>2</sub><sup>-</sup> can be monitored spectroscopically by following its reaction with NBT, which leads to an absorbance change at 560 nm (Eq 2.2).

O<sub>2</sub><sup>-</sup> production by different concentrations of PMS was investigated in solutions of NBT and NADPH in PBS (pH 7.4). Figure 3.12 shows that the absorbance at 560 nm

due to NBT reduction by  $O_2^-$  (Eq 2.2) increased after PMS addition, indicating that PMS reacted with NADPH to generate  $O_2^-$  (Eq 2.2). From Figure 3.13, it is observed that absorbance increased linearly over  $\sim 0.7$  min and the initial rate increased with the PMS concentration but the final absorbance ( $A_{560} \sim 0.9$ , Fig. 3.12) was the same as expected since NADPH was the limiting reagent. Figure 3.14 shows that both the rate of  $O_2^-$  generation and its final concentration increased with the NADPH concentration, supporting the NADPH dependence of  $O_2^-$  production. These results are consistent with PMS catalysis of  $O_2^-$  generation using NADPH as a reducing agent (Eq 2.2 and 2.3).

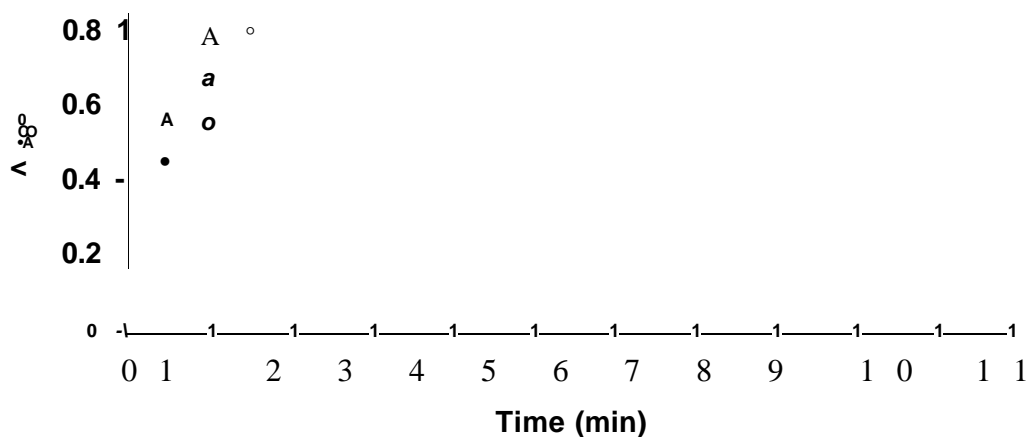


**Figure 3.12. PMS-catalyzed superoxide generation.** Superoxide was generated by 1.6  $\mu$ M ( $\circ$ ), 4.7  $\mu$ M ( $\bullet$ ), or 7.9  $\mu$ M (A) PMS, and 46.3  $\mu$ M NADPH in 2 mL of PBS in an open 1-cm cuvette without stirring. The reaction was initiated by PMS addition and monitored spectrophotometrically by NBT (302  $\mu$ M) reduction at 560 nm in the 1-cm cuvette at ambient temperature.

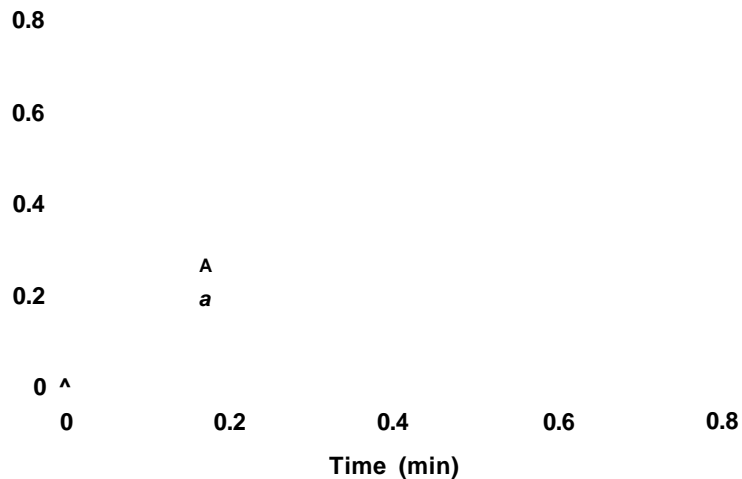


**Figure 3.13. Initial rates of superoxide generation by PMS/NADPH in 2 mL of PBS in an open 1-cm cuvette at room temperature.** The absorbance changes (data points) over the first 0.7 min are plotted using data from Figure 3.12.

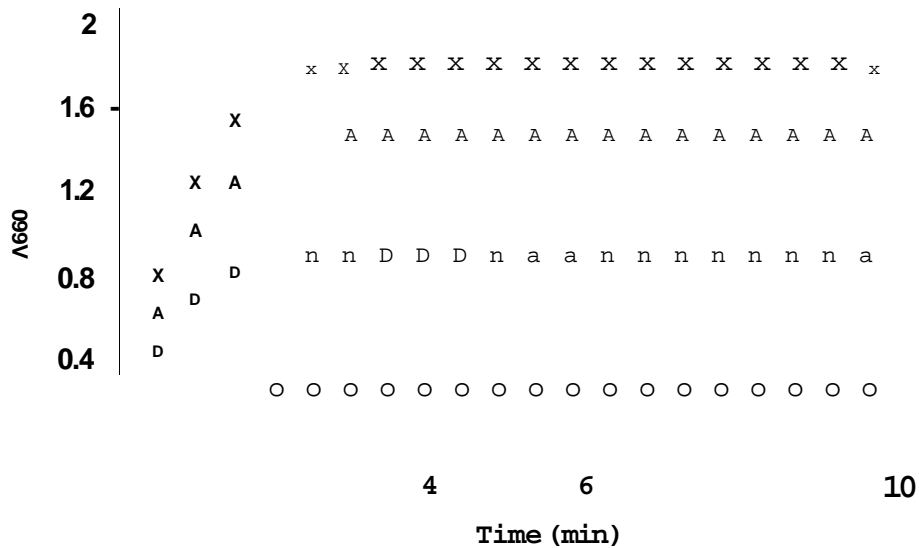


**Figure 3.14. NADPH concentration dependence of superoxide generation.** Superoxide was generated by 4.7 uM PMS and 23 uM (○), 46.3 uM (●), 70 uM (▲) or 85 uM (×) NADPH in 2 mL of PBS in an open 1-cm cuvette at room temperature without stirring. The reaction was initiated by PMS addition and monitored spectrophotometrically by NBT (302 uM) reduction at 560 nm in the 1-cm cuvette at ambient temperature.

The reduction of NBT by superoxide should be inhibited by SOD activity. Figure 3.15 shows that in the presence of 60 nM CuZnSOD, the absorbance increase is almost half that in the absence of the enzyme. The reduction of NBT by  $O_2^-$  is inhibited by CuZnSOD specifically and efficiently. Also CuZnSOD has negligible absorbance at the concentration used and thus does not interfere with the absorbance measurements at 560 nm.

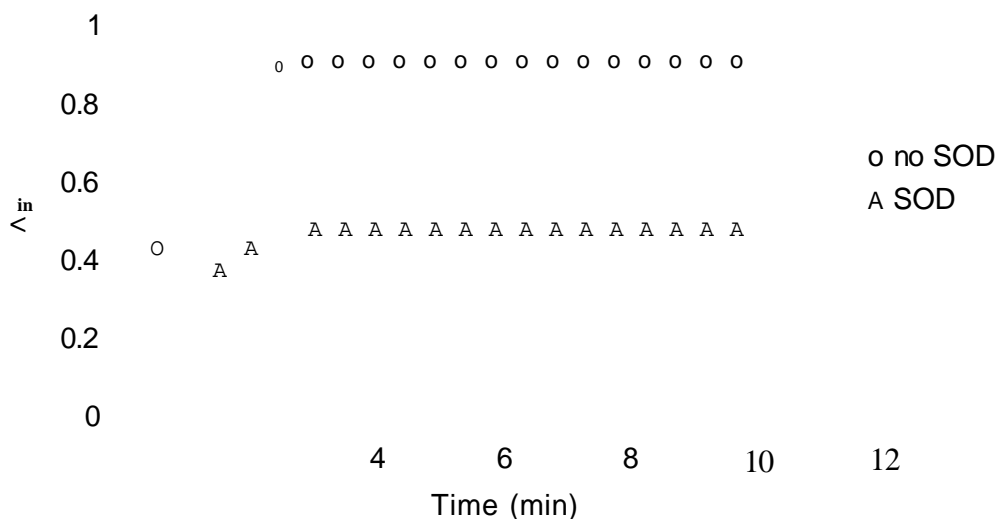


**Figure 3.15. CuZnSOD inhibits superoxide generated by NADPH/PMS.** Superoxide was generated by 4.7  $\mu$ M PMS and 46.3  $\mu$ M NADPH in 2 mL of PBS in an open 1-cm cuvette without stirring at room temperature in the absence (O) and presence (A) of 60 nM CuZnSOD. The reaction was initiated by PMS addition and monitored spectrophotometrically by NBT (302  $\mu$ M) reduction at 560 nm in the 1-cm cuvette at ambient temperature.

### 3.8 Localization of CuZnSOD, catalase, GPx, and GSH in fixed human RBCs under an exogenous $H_2O_2$ flux

CuZnSOD, catalase, GPx, and GSH play a major role in the protection of RBCs from oxidative stress. The localization of these enzymes in response to exogenous  $H_2O_2$

was first examined. Washed RBCs at 10% Ht in G-PBS were exposed to an 8  $\mu\text{M}/\text{min}$   $\text{H}_2\text{O}_2$  flux (Section 3.7.1). The cells were incubated in the same glucose buffer both without GOx and with 35 nM catalase as controls. In the absence of GOx, RBCs were not exposed to exogenous  $\text{f}^{\text{C}}$  while with exogenous catalase present, RBCs were exposed to decreased  $\text{H}_2\text{O}_2$  flux since catalase decomposes  $\text{H}_2\text{O}_2$  efficiently (Section 1.6.1).

The confocal images in Figure 3.16 show that the RBC catalase staining patterns (A-C) were similar under all three conditions. Catalase was partially membrane stained and partially cytosol stained in G-PBS with or without exogenous catalase and GOx. In contrast, GPx exhibited staining patterns that were different for the negative controls and the test sample. In glucose only (D) and glucose with GOx plus catalase (F), GPx was partially membrane stained and partially cytosol stained. However, GPx was predominantly membrane stained in glucose plus GOx (E). The staining patterns of CuZnSOD (Fig. 3.16G-I) and GSH (Fig. 3.16J-L) were the same, and showed that these species are evenly distributed throughout the cytosol under all three working conditions.

### 3.9 Localization of CuZnSOD, catalase, GPx, and GSH in fixed human RBCs under intracellular $\text{O}_2^-$ generation

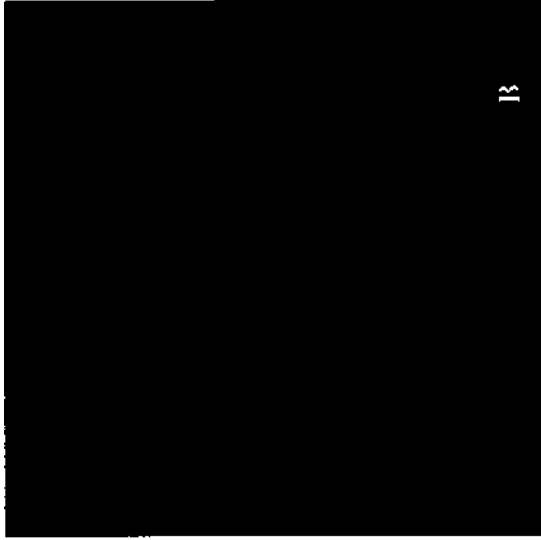
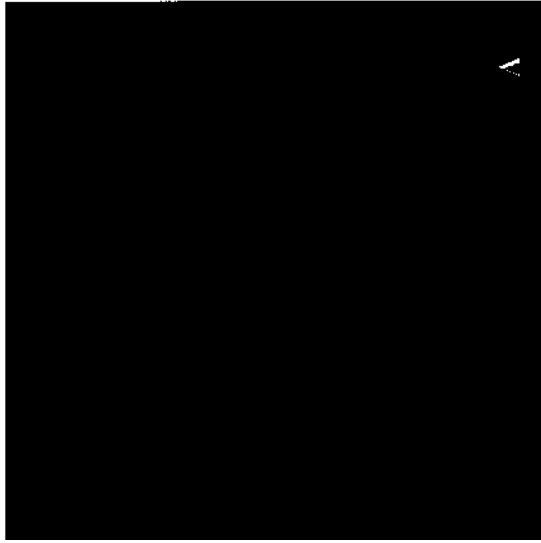
The main source of  $\text{O}_2^-$  inside RBCs is the autoxidation of Hb (25). The response of CuZnSOD, catalase, GPx, and GSH to additional superoxide generated intracellularly by PMS was examined. Washed RBCs were incubated in G-PBS with 5  $\mu\text{M}$  PMS for 10 min (Section 3.7.2). Cells were also incubated in the same buffer without PMS as a negative control.

**Figure 3.16. Confocal immunofluorescence images of CuZnSOD, catalase, GPx, and GSH in fixed intact human RBCs under H<sub>2</sub>O<sub>2</sub> flux.** A-C. Catalase stained by sheep polyclonal anti-human catalase and Alexa conjugated anti-sheep IgG. D-E. GPx stained by sheep anti-human GPx-1 and Alexa conjugated anti-sheep IgG. G-H. CuZnSOD stained by rabbit polyclonal anti-human CuZnSOD and Cy2 conjugated anti-rabbit IgG. J-K. GSH stained by rabbit polyclonal anti-human GSH and Cy2 conjugated anti-rabbit IgG. Within 3 h of drawing blood, RBCs at 10% Ht in G-PBS at ambient temperature were exposed to 8  $\mu$ M/min exogenous H<sub>2</sub>O<sub>2</sub> for 10 min. The cells were then stained as outlined in Section 2.2.3.1. Left column, control (5 mM glucose only). Middle column, 5 mM glucose plus 1.22 units GOx. Right column, 5 mM glucose plus 1.22 units GOx and 35 nM catalase. Filter settings were as follows: for both Cy2 and Alexa, excitation 488 nm; emission 500-530 nm.

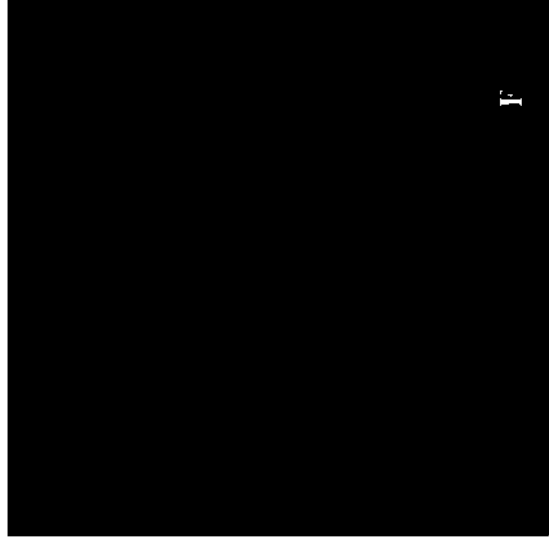
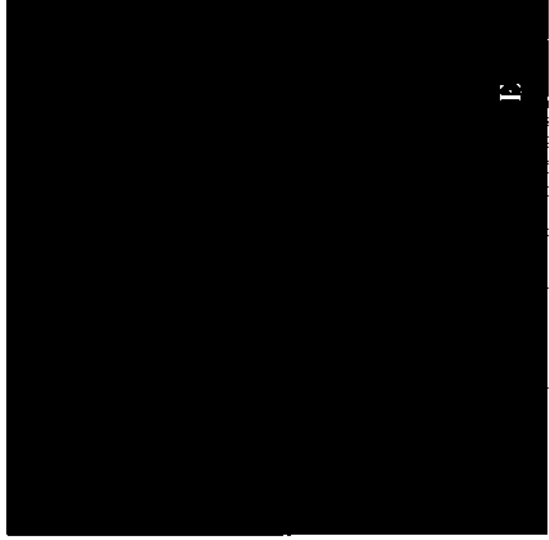
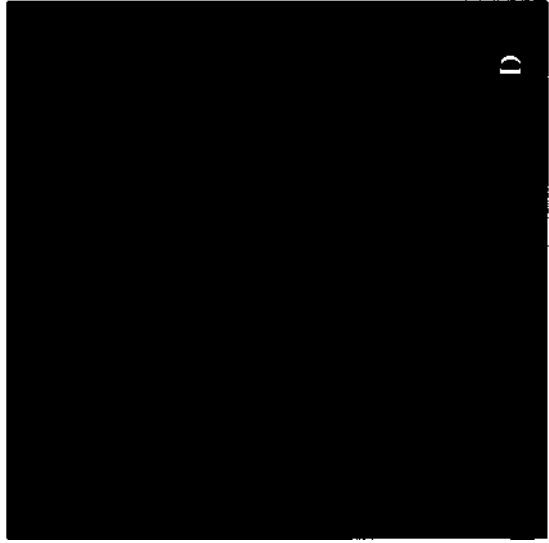
Control (glucose only)

Glucose/GOx

Glucose/GOx/catalase



n

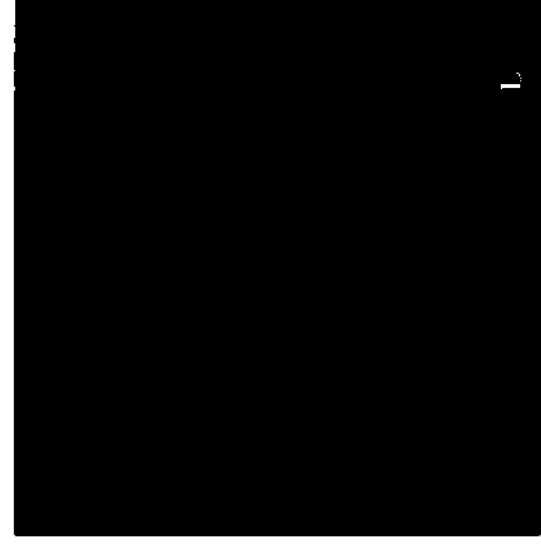
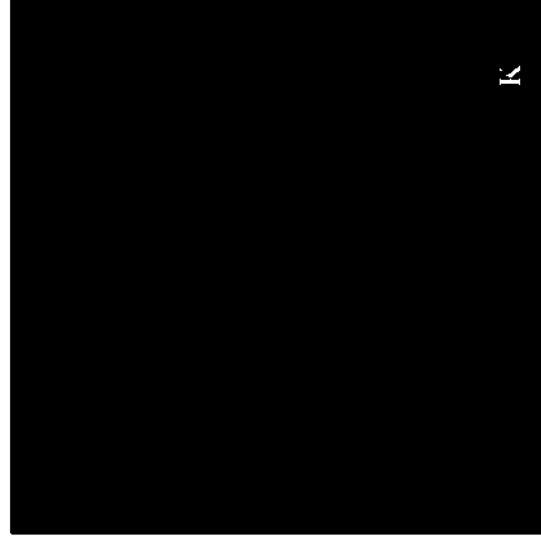
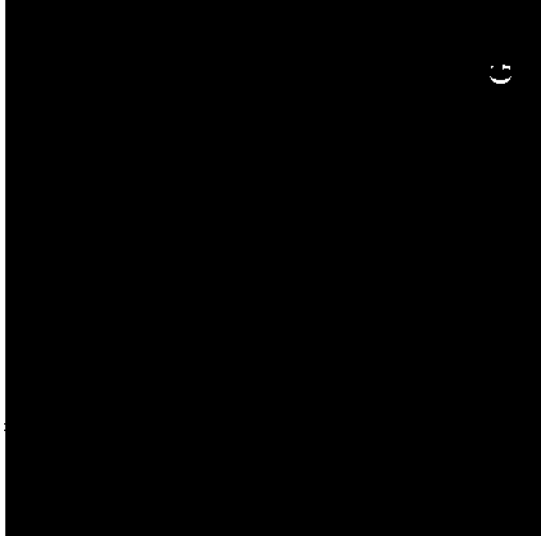


o

Control (glucose only)

Glucose/GOx

Glucose/GOx/catalase



n N 3 0 0

o ca

The confocal images in Figure 3.17 show that the staining patterns of catalase are similar in both the negative control (A) and test sample (B). Most of the catalase is distributed in the cytosol with less localized at the membrane. The staining patterns of GPx are different for the negative control (C) and test sample (D). In the negative control, GPx was partially membrane stained and partially cytosol stained, but GPx was predominantly membrane stained in the test sample. The staining patterns of CuZnSOD (Fig. 3.17E,F) and GSH (Fig. 3.17G,H) showed an even cytosolic distribution in the presence and absence of PMS.

### 3.10 ICP-MS determination of RBC Cu and Fe concentrations

The concentration of copper and iron detected by ICP-MS is summarized in Table 3.1. The [Fe]/[Cu] ratio is ~2000 based on the ICP-MS results. Each human RBC contains ~270,000,000 copies of Hb (102), the most abundant protein (5 mM) in these cells (9). The concentration of other heme proteins in human RBCs are in the micromolar range; for example, 2.6 uM catalase has been reported (33). Assuming that all sources of Fe detected by ICP-MS come from Hb, we estimate the CuZnSOD copy number to be ~270,000 from the ICP-MS data. This calculation took into consideration that there are four hemes per Hb tetramer and two copper ions per CuZnSOD dimer. We also assumed that all the copper in the RBC was from CuZnSOD.

Table 3.1: ICP-MS analysis of Cu and Fe concentrations in human RBCs

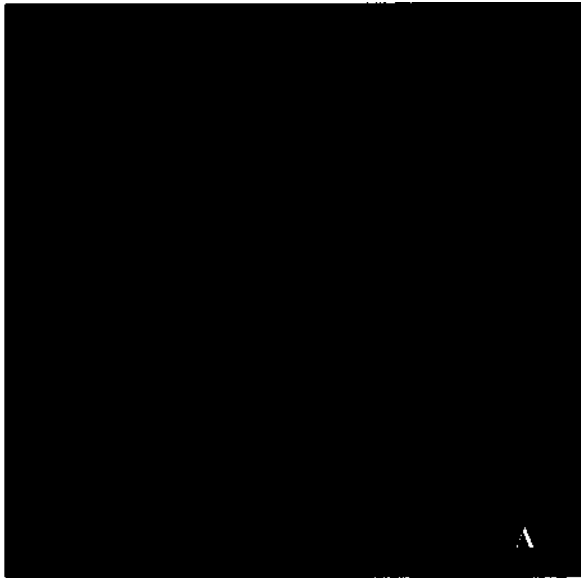
	Cu (uM)	Fe (mM)
Trial 1	12.64	23.59
Trial 2	14.86	25.49
Average	13.75	24.54

**Figure 3.17. Confocal immunofluorescence images of CuZnSOD, catalase, GPx, and GSH in fixed intact human RBCs under intracellular O<sub>2</sub>- generation.** A-B. Catalase stained by sheep polyclonal anti-human catalase and Alexa conjugated anti-sheep IgG. C-D. GPx stained by sheep anti-human GPx-1 and Alexa conjugated anti-sheep IgG. E-F. CuZnSOD stained by rabbit polyclonal anti-human CuZnSOD and cy2 conjugated anti-rabbit IgG. G-H. GSH stained by rabbit polyclonal anti-human GSH and cy2 conjugated anti-rabbit IgG. Within 3 h of drawing blood, RBCs at 10% Ht in G-PBS at ambient temperature were exposed to intracellular O<sub>2</sub> generated by 5 uM PMS for 10 min. The cells were then stained as outlined in Section 2.2.3.1. Left column, G-PBS only. Right column, G-PBS plus 5 uM PMS. Filter settings were as follows: for both cy2 and Alexa, excitation window, 488 nm; emission window, 500-530 nm.

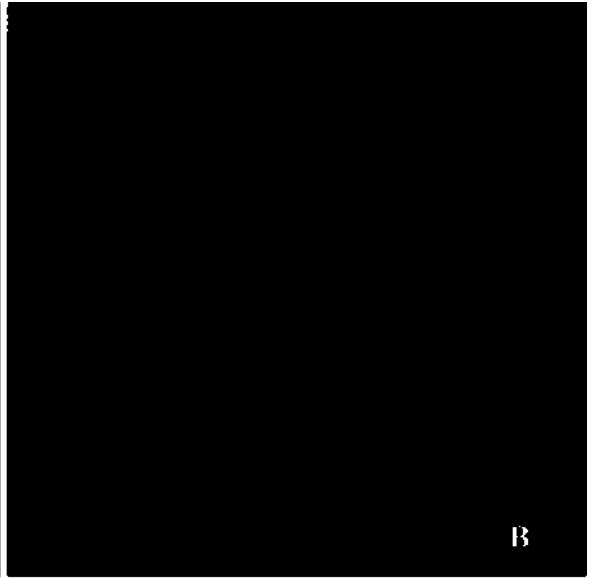
NoPMS

PMS

Catalase

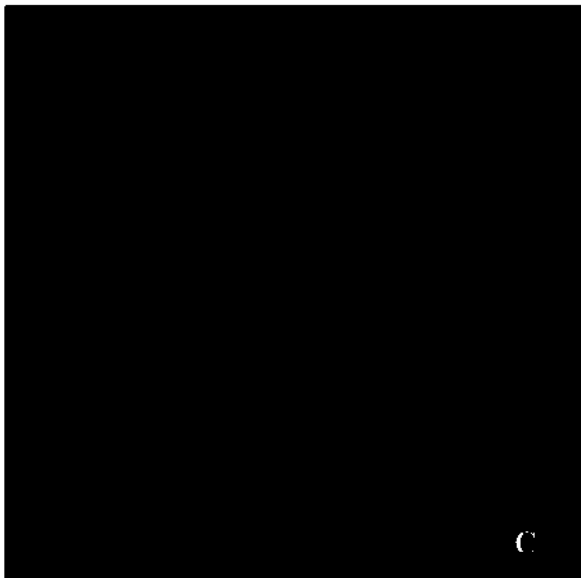


A

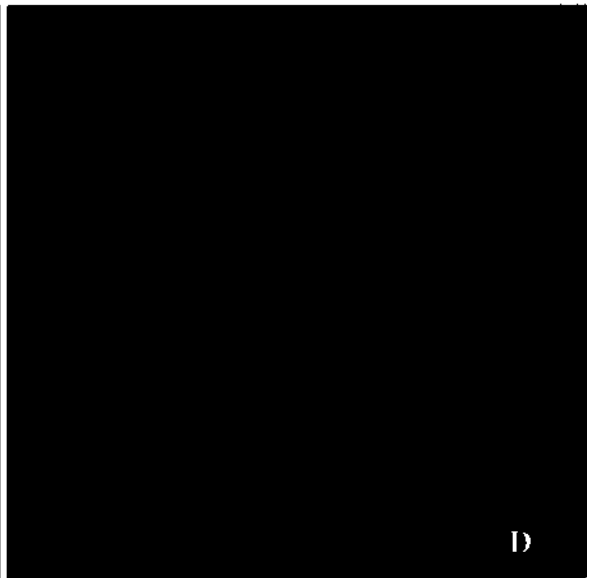


B

GPx



C

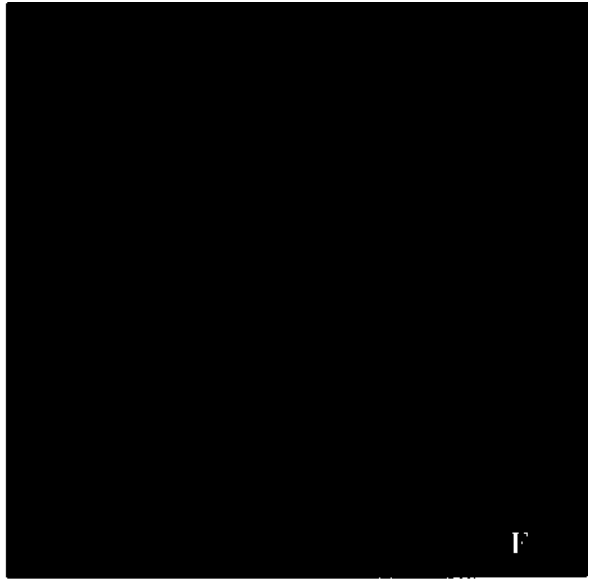
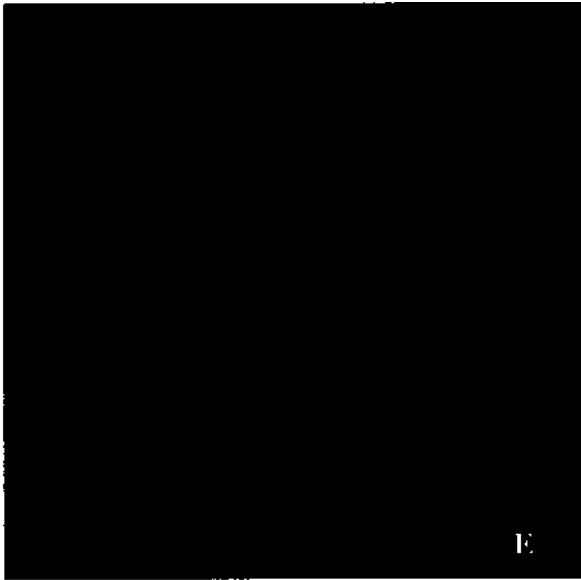


D

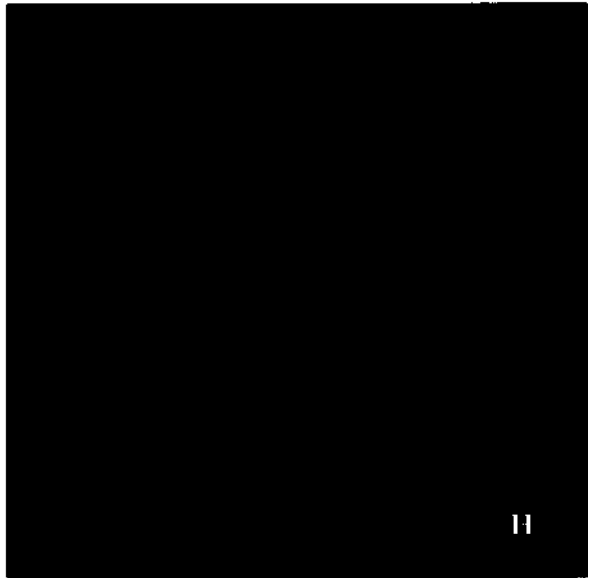
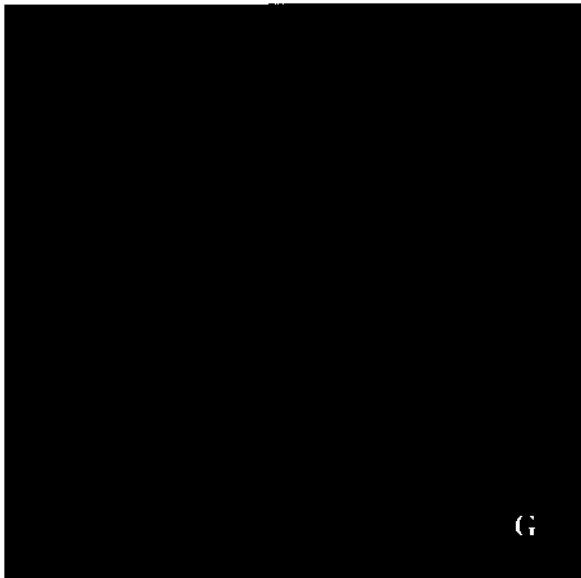
NoPMS

PMS

CuZnSOD



GSH



## Chapter 4: Discussion

### 4.1 Evaluation of methods

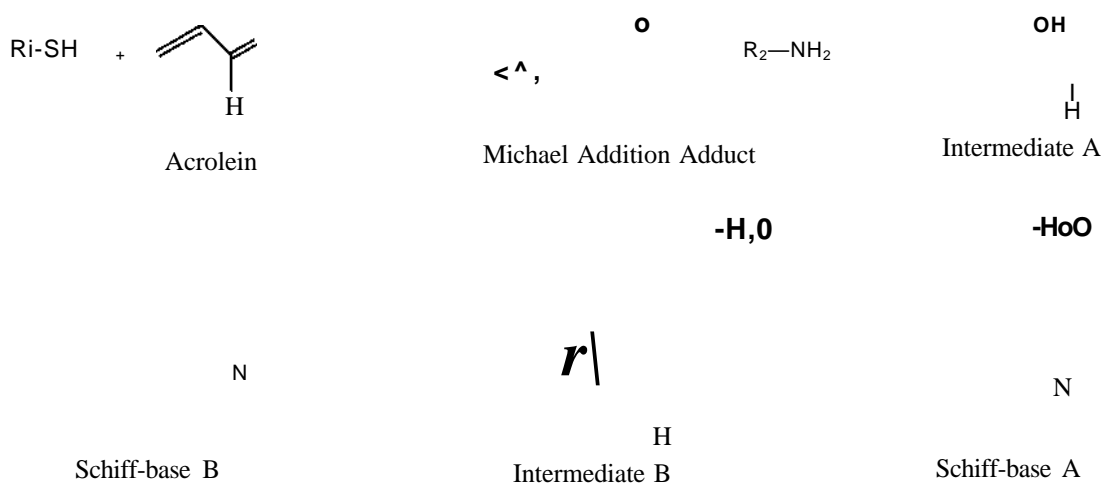
Determining subcellular localization is important for understanding protein function as proteins must migrate to the appropriate location to perform their desired function. Localization of the antioxidant enzymes, CuZnSOD, catalase, GPx-1 as well as GSH in human RBC was studied to determine their responses under physiological and oxidative-stress conditions. Proteins are too small to visualize directly under the microscope, so an immunofluorescence technique was adopted in this project. Antibodies are an important tool for detecting both the presence and the subcellular localization of an antigen. Since antibodies can not freely penetrate cell membranes, the first step is to fix and permeabilize the cells. This ensures free access of the antibody to its immobilized antigen (103).

Fixation arrests biological activity and stabilizes cellular components with minimal alteration of conformational and spatial relationships between the cellular constituents (104). If cells are not fixed within 1 h after washing, considerable autolysis would be noticed in most samples. Fixation is a critical step in ensuring accuracy of detection protocols and in determining the subsequent success or failure of a given experiment. An ideal fixative maintains the original *in vivo* distribution of the antigen without diffusion or rearrangement. Ideally, cell morphology should be conserved, the antigen of interest should remain accessible to the probe, and the fixation should cause negligible denaturation of the antigen. Perfect fixation would immobilize the antigen to minimize post-fixation changes. At the same time it should retain cellular and subcellular structure while permitting free access of antibodies to all subcellular compartments (103).

Both chemical and physical fixation methods are used, but chemical fixation is most commonly employed (104). A broad range of chemical fixatives are available, and can be divided into two classes: organic solvents and crosslinking reagents. Organic solvents such as alcohols and acetone remove lipids and water from the cells, while precipitating the proteins. They could alter the localization of some antigens (103). Crosslinking reagents, such as formaldehyde, form intermolecular bridges through free amino groups, creating a network of linked antigens (103). Since crosslinkers preserve cell structure better than organic solvents, the former were used here to examine protein localization.

Several considerations should be taken into account when selecting a fixative. The speed of penetration of the fixative is the most important consideration because the speed determines the success of the procedure. Smaller fixative molecules penetrate more rapidly than larger ones. There is a variety of small fixatives, such as acrolein, formaldehyde, and glutaraldehyde. Acrolein and formaldehyde penetrate more rapidly than glutaraldehyde (104). The former was selected for human RBC fixation because formaldehyde would have been washed out when rinsed with an aqueous solution (103). Acrolein reacts with protein side chains in the cell (Scheme 4.1) (105) after which the non-reacted fixative is washed out with rinsing buffer. Acrolein optimally fixes RBCs within 5 min under the experimental conditions adopted here (90). Different fixation times (3 min, 10 min) were also tested here. As reported (103), 3-min fixation of the sample led to altered cell morphology, whereas 10-min fixation led to high nonspecific background signals. Incubation in rinsing buffer, which contained 0.1 M glycine, for 30 min after permeabilization was also important because the glycine scavenged any unreacted acrolein. In the absence of this step, a strong background signal was detected

even when fixation lasted only 5 min. Acrolein, the simplest unsaturated aldehyde, is also subject to polymerization to an insoluble, crosslinked solid. This is catalyzed by light and air at room temperature (106), so to minimize polymerization when exposed to air, diluted acrolein needs to be freshly prepared. If the acrolein stock becomes yellow or the pH drops below 3.5, it should be discarded (104). Intermediate A and Schiff-base A in Scheme 4.1 correspond to the forms that give rise to the protein crosslinks expected after fixation with acrolein.



**Scheme 4.1. Reaction of acrolein with proteins** (Adapted from (105)).

Crosslinkers maintain the spatial relationships within cells, but may diminish the antigenicity of some cell components (103). Assessing how fixation affects the distribution of proteins is necessary before examining target proteins (88). The monoclonal anti-CDB3 antibody used in these studies specifically recognizes an epitope within residues 1-136 of CDB3 (107), which contains 403 residues (92). The membrane pattern of CDB3 staining in intact RBCs (Fig. 3.2) indicated that this antibody could penetrate through the membrane after cell fixing and permeabilizing. Also, the uniform Hb staining with a polyclonal antibody (Fig. 3.2) demonstrated that the highly dense

macromolecular network formed by crosslinked Hb after chemical fixation does not restrict access of the antibody to the cell interior. Therefore, the staining patterns observed for the target proteins of interest here should reflect their actual localization as assumed previously for the enzymes involved in glycolysis (90).

A buffering system is used to maintain the pH of the cells near physiological levels during fixation and to maintain near-isotonic conditions. The tonicity of a solution can be adjusted by adding an electrolyte (sodium chloride) or a nonelectrolyte (sucrose). The buffer (G-PBS, Section 2.2.1) used to preserve RBCs during preparation contains 5 mM glucose (108) as glucose is present at ~ 5 mM in plasma. Glucose is the only sugar used in RBC anaerobic glycolysis. It tends to decrease the rate of fixative penetration into the cells and it also increases the extraction of cellular components (104). Thus, RBCs were fixed in acrolein diluted into PBS instead of G-PBS.

Following fixation by crosslinking, the plasma membrane is permeabilized to allow entry of impermeable species. Permeabilization is required for immunofluorescence detection of intracellular and transmembrane membrane proteins because it allows the antibody to enter the cell (103). The target proteins, Hb, CuZnSOD, catalase, and GPx-1, as well as the GPx substrate (GSH) are localized in the cytosol, while CDB3 is at the cytosolic face of the membrane. Thus, we permeabilized RBCs before antibody staining. Detergents are used to increase permeability and organic solvents to extract lipids from the plasma membrane (103). There is a wide variety of available detergents which differ in their efficiency in extracting lipids from membranes. Triton X-100 is the most commonly used permeabilization agent for immunofluorescence

staining as it efficiently solubilises phospholipid membranes without altering protein-protein interactions (103).

The last step involves incubation of the cell preparation with the primary antibody. Unbound antibody is removed by washing, and the bound antibody is detected indirectly using a fluorochrome-labelled secondary antibody. Selection of an appropriate primary antibody is an important step in the protocol. Monoclonal antibodies recognize only one epitope and have weaker avidity relative to polyclonal antibodies, which recognize different epitopes on their target protein. As some antigenic sites on the protein may be destroyed or masked during fixation, loss of one or two epitope sites on the protein may not be critical when working with polyclonal antibodies, but may be of crucial importance with monoclonal antibodies. Partial masking or destruction of a particular antigen recognized by a monoclonal antibody could result in misleading immunofluorescence data.

Band 3 is the major erythrocyte membrane protein with  $1.2 \times 10^6$  copies per RBC (91). Its cytoplasmic domain (CDB3) is the binding site of cytoskeletal proteins (ankyrin, protein 4.1, protein 4.2), glycolytic enzymes (aldolase, GAPDH, phosphofructokinase), deoxyHb, Hb denaturation products (hemichromes), and the protein tyrosine kinase (p72<sup>Syk</sup>). Each of these interactions appears to be of importance for the structure and function of RBCs (97). A monoclonal anti-CDB3 antibody was used to specifically recognize CDB3 and not the transmembrane domain, which might have been recognized by a polyclonal antibody. Compared with band 3, CuZnSOD, catalase, and GPx-1 have relatively low copy number ( $< 3 \times 10^5$ ), so polyclonal antibodies were selected as the primary antibodies for these proteins. Although Hb has a high copy number ( $2.7 \times 10^8$ ),

we used polyclonal anti-Hb antibodies for its detection because the Hb epitope is irrelevant here, so monoclonal and polyclonal antibodies would accomplish the same task.

The secondary antibodies used to label the target proteins were attached to fluorescent probes. These probes are more environmentally friendly than radioactive labels and are highly selective. Fluorescent probes are grouped according to their excitation and emission characteristics, as well as their chemical and biological properties. Based on excitation wavelength, the common commercial fluorescent probes are divided into seven groups, excited by laser lines at 351 nm, 488 nm, 514 nm, 543 nm, 568 nm, 633 nm, and 647 nm, which correspond to the lines available with confocal microscopes. The laser lines available for this study were 488 nm, 543 nm, and 633 nm, so the selection of fluorescent probes was limited to those that could be excited by these laser lines.

There is a variety of green fluorescence dyes including FITC, Cy2, and Alexa 488 (Fig. 4.1), which were selected here. Fluorescein isothiocyanate (FITC), a derivative of fluorescein, has an excitation maximum at 494 nm, which is close to the 488-nm line of the argon laser. Cy2, a cyanine dye, absorbs at 492 nm; Alexa 488, a sulfonated compound, has an excitation maximum at 488 nm. These probes possess the advantages of relatively high molar absorptivity ( $\epsilon$  68,000-150,000  $M^{-1}cm^{-1}$ ), excellent fluorescence quantum yields ( $\phi=0.7-0.85$ ), and good solubility in water. They also possess distinct characteristics including variable photostability, brightness, and a tendency to self-quench. FITC has a relatively high rate of photobleaching compared to Cy2 and Alexa 488, and a greater tendency to self-quench (109). In fact, photobleaching limits FITC

sensitivity, which is undesirable for the localization of low abundance proteins (109). Cy2 and Alexa 488 can be visualized longer and brighter than FITC, so these dyes are used to detect target proteins when a strong signal is needed (110). In fact, Alexa 488 is the brightest of all dyes that absorb at 488 nm (110).

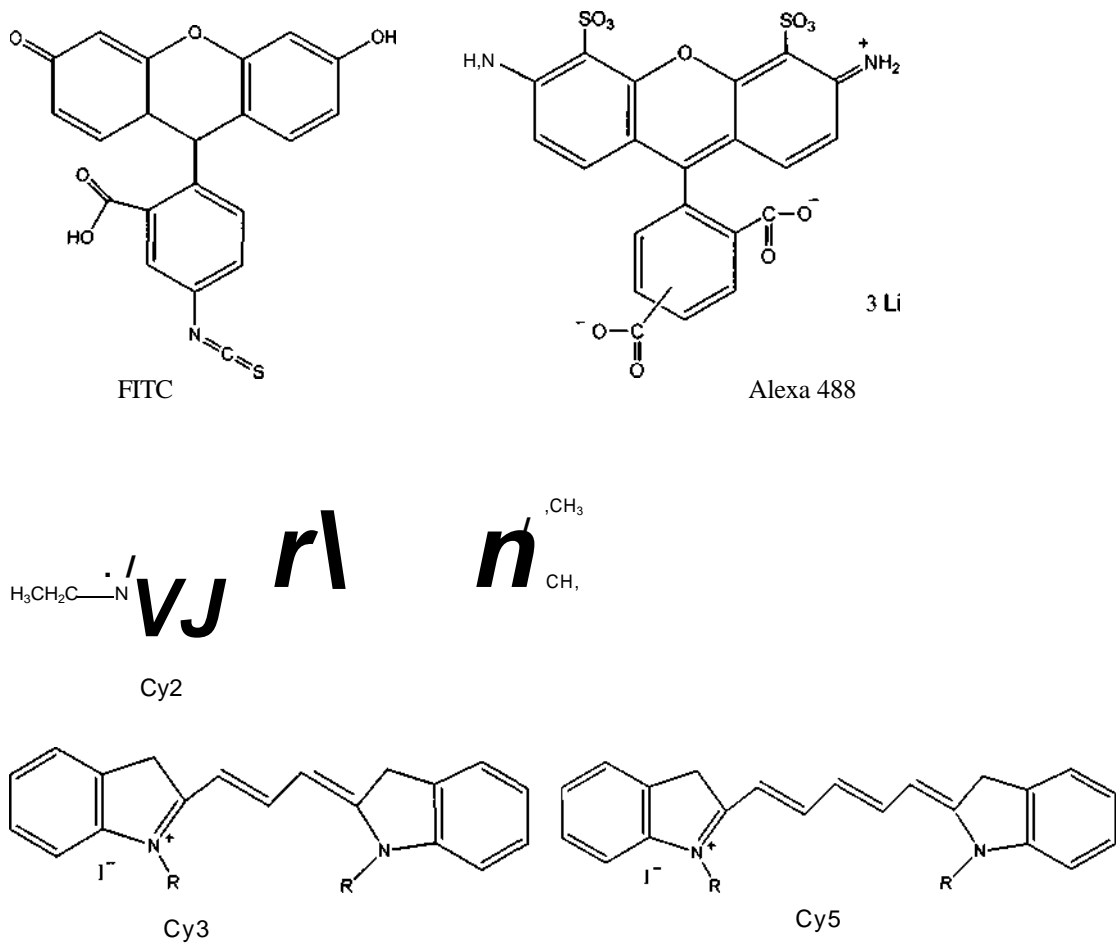
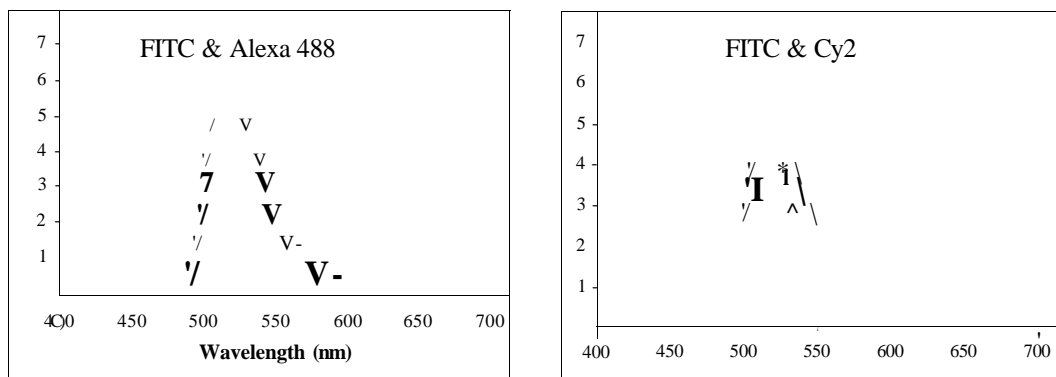


Figure 4.1. Structures of the dyes used in this work.

Multiple staining probes with distinct emission spectra are used for simultaneous visualization of multiple targets within a single image. Alexa 488 and FITC have similar broad emission spectra, which limits their efficiency in multicolor applications (Fig. 4.2), so Cy2 is used with Cy3 and Cy5 in multiple staining. To avoid the crosstalk of two dyes, orange-red (Cy3) or far-red (Cy5) emitting dyes are selected with green-emitters for

multiple staining. TRITC and Cy3 (Fig. 4.1), the orange-red emitters, can be excited maximally at 550 nm, which is close to the 543-nm laser line, and they exhibit peak emission at 570 nm. However, Cy3 is brighter, more photostable, and gives less background than TRITC. Cy5 (Fig. 4.1), a far-red fluorescing dye, is excited maximally at 650 nm, which is close to the 633-nm laser line, and it fluoresces maximally at 670 nm.



**Figure 4.2. Normalized emission spectra of Cy2, FITC, and Alexa 488.** Left: Overlapping emission of FITC and Alexa 488. Right: Resolved emission of FITC and Cy2. Modified from [http://www.mcb.arizona.edu/IPC/spectra\\_page.htm](http://www.mcb.arizona.edu/IPC/spectra_page.htm).

#### 4.2 RBC response to changes in oxygenation

The high Hb concentration exposes RBCs to continuous intracellular oxidative stress due to autoxidation of oxyHb (9). RBCs not only generate free radicals but are additionally exposed to xenobiotics, pathogens, hyperglycemic conditions, and to radical generating cells of the immune system. Superoxide and hydroxyl radicals produced by neutrophils and other phagocytes during phagocytosis have an important role in bactericidal and inflammatory processes. However, ROS release from these cells may cause tissue damage (5, 111).

RBCs possess efficient intracellular reducing machinery which, when coupled with their high density, makes them an effective circulating 'sink' for reactive species

(772). Not only the blood, but also the whole organism benefits from the RBC's scavenging ability (772). The non-enzymatic antioxidants in RBCs include GSH, ascorbic acid, NAD(P)H, and vitamin E. Furthermore, compared with other cell types, RBCs exhibit high activities of the most important antioxidant enzymes, including CuZnSOD, catalase, GPx, glutathione reductase, and plasma membrane oxidoreductases (772). Altogether, this powerful antioxidant machinery makes the RBC a highly efficient antioxidant system.

The confocal results (Fig. 3.3A,B, Fig. 3.3C) reveal different localization patterns for the antioxidant enzymes, CuZnSOD, catalase, and GPx in RBCs. Both CuZnSOD and catalase are distributed between the membrane and the cytosol, while GPx is largely localized at the membrane. As discussed above, RBCs scavenge both intracellular and intercellular ROS, so the distribution of CuZnSOD and catalase between the membrane and cytosol may reflect these two different roles. The antioxidant enzyme population at the membrane deactivates ROS produced outside the RBC as these species pass through the membrane either by free diffusion or via a transporter, thereby protecting membrane proteins. The cytosolic enzyme population scavenges the ROS produced by the RBC itself, and protects the cytosolic proteins, especially Hb.

The repeated uptake and release of O<sub>2</sub> by RBCs causes them to switch between high- and low-oxygenation states. Many studies have suggested that the oxygenation state regulates RBC properties. First, the activity of many membrane transporters changes with the O<sub>2</sub> content of the cell. The K<sup>+</sup>/Cl<sup>-</sup> cotransporter, for example, is reported to be 20-fold more active in oxygenated than in deoxygenated RBCs (773, 774). Second, RBC metabolism is adjusted according to the O<sub>2</sub> tension of the medium. Glucose, the only

energy source in the RBC, is metabolized via the pentose phosphate pathway twice as quickly in oxygenated as in deoxygenated cells (115). Third, RBC oxygenation-deoxygenation cycles may affect membrane properties (91).

Our data show that high O<sub>2</sub> tension drives CuZnSOD and catalase to relocate at the membrane in highly aerated RBCs (Fig. 3.5A,B). We question the physiological importance of their relocation under high O<sub>2</sub>. The molecular events that link the modulation of RBC properties to its O<sub>2</sub> state are very complex and cannot be easily elucidated. Several of these events are probably confined to the membrane with band 3 playing a primary role (91). The transmembrane domain of band 3 responsible for anion exchange across the membrane and CDB3 binds cytoskeletal proteins and several glycolytic enzymes, such as aldolase, phosphofructokinase, glyceraldehyde-3-phosphate dehydrogenase (GAPDH), lactate dehydrogenase, and protein tyrosine kinase (91). In addition, CDB3 binds deoxyHb (116).

The accepted transport function of band 3 is the exchange of Cl<sup>-</sup> and HCO<sub>3</sub><sup>-</sup> through its transmembrane domain. However, it is reported that band 3 can exchange anions other than Cl<sup>-</sup> and HCO<sub>3</sub><sup>-</sup>, and the anion transport rate is Ch-dependent in human RBCs (91). Band 3 anion transport works about three times faster when Hb is 100% vs 15% saturated with O<sub>2</sub> (91). Some studies have shown that band 3 also has the capacity to exchange O<sub>2</sub> for HCO<sub>3</sub><sup>-</sup> (117). Thus, we can speculate that high O<sub>2</sub> tension stimulates O<sub>2</sub> transport by band 3 from the external environment, and increases the intracellular H<sub>2</sub>O<sub>2</sub> concentration as a consequence of O<sub>2</sub> dismutation, especially near the membrane.

The non-nucleated RBC is unique among human cells in that the plasma membrane, its only structural component, accounts for all of its antigenic, transport, and

mechanical characteristics. Protection of its membrane by antioxidant enzymes is critical for RBC survival. This is supported by the relocalization observed here of CuZnSOD and catalase to the membrane in highly aerated RBCs (Fig 3.5A,B). To effectively remove the  $O_2$  transported by band 3, CuZnSOD not only concentrates at the membrane, but it also likely binds to CDB3 as supported by our colocalization data (Fig 3.6D). This conclusion is further supported by the competitive antibody binding results (Fig. 3.7). Catalase also binds to CDB3, and since the catalase substrate,  $H_2O_2$ , is a product of CuZnSOD catalysis, we speculate that CuZnSOD and catalase are organized into a complex at CDB3 to effectively remove ROS transported by the transmembrane domain of band 3. This is also supported by the colocalization of these two proteins as revealed by confocal microscopy (Fig. 3.6L). Such a complex would serve to compartmentalize ROS by the channelling of substrates through this assembly. ROS escape by diffusion from the complex would be dangerous for the RBC membrane and tissues. The glycolytic enzymes form a complex for the efficient metabolism of glucose, and some enzymes of this complex bind to CDB3 (90). Carbonic anhydrase isoform II (CAII) is an enzyme that catalyzes the conversion of  $CO_2$  to  $HCO_3^-$  in RBC. CAII attaches to the cytoplasmic C-terminus of band 3 to form a complex that has been called a bicarbonate transport metabolon. This metabolon increases the  $HCO_3^-$ -transmembrane flux (118).

In addition to its superoxide dismutase activity, CuZnSOD exhibits anion-binding capacity (119, 120), as well as inactivation by its own reaction product,  $H_2O_2$  (121-123). The rate of CuZnSOD inactivation by  $H_2O_2$  is significantly enhanced in the presence of physiologically relevant concentrations (~25 mM) of bicarbonate (124). Complex

formation at CDB3 may protect CuZnSOD from inactivation and metal release, especially at the RBC membrane where high concentrations of bicarbonate exist (118).

The membrane localization of GPx is not affected by increasing oxygen exposure (Fig 3.3C vs 3.5C). GPx not only shares the same substrate, H<sub>2</sub>O<sub>2</sub>, with catalase, but it also metabolizes a range of organic peroxides, including cholesterol and long-chain fatty acid peroxides (77). Thus, the membrane localization of GPx allows it to specifically stabilize cell membranes since these are composed of unsaturated fatty acids and cholesterol that are susceptible to oxidation (725).

The band 3 transport activity curve is of similar shape to the oxygen binding curve of human Hb when plotted against  $pO_2$  (91). Therefore, band 3 activity may be regulated by deoxyHb binding. DeoxyHb binds to CDB3 more tightly than oxyHb (126) and it has been reported that a number of glycolytic enzymes also bind to CDB3 (127). Thus, deoxyHb-CDB3 association may be responsible for the O<sub>2</sub>-dependent modulation of RBC glucose metabolism (775). If the association between CDB3 and CuZnSOD and/or catalase is physiological, one would expect to observe at least partial displacement of the enzymes upon deoxygenation. Binding of deoxyHb to CDB3 induces structural changes throughout the entire band 3 molecule (128, 129), and a gradual increase in bound Hb will consequently increase the structural hindrance to other protein binding. Since CuZnSOD and catalase are not membrane bound in deaerated RBCs (Fig. 3.4D,E), we conclude that both enzymes bind at or near the N-terminus of CDB3. This binding site is also supported by the observation that the monoclonal anti-CDB3 antibody, which recognizes an epitope within residues 1-136 of CDB3 (36), competed with the binding of anti-CuZnSOD to CuZnSOD at the membrane (Fig 3.7A,B). As the antibody used for

CuZnSOD staining was polyclonal, we did not expect complete inhibition of anti-CuZnSOD binding. The binding of anti-CDB3 to CDB3 should also be reduced by first staining with anti-CuZnSOD; however, the intensity was similar in the present and absent of anti-CuZnSOD (Fig. 3.7C vs Fig. 3.7D). The likely explanation for this observation is that the number of band 3 molecules in the membrane is  $1.2 \times 10^6$  (91), which is over 4-fold greater than the total number of CuZnSOD molecules ( $\sim 2.7 \times 10^5$ ) per RBC as estimated from the ICP-MS results, Section 3.10. Assuming that 50% or less of CuZnSOD is bound to the membrane, the CDB3 concentration at the membrane could be up to 10-fold higher than that of CuZnSOD. Thus, the drop in fluorescence intensity on anti-CuZnSOD binding gives rise to no detectable changes in CDB3 fluorescence. The images in Figures 3.3-3.5 clearly demonstrate that the association of CuZnSOD and catalase with the RBC membrane is regulated by its oxygenation state.

Comparing the images for immunofluorescence of CDB3 and the antioxidant enzymes in the same RBC field reveals that membrane staining for the former is obviously smooth whereas staining for the enzymes is measurably punctate. This indicates that a fraction of the enzymes are organized into larger complexes, which appear as discrete fluorescent spots on the membrane (e.g., Fig. 3.3). The significance of this punctate staining as well as the aggregation of CuZnSOD towards the center of the biconcave membrane in highly aerated RBCs (Fig. 3.5) is not clear at the present time. It was reported that Hb degradation products (hemichromes) have a strong affinity for CDB3. The association of hemichromes with CDB3 triggers band 3 clustering and the clusters show increased affinity for naturally occurring band 3 antibodies (NAbs). The binding of NAbs to the surface of RBCs triggers the phagocytosis of altered RBCs.

However, the reasons for band 3 aggregation and its importance are still not clear (21). We suspected that CuZnSOD aggregation at the RBC membrane after air exposure (Fig 3.5) was the result of band 3 clustering. However, CDB3 did not show punctate distribution in post-oxygenated RBCs. These results warrant further investigation.

In addition to being a binding site for proteins, another major function of CDB3 is to anchor the RBC membrane to the underlying cytoskeleton by association with multiple cytoskeletal components. This is essential for the structure and function of the entire RBC. The biconcave disk shape of the cell is maintained by the strong cohesion between the bilayer and the membrane skeleton through interaction with CDB3. Missense mutations in CDB3 result in global changes in RBC shape and deformability (98). For example, hereditary spherocytosis (HS) is caused by mutations in a variety of RBC proteins, including CDB3 (130). A common feature of all forms of HS is the loss of membrane surface area and a change in cell shape from discocytes (normal cells) to stomatocytes (cup cells) and spherocytes (spherical cells) (131). Thus, we can assume that oxidation of band 3 at the center of the RBC membrane causes cell deformation. Under air-saturated conditions, oxyHb is considerably oxidized to metHb with generation of O<sub>2</sub> (132). The biconcave site allows O<sub>2</sub> and CO<sub>2</sub> to move more quickly through the membrane, so band 3 may be more active, and more O<sub>2</sub> may be generated and transported at this site. Hence, we speculate that CuZnSOD concentrates at this site to protect membrane proteins from oxidative damage.

In addition to changes in localization of the antioxidant enzymes, we also noticed that the cells clump together in deaerated and aerated RBCs (Figs. 3.4 and 3.5, bright-field images). A possible reason may be that the properties of the membrane's outer face

change on prolonged exposure to air or N<sub>2</sub> (1 h air and 2 min N<sub>2</sub>). In contrast, RBC gas exchange occurs within seconds in the lung (98, 133). Alteration of RBC surface properties caused cell clustering and the cells were not well spread out on the slides. Thus, too many cells were visualized in one image and too few in another (Fig 3.5 A and C).

The fluorescence signal of the target enzymes in deaerated RBCs was weaker (Fig 3.4 D, E, F) compared with their signal in RBCs exposed to air for < 5 min (Fig 3.3). An explanation is that proteins dissociated from CDB3 and were evenly distributed throughout the cytosol in deaerated cells. Since the protein concentration per unit area in the cytosol was lower than that at the membrane, the fluorescence intensity was lower. Also, formaldehyde may be less efficient than acrolein at cell fixation (Section 4.1).

#### 4.3 RBC response to H<sub>2</sub>O<sub>2</sub> and O<sub>2</sub>~

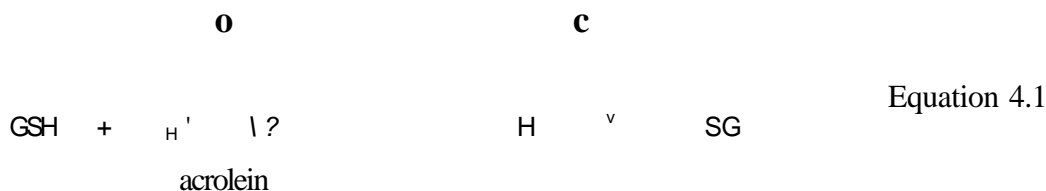
The antioxidant enzymes catalase and CuZnSOD change their localization in response to increased O<sub>2</sub> tension (Fig. 3.3A,B vs Fig. 3.5A,B). Under this condition, it is speculated that the ROS concentration increases both intracellular<sup>^</sup> and extracellularly. Response to increased O<sub>2</sub> tension provides indirect evidence for the response of these enzymes to ROS. Direct responses are examined by artificially increasing extracellular or intracellular ROS. RBCs are exposed to both endogenous and exogenous peroxides during their lifetime. H<sub>2</sub>O<sub>2</sub> sources outside the RBC include phagocytic cells, leukocytes, and macrophages. Peroxides are the by-products of the oxidative destruction of foreign matter in these cells. The main endogenous source of H<sub>2</sub>O<sub>2</sub> is the dismutation of O<sub>2</sub> (134). RBCs have efficient enzymes for the decomposition of H<sub>2</sub>O<sub>2</sub> and the best characterized ones are catalase and GPx (735).

The discovery of GPx initiated an intense debate as to which enzyme plays the predominant role in scavenging H<sub>2</sub>O<sub>2</sub> (136). GPx catalyzes H<sub>2</sub>O<sub>2</sub> decomposition at the expense of two GSH molecules, which are very important for maintenance of intracellular redox status. From our experiments, we can not say which enzyme is more important in H<sub>2</sub>O<sub>2</sub> metabolism but our data support GPx's role in scavenging organic peroxides as discussed in Section 4.2. However, the production of organic peroxides is not critical to the functioning of the RBCs as these are by-products of the reactions between lipids, ROS and xenobiotics (137). Therefore, we want to determine whether GPx also plays a role in protecting RBCs from H<sub>2</sub>O<sub>2</sub>. GPx is seen to respond to the exogenous H<sub>2</sub>O<sub>2</sub> generated *in situ* by GOx and glucose in the medium as the peroxidase concentrates at the membrane (Fig. 3.16). Under saturating conditions, the H<sub>2</sub>O<sub>2</sub> degradation rate depends linearly on the GPx concentration, and GPx becomes saturated at >1 uM H<sub>2</sub>O<sub>2</sub> (136). The rate of H<sub>2</sub>O<sub>2</sub> generation is ~8 uM/min (Fig. 3.11) in our experiment, so more GPx relocates to the membrane to decompose H<sub>2</sub>O<sub>2</sub> compared with control cells where H<sub>2</sub>O<sub>2</sub> is present at basal levels. Catalase is efficient at H<sub>2</sub>O<sub>2</sub> deactivation as it exhibits the highest turnover number (10<sup>6</sup> s) of known enzymes. In fact, 1% of the catalase activity of RBCs would remove most of the H<sub>2</sub>O<sub>2</sub> generated in these cells (e.g., ~ 50% at 10<sup>5</sup> mol/L H<sub>2</sub>O<sub>2</sub>) (136). GPx attains only ~8% of the rate at which catalase decomposes H<sub>2</sub>O<sub>2</sub> (136), and two molecules of GSH are oxidized per H<sub>2</sub>O<sub>2</sub> molecule. Thus, H<sub>2</sub>O<sub>2</sub> removal by catalase is efficient and economic. However, catalase can not replace GPx in organic peroxides detoxification, which is critical for protection of the RBC membrane. Thus, H<sub>2</sub>O<sub>2</sub> removal in normal RBCs is mainly the domain of

catalase (136), while GPx works as a deactivator of organic peroxides, especially at the RBC membrane (137).

H<sub>2</sub>O<sub>2</sub> is the main substrate of catalase (55), so we expected it to respond to an exogenous source of H<sub>2</sub>O<sub>2</sub> and localize at the membrane as observed at high O<sub>2</sub> tension (Section 4.2). However, catalase remained distributed between the membrane and the cytosol in both control and H<sub>2</sub>O<sub>2</sub>-exposed cells (Fig. 3.16). Possible explanations are: first, during H<sub>2</sub>O<sub>2</sub> generation by GO<sub>x</sub>-catalyzed glucose oxidation, oxygen is consumed at a 1:1 ratio of O<sub>2</sub> per H<sub>2</sub>O<sub>2</sub> produced (Eq 3.1). Hence, the O<sub>2</sub> concentration in the RBC incubation would have decreased since the 2-mL Eppendorf tube was sealed. The increased deoxyHb concentration would displace catalase from the membrane even in the presence of increased H<sub>2</sub>O<sub>2</sub>. The partial cytosolic localization of GPx in the glucose/GO<sub>x</sub>/catalase control (Fig. 3.16F), in which there was less H<sub>2</sub>O<sub>2</sub> influx into the PvBC but similar deoxyHb generation as in the absence of exogenous catalase, suggests that GPx might not compete with deoxyHb for CDB3. Second, catalase forms a complex with CuZnSOD at the membrane when the O<sub>2</sub> level is high (Fig. 3.6L). However, CuZnSOD redistributes to the cytosol when RBCs are exposed to exogenous H<sub>2</sub>O<sub>2</sub> (Fig. 3.16H), suggesting that CuZnSOD may anchor catalase at the membrane. Third, H<sub>2</sub>O<sub>2</sub> entering the cell may react with GPx more efficiently than with catalase. Catalase could execute a dual function in the cell. Since catalase is more abundant in the cytosol than at the membrane, it possibly protects cytosolic proteins from oxidative damage. Yet, catalase found in the membrane possibly reacts with H<sub>2</sub>O<sub>2</sub> to maintain GSH levels and thereby GPx activity (136).

As the substrate of GPx in H<sub>2</sub>O<sub>2</sub> decomposition, GSH was expected to show partial membrane staining, but Figures 3.16J,K,L reveal even distribution of the tripeptide throughout the cytosol. GSH-associated metabolism is a major mechanism of cellular protection against agents that generate oxidative stress (136). Thus, GSH provides the cell with multiple defences not only against ROS but also against their toxic products (136). It can directly scavenge free radicals or act as a substrate for GPx during the detoxification of H<sub>2</sub>O<sub>2</sub>. GSH near the membrane, where the H<sub>2</sub>O<sub>2</sub> concentration is high, will react with H<sub>2</sub>O<sub>2</sub> directly or as a GPx substrate and form GSSG (136). Furthermore, acrolein rapidly binds and depletes cellular GSH (89, 138), and membrane localized GSH will likely be consumed first. The formation of acrolein-GSH adducts (Eq 4.1) or protein S-glutathionylation (89, 138, 139) may influence antibody binding to GSH. Note that the antibody used (ab9443), recognized both oxidized and reduced GSH. Furthermore, the pores in the RBC membrane after permeabilization are large enough for antibody access. Antibodies are large macromolecules (~150 kDa), whereas GSH is a small soluble molecule (307 Da). Thus, GSH close to the membrane may diffuse out of the permeabilized cells before staining. No membrane-localized GSH was detected in our confocal results (Fig. 3.16).



Basal ROS in RBCs come from the autoxidation of oxyHb which produces O<sub>2</sub><sup>-</sup>. To mimic the autoxidation of oxyHb, RBCs were incubated with PMS, which reacts with hydrogen donors (e.g., NADPH) in RBCs to generate intracellular O<sub>2</sub><sup>-</sup> (Eq 2.3) (100). *In*

*vitro*,  $O_2$  production by PMS was confirmed in a preliminary experiment, and the generation of  $O_2^-$  was found to be dependent on the NADPH concentration and inhibited by CuZnSOD (Figs. 3.14 and 3.15).

CuZnSOD is the only known SOD in RBCs, and partial CuZnSOD localization at the membrane under physiological conditions was observed here (Fig. 3.3). We expected to observe increased membrane localization of CuZnSOD in the PMS-treated RBCs. However, even distribution throughout the cytosol is seen in the confocal images of CuZnSOD in PMS-treated RBCs (Fig. 3.17F). CuZnSOD localized at the membrane will dismutate  $O_2^-$  generated by oxyHb autoxidation near the membrane. Since the RBC membrane is the  $O_2$  exchange site, we speculated that endogenous  $O_2^-$  generation from oxyHb is greater near the membrane than in the cytosol. Thus, CuZnSOD is more concentrated at the membrane than in the cytosol where  $O_2^-$  generation may be lower. In PMS-treated RBCs,  $O_2^-$  may be uniformly produced throughout the RBC without any compartmentalization. But  $O_2^-$  generation over 5 min by PMS consumes  $O_2$  (Eq 2.3) so the  $O_2$  level will decrease as the 2-mL Eppendorf tube was sealed. The deoxyHb formed on  $O_2$  consumption will bind to CDB3, hindering the binding of CuZnSOD.

The RBC substrates that react with PMS are not completely understood (100). We question if there are other reactions of PMS in RBCs. Indirect evidence for PMS-catalyzed  $O_2^-$  formation in RBCs was reported by Ricardo (100) at high concentrations of PMS (0.1-2.0 mM). However, it was reported that RBCs become significantly altered from control cells at 25  $\mu$ M PMS, and even 10  $\mu$ M PMS caused alterations slightly exceeding those seen for sickle RBCs (140). Thus, we chose to incubate RBCs with only 5  $\mu$ M PMS (Section 2.2.9), but we have no evidence that endogenous  $O_2^-$  production

would be significantly increased by 5  $\mu$ M PMS in the cells. In any event, CuZnSOD distributed in the cytosol would be able to dismutate the additional  $O_2^-$  generated intracellularly by PMS.

In addition to NAD(P)H, PMS may be reduced to generate  $O_2^-$  by other RBC metabolites such as GSH. Oxidation of GSH by PMS and acrolein may affect antibody recognition such that no membrane staining of GSH is seen in the confocal images (Figs. 3.16J-L and 3.17G,H). GPx shows similar distribution in GOx-treated and PMS-treated RBCs (Figs. 3.16E and 3.17D). Since GPx mainly protects the membrane, this may be a response to enhanced cytosolic  $H_2O_2$  or  $O_2^-$  dismutation in PMS-treated cells and elevated extracellular  $H_2O_2$  in the GOx-treated cells.

The CuZnSOD, catalase, and GPx staining patterns in control samples as well as in the GOx- and PMS-treated samples (Fig. 3.16 A,D,G and Fig. 3.17A,C,E) are different from those in cells exposed to air for < 5 min and fixed immediately after washing ("fresh RBCs") (Fig. 3.3). Less membrane localization is seen in the control samples in Figures 3.16 and 3.17 than in the fresh RBCs (Fig. 3.3). The reasons for this are not clear. Comparing the experimental procedures, the only difference is that before fixing, the control RBCs were incubated in G-PBS for 10 min in sealed 2-mL Eppendorf tubes (Section 2.2.9) whereas the fresh RBCs were incubated in G-PBS for < 1 min in unsealed 2-mL Eppendorf tubes (Section 2.2.1). Further experiments are required to clarify the role of glucose exposure, if any, on protein localization.

## Chapter 5: Conclusions and future studies

RBCs function both in O<sub>2</sub> transport and as ROS sinks for tissues to maintain homeostasis. Defenses against ROS, such as O<sub>2</sub><sup>-</sup> and H<sub>2</sub>O<sub>2</sub>, are clearly mandatory. RBCs possess a strong antioxidant system, including enzymatic and non-enzymatic antioxidants. CuZnSOD, catalase, and GPx are key players. CuZnSOD protects RBCs from oxidative damage by scavenging O<sub>2</sub> and keeping its concentration low. Catalase and GPx serve the same function by decomposing H<sub>2</sub>O<sub>2</sub> and organic peroxides. GPx mainly protects membrane lipids and proteins, and catalase protects the cytosolic proteins. Their combined effects minimize the likelihood of interaction between RBC components and ROS. Furthermore, their effective scavenging actions are maintained by their localization, which is regulated by the oxygenation state of the RBC.

The presence of CuZnSOD, catalase, and CDB3 within one structural macrocomplex makes it likely that the individual components have linked roles. We can speculate on the possible nature of this function: CuZnSOD, catalase, and CDB3 form a metabolon at the cytosolic surface of the RBC membrane that accepts O<sub>2</sub><sup>-</sup> transported by band 3 into the cell. The O<sub>2</sub><sup>-</sup> is dismutated by CuZnSOD to H<sub>2</sub>O<sub>2</sub>, which is then channelled to catalase for decomposition (Eq 1.4). The membrane localization and substrate channelling offered by this metabolon would control O<sub>2</sub><sup>-</sup> and H<sub>2</sub>O<sub>2</sub> diffusion and promote their efficient deactivation thereby protecting the RBC from oxidative damage. In summary, this very efficient antioxidant machinery ensures a reducing environment in RBCs to maintain both a functional membrane and Hb in its active form for efficient O<sub>2</sub> delivery and waste removal.

There are a number of interesting results observed here that we can not explain clearly. Thus, more investigations need to be performed to clarify several observations.

Suggested future studies include:

- 1) It is speculated that CuZnSOD, catalase, and CDB3 form a metabolon for ROS deactivation based on the experiments described in this thesis, but more direct evidence for their binding is required. *In vitro* binding experiments using recombinant CDB3 could be performed as was carried out for Hb (141).
- 2) Binding of catalase and GPx-1 to CDB3 should also be examined in the RBC by competitive antibody binding experiments similar to those described in Section 3.6. If evidence for association is obtained, then *in vitro* experiments could be carried out to characterize the protein-protein complexes in greater detail as proposed in (1) above. Furthermore, competition with carbonic anhydrase II (CAII) should be carried out to confirm that the antioxidant enzymes bind to CDB3 and not the C-terminus of band 3. Anti-CAII should compete with the protein binding to the C-terminus but not CDB3.
- 3) In addition to catalase and GPx-1, peroxiredoxin 2 (Prx2) is an abundant peroxidase in RBCs (142). Prx2 uses cysteine residues to decompose H<sub>2</sub>O<sub>2</sub> and is the third most abundant protein in RBCs after Hb and carbonic anhydrase (142). Thus, Prx2 could compete effectively with catalase and GPx to scavenge low levels of H<sub>2</sub>O<sub>2</sub>, including that derived from oxyHb autoxidation. In fact, due to its high cellular concentration, Prx2 acts as a non-catalytic scavenger of H<sub>2</sub>O<sub>2</sub> at concentrations up to 250  $\mu$ M (142). Prx2 rapidly decomposes not only H<sub>2</sub>O<sub>2</sub> but also organic peroxides, including lipid

hydroperoxides, and peroxyxynitrite. Prx2 associates with the RBC membrane (142), but what controls its membrane association and whether it competes with catalase or GPx for CDB3 binding have not been established. The localization of Prx2 under both physiological and oxidative-stress conditions should be examined in future work.

- 4) Antioxidant enzyme relocation was examined in Chapter 3 in response to prolonged exposure (1 h) of RBCs to air. However, RBC gas exchange occurs within seconds (98, 133). If the membrane association of antioxidant enzymes in highly aerated RBCs is physiologically relevant, then this association should be reversible. Thus, enzyme localization in RBCs exposed to air for shorter times and association-dissociation mediated by the RBC oxygenation state should be examined in further detail. Also, quantitation of cytosol vs membrane stained protein should be performed using the appropriate software. It would additionally be of interest to repeat the O<sub>2</sub>-dependent localization at 37°C.
- 5) RBCs should be exposed to exogenous H<sub>2</sub>O<sub>2</sub> and O<sub>2</sub> in open vessels and O<sub>2</sub> levels should be monitored. This would allow full evaluation of competition between deoxyHb and the antioxidant enzymes for CDB3 binding under oxidative stress. Fluorescent dyes (e.g., hydroethidine for O<sub>2</sub>, 2,7-dichlorodihydrofluorescein for H<sub>2</sub>O<sub>2</sub>) could also be used to monitor O<sub>2</sub> and H<sub>2</sub>O<sub>2</sub> levels within RBCs.
- 6) RBCs fixed with formaldehyde under air should be carried out as an additional control for the studies on cells exposed to N<sub>2</sub> (Section 2.2.5).

## References

1. Vander, A.J. (2001) Blood in *Human Physiology: The Mechanism of Body Function*, 8th ed., McGraw-Hill Education, Singapore, p 377.
2. Gerschman, R., Gilbert, D. L., Nye, S. W., Dwyer, P., and Fenn, W. O. (1954) Oxygen poisoning and x-irradiation: a mechanism in common. *Science* 119, 623-6.
3. Miller, D. M, Buettner, G. R., and Aust, S. D. (1990) Transition metals as catalysts of "autoxidation" reactions. *Free Radic Biol Med* 8, 95-108.
4. Valko, M., Rhodes, C. J., Moncol, J., Izakovic, M, and Mazur, M. (2006) Free radicals, metals and antioxidants in oxidative stress-induced cancer. *Chem Biol Interact* 160, 1-40.
5. Valko, M, Leibfritz, D., Moncol, J., Cronin, M. T., Mazur, M., and Telser, J. (2007) Free radicals and antioxidants in normal physiological functions and human disease. *Int J Biochem Cell Biol* 39, 44-84.
6. Halliwell, B., and Gutteridge, J. M.C. (1999) in *Free Radicals in Biology and Medicine*, 3rd ed., Oxford University Press Inc., New York, p 143.
7. Stadtman, E. R. (2004) Role of oxidant species in aging. *Curr Med Chem* 11, 1105-12.
8. Turrens, J. F. (2003) Mitochondrial formation of reactive oxygen species. *J Physiol* 552, 335-44.
9. Cimen, M. Y. (2008) Free radical metabolism in human erythrocytes. *Clin Chim Acta* 390, 1-11.

10. Hebbel, R. P., Eaton, J. W., Balasingam, M., and Steinberg, M. H. (1982) Spontaneous oxygen radical generation by sickle erythrocytes. *J Clin Invest* 70, 1253-9.
11. Claster, S., Chiu, D. T., Quintanilha, A., and Lubin, B. (1984) Neutrophils mediate lipid peroxidation in human red cells. *Blood* 64, 1079-84.
12. Baynes, JW. (2005) Oxygen and life in *Medical Biochemistry*, 2nd ed. (Baynes JW, Domoniczal MH, Ed.), Elsevier Mosby, Philadelphia, pp 497-506.
13. Dumaswala, U. J., Zhuo, L., Jacobsen, D. W., Jain, S. K., and Sukalski, K. A. (1999) Protein and lipid oxidation of banked human erythrocytes: role of glutathione. *Free Radic Biol Med* 27, 1041 -9.
14. Kaul, R. K., and Kohler, H. (1983) Interaction of hemoglobin with band 3: a review. *Klin Wochenschr* 61, 831-7.
15. Shalev, O., Leida, M. N., Hebbel, R. P., Jacob, H. S., and Eaton, J. W. (1981) Abnormal erythrocyte calcium homeostasis in oxidant-induced hemolytic disease. *Blood* 58, 1232-5.
16. Giulivi, C, and Davies, K. J. (2001) Mechanism of the formation and proteolytic release of H<sub>2</sub>O<sub>2</sub>-induced dityrosine and tyrosine oxidation products in hemoglobin and red blood cells. *J Biol Chem* 276, 24129-36.
17. Caprari, P., Scuteri, A., Salvati, A. M., Bauco, C, Cantafora, A., Masella, R., Modesti, D., Tarzia, A., and Marigliano, V. (1999) Aging and red blood cell membrane: a study of centenarians. *Exp Gerontol* 34, 47-57.
18. Fujino, T., Ando, K., Beppu, M., and Kikugawa, K. (2000) Enzymatic removal of oxidized protein aggregates from erythrocyte membranes. *JBiochem* 127, 1081-6.

19. Snyder, L. M., Fortier, N. L., Trainor, J., Jacobs, J., Leb, L., Lubin, B., Chiu, D., Shohet, S., and Mohandas, N. (1985) Effect of hydrogen peroxide exposure on normal human erythrocyte deformability, morphology, surface characteristics, and spectrin-hemoglobin cross-linking. *J Clin Invest* 76, 1971-7.
20. Leb, L., Snyder, L. M., Fortier, N. L., and Andersen, M. (1987) Antiglobulin serum mediated phagocytosis of normal senescent and oxidized RBC: role of anti-IgM immunoglobulins in phagocytic recognition. *Br J Haematol* 66, 565-70.
21. Pantaleo, A., Giribaldi, G., Mannu, F., Arese, P., and Turrini, F. (2008) Naturally occurring anti-band 3 antibodies and red blood cell removal under physiological and pathological conditions. *Autoimmun Rev* 7, 457-62.
22. Kiefer, C. R., Trainor, J. F., McKenney, J. B., Valeri, C. R., and Snyder, L. M. (1995) Hemoglobin-spectrin complexes: interference with spectrin tetramer assembly as a mechanism for compartmentalization of band 1 and band 2 complexes. *Blood* 86, 366-71.
23. Yahya, H. (2007) in *The Miracle of the Blood and Heart*, 1st ed., Global Publishing, Istanbul, p 25.
24. Al-Omar MA, Beedham C, Alsarra IA. (2004) Pathological roles of reactive oxygen species and their defence mechanism. *Saudi Pharm J* 12, 1-18.
25. Johnson, R. M., Goyette, G., Jr., Ravindranath, Y., and Ho, Y. S. (2005) Hemoglobin autoxidation and regulation of endogenous H<sub>2</sub>O<sub>2</sub> levels in erythrocytes. *Free Radic Biol Med* 39, 1407-17.
26. Chiu, D., Kuypers, F., and Lubin, B. (1989) Lipid peroxidation in human red cells. *Semin Hematol* 26, 257-76.

27. Scott, M. D., Eaton, J. W., Kuypers, F. A., Chiu, D. T., and Lubin, B. H. (1989) Enhancement of erythrocyte superoxide dismutase activity: effects on cellular oxidant defense. *Blood* 74, 2542-9.
28. Bielski, B. H., and Cabelli, D. E. (1991) Highlights of current research involving superoxide and perhydroxyl radicals in aqueous solutions. *Int J Radiat Biol* 59, 291-319.
29. Miller, N. J., Sampson, J., Candeias, L. P., Bramley, P. M, and Rice-Evans, C. A. (1996) Antioxidant activities of carotenes and xanthophylls. *FEBS Lett* 384, 240-2.
30. Dumaswala, U. J., Zhuo, L., Mahajan, S., Nair, P. N., Shertzer, H. G., Dibello, P., and Jacobsen, D. W. (2001) Glutathione protects chemokine-scavenging and antioxidative defense functions in human RBCs. *Am J Physiol Cell Physiol* 280, C867-73.
31. Somani, S. M., Husain, K., and Schlorff, E. C. (1997) Response of antioxidant system to physical and chemical stress in *Oxidants, Antioxidants, and Free Radicals*, 1st ed. (Steven I. Baskin, Harry Salem, Ed.), CRC press, Washington, p127.
32. McCord, J. M., and Fridovich, I. (1988) Superoxide dismutase: the first twenty years (1968-1988). *Free Radio Biol Med* 5, 363-9.
33. Rigo, A., and Rotilio, G. (1977) Simultaneous determination of superoxide dismutase and catalase in biological materials by polarography. *Anal Biochem* 81, 157-66.

34. Bannister, J. V., Bannister, W. H., and Rotilio, G. (1987) Aspects of the structure, function, and applications of superoxide dismutase. *CRC Crit Rev Biochem* 22, 111-80.
35. Valentine, J. S., Doucette, P. A., and Zittin Potter, S. (2005) Copper-zinc superoxide dismutase and amyotrophic lateral sclerosis. *Annu Rev Biochem* 74, 563-93.
36. Hart, P. J., Balbirnie, M. M., Ogihara, N. L., Nersissian, A. M., Weiss, M. S., Valentine, J. S., and Eisenberg, D. (1999) A structure-based mechanism for copper-zinc superoxide dismutase. *Biochemistry* 38, 2167-78.
37. Tainer, J. A., Getzoff, E. D., Beem, K. M., Richardson, J. S., and Richardson, D. C. (1982) Determination and analysis of the 2-A structure of copper, zinc superoxide dismutase. *JMol Biol* 160, 181-217.
38. Tainer, J. A., Getzoff, E. D., Richardson, J. S., and Richardson, D. C. (1983) Structure and mechanism of copper, zinc superoxide dismutase. *Nature* 306, 284-7.
39. Rakhit, R., and Chakrabarty, A. (2006) Structure, folding, and misfolding of Cu,Zn superoxide dismutase in amyotrophic lateral sclerosis. *Biochim Biophys Acta* 1762, 1025-37.
40. Goodsell, D. S., and Olson, A. J. (2000) Structural symmetry and protein function. *Annu Rev Biophys Biomol Struct* 29, 105-53.
41. Lepock, J. R., Arnold, L. D., Torrie, B. H., Andrews, B., and Kruuv, J. (1985) Structural analyses of various Cu<sup>+</sup>, Zn<sup>+</sup>-superoxide dismutases by differential

- scanning calorimetry and Raman spectroscopy. *Arch Biochem Biophys* 241, 243-51.
42. Forman, H. J., and Fridovich, I. (1973) On the stability of bovine superoxide dismutase. The effects of metals. *J Biol Chem* 248, 2645-9.
  43. Getzoff, E. D., Tainer, J. A., Weiner, P. K., Kollman, P. A., Richardson, J. S., and Richardson, D. C. (1983) Electrostatic recognition between superoxide and copper, zinc superoxide dismutase. *Nature* 306, 287-90.
  44. Imlay, J. A., and Fridovich, I. (1991) Assay of metabolic superoxide production in *Escherichia coli*. *J Biol Chem* 266, 6957-65.
  45. Poderoso, J. J., Lisdero, C., Schopfer, F., Riobo, N., Carreras, M. C, Cadenas, E., and Boveris, A. (1999) The regulation of mitochondrial oxygen uptake by redox reactions involving nitric oxide and ubiquinol. *J Biol Chem* 274, 37709-16.
  46. Pelmeshnikov, V., and Siegbahn, P. E. (2005) Copper-zinc superoxide dismutase: theoretical insights into the catalytic mechanism. *Inorg Chem* 44, 3311-20.
  47. Elchuri, S., Oberley, T. D., Qi, W., Eisenstein, R. S., Jackson Roberts, L., Van Remmen, H., Epstein, C. J., and Huang, T. T. (2005) CuZnSOD deficiency leads to persistent and widespread oxidative damage and hepatocarcinogenesis later in life. *Oncogene* 24, 367-80.
  48. Muller, F. L., Song, W., Liu, Y., Chaudhuri, A., Pieke-Dahl, S., Strong, R., Huang, T. T., Epstein, C. J., Roberts, L. J., 2nd, Csete, M., Faulkner, J. A., and Van Remmen, H. (2006) Absence of CuZn superoxide dismutase leads to

- elevated oxidative stress and acceleration of age-dependent skeletal muscle atrophy. *Free Radic Biol Med* 40, 1993-2004.
49. Zamocky, M., and Koller, F. (1999) Understanding the structure and function of catalases: clues from molecular evolution and in vitro mutagenesis. *Prog Biophys Mol Biol* 72, 19-66.
  50. Loew, O. (1900) A new enzyme of general occurrence in organisms. *Science* 11, 701-702.
  51. Sumner, J. B., and Gralen, N. (1938) The molecular weight of crystalline catalase. *Science* 87, 284.
  52. Schroeder, W. A., Shelton, J. R., Shelton, J. B., Robberson, B., and Apell, G. (1969) The amino acid sequence of bovine liver catalase: a preliminary report. *Arch Biochem Biophys* 131, 653-5.
  53. Chelikani, P., Fita, I., and Loewen, P. C. (2004) Diversity of structures and properties among catalases. *Cell Mol Life Sci* 61, 192-208.
  54. Nicholls P., Fita I., Loewen P.C. (2001) Enzymology and structure of catalases, *Advances in Inorganic Chemistry* 51, 51-106.
  55. Kirkman, H. N., and Gaetani, G. F. (2007) Mammalian catalase: a venerable enzyme with new mysteries. *Trends Biochem Sci* 32, 44-50.
  56. Putnam, C. D., Arvai, A. S., Bourne, Y., and Tainer, J. A. (2000) Active and inhibited human catalase structures: ligand and NADPH binding and catalytic mechanism. *J Mol Biol* 296, 295-309.

57. Deisseroth, A., and Dounce, A. L. (1970) Catalase: physical and chemical properties, mechanism of catalysis, and physiological role. *Physiol Rev* 50, 319-75.
58. Lardinois, O. M, and Rouxhet, P. G. (1996) Peroxidatic degradation of azide by catalase and irreversible enzyme inactivation. *Biochim Biophys Acta* 1298, 180-90.
59. Ogura, Y., and Yamazaki, I. (1983) Steady-state kinetics of the catalase reaction in the presence of cyanide. *J Biochem* 94, 403-8.
60. Maehly, A. C, and Chance, B. (1954) The assay of catalases and peroxidases. *Methods Biochem Anal* 1, 357-424.
61. Aebi, H. (1984) Catalase in vitro. *Meth Enzymol.* 105, 121.
62. Ho, Y. S., Xiong, Y., Ma, W., Spector, A., and Ho, D. S. (2004) Mice lacking catalase develop normally but show differential sensitivity to oxidant tissue injury. *J Biol Chem* 279, 32804-12.
63. Scott, T., and Mercer, E. L. (1997) in *Concise Encyclopedia Biochemistry and Molecular Biology*, 3rd ed., Walter de Gruyter Berlin, New York, p314.
64. Mills, G. C. (1957) Hemoglobin catabolism. I. Glutathione peroxidase, an erythrocyte enzyme which protects hemoglobin from oxidative breakdown. *J Biol Chem* 229, 189-97.
65. Rotruck, J. T., Pope, A. L., Ganther, H. E., Swanson, A. B., Hafeman, D. G., and Hoekstra, W. G. (1973) Selenium: biochemical role as a component of glutathione peroxidase. *Science* 179, 588-90.

66. Flohe, L., Gunzler, W. A., and Schock, H. H. (1973) Glutathione peroxidase: a selenoenzyme. *FEBS Lett* 32, 132-4.
67. Arthur, J. R. (2000) The glutathione peroxidases. *Cell Mol Life Sci* 57, 1825-35.
68. Behne, D., and Kyriakopoulos, A. (2001) Mammalian selenium-containing proteins. *Annu Rev Nutr* 21, 453-73.
69. Hardy, I. J., and Hardy, G. (2007) Immune-modulating effects of sulfur-containing nutraceuticals. *Nutrition* 23, 514-6.
70. Townsend, D. M, Tew, K. D., and Tapiero, H. (2003) The importance of glutathione in human disease. *BiomedPharmacother* 57, 145-55.
71. Sunde, R. A. (1997) Selenium in *Handbook of Nutritionally Essential Mineral Elements*, 1st ed. (Boyd L. O'Dell, Roger Allan Sunde, Ed.), CRC Press, New York, pp 493-556.
72. Epp, O., Ladenstein, R., and Wendel, A. (1983) The refined structure of the selenoenzyme glutathione peroxidase at 0.2-nm resolution. *Eur J Biochem* 133, 51-69.
73. Shigeoka, S., Takeda, T., and Hanaoka, T. (1991) Characterization and immunological properties of selenium-containing glutathione peroxidase induced by selenite in *Chlamydomonas reinhardtii*. *Biochem J* 275 (Pt 3), 623-7.
74. Mates, J. M., Perez-Gomez, C, and Nunez de Castro, I. (1999) Antioxidant enzymes and human diseases. *Clin Biochem* 32, 595-603.
75. Ho, Y. S., Magnenat, J. L., Bronson, R. T., Cao, J., Gargano, M., Sugawara, M., and Funk, C. D. (1997) Mice deficient in cellular glutathione peroxidase develop

- normally and show no increased sensitivity to hyperoxia. *J Biol Chem* 272, 16644-51.
76. Lakowicz, J. R. (2006) Introduction to fluorescence in *Principles of Fluorescence Spectroscopy*, 3rd ed., Springer, Singapore, p 5.
  77. Ramos-Vara, J. A. (2005) Technical aspects of immunohistochemistry. *Vet Pathol* 42, 405-26.
  78. Shepard, C.J.R. (1999) Confocal microscopy-principles, practice and options in *Fluorescent and luminescent Probes for Biological Activity*, (Mason, WT, Ed.), Academic Press, London, pp 303-309.
  79. Wilhelm, S., Grobler, B., Gluch, M., and Heinz, H. in *Confocal Laser Scanning Microscopy Principles*, Carl Zeiss Jena,
  80. Confocal microscopy. [http://en.wikipedia.org/wiki/Confocal\\_microscope](http://en.wikipedia.org/wiki/Confocal_microscope).
  81. Tsantes, A. E., Bonovas, S., Travlou, A., and Sitaras, N. M. (2006) Redox imbalance, macrocytosis, and RBC homeostasis. *Antioxid Redox Signal* 8, 1205-16.
  82. Delincee, H., and Radola, B. J. (1975) Fractionation of horseradish peroxidase by preparative isoelectric focusing, gel chromatography and ion-exchange chromatography. *Eur J Biochem* 52, 321-30.
  83. Koh, M., and Kim, H.J. (2001) The effects of metallothionein on the activity of enzymes involved in removal of reactive oxygen species. *Bull Korean Chem Soc* 22, 362-6.
  84. Hung, K. T., and Kao, C. H. (2003) Nitric oxide counteracts the senescence of rice leaves induced by hydrogen peroxide. *J Plant Phys* 160, 871-9.

85. Ghosh, R., and Quayle, J. R. (1979) Phenazine ethosulfate as a preferred electron acceptor to phenazine methosulfate in dye-linked enzyme assays. *Anal Biochem* 99, 112-7.
86. Altman, F. P. (1976) Tetrazolium salts: a consumer's guide. *Histochem J* 8, 471-85.
87. Ivanov, Y. D., Kanaeva, I. P., Kuznetsov, V. Y., Lehnerer, M., Schulze, J., Hlavica, P., and Archakov, A. I. (1999) The optical biosensor studies on the role of hydrophobic tails of NADPH-cytochrome P450 reductase and cytochromes P450 2B4 and b5 upon productive complex formation within a monomeric reconstituted system. *Arch Biochem Biophys* 362, 87-93.
88. Hayat, M. A. (1989) Chemical fixation in *Principles and Techniques of Electron Microscopy: Biological Applications*, 3rd ed., CRC Press, Boca Raton, pp 6-80.
89. Kehrer, J. P., and Biswal, S. S. (2000) The molecular effects of acrolein. *Toxicol Sci* 57, 6-15.
90. Campanella, M. E., Chu, H., and Low, P. S. (2005) Assembly and regulation of a glycolytic enzyme complex on the human erythrocyte membrane. *Proc Natl Acad Sci USA* 102, 2402-7.
91. Galtieri, A., Tellone, E., Romano, L., Misiti, F., Bellocco, E., Ficarra, S., Russo, A., Di Rosa, D., Castagnola, M., Giardina, B., and Messina, I. (2002) Band-3 protein function in human erythrocytes: effect of oxygenation-deoxygenation. *Biochim Biophys Acta* 1564, 214-8.
92. Yawata, Y. (2003) Integral proteins in *Cell Membrane: the Red Blood Cell As a Model*, Wiley-VCH, Darmstadt, p 81.

93. Ellsworth, M. L. (2000) The red blood cell as an oxygen sensor: what is the evidence? *Acta Physiol Scand* 168, 551-9.
94. Fan, J., Cai, H., Yang, S., Yan, L., and Tan, W. (2008) Comparison between the effects of normoxia and hypoxia on antioxidant enzymes and glutathione redox state in ex vivo culture of CD34(+) cells. *Comp Biochem Physiol B Biochem Mol Biol* 151, 153-8.
95. Cicha, I., Suzuki, Y., Tateishi, N., and Maeda, N. (2003) Changes of RBC aggregation in oxygenation-deoxygenation: pH dependency and cell morphology. *Am J Physiol Heart Circ Physiol* 284, H2335-42.
96. Tuvia, S., Levin, S., and Korenstein, R. (1992) Oxygenation-deoxygenation cycle of erythrocytes modulates submicron cell membrane fluctuations. *Biophys J* 63, 599-602.
97. Zhang, D., Kiyatkin, A., Bolin, J. T., and Low, P. S. (2000) Crystallographic structure and functional interpretation of the cytoplasmic domain of erythrocyte membrane band 3. *Blood* 96, 2925-33.
98. Bruce, L. J., Beckmann, R., Ribeiro, M. L., Peters, L. L., Chasis, J. A., Delaunay, J., Mohandas, N., Anstee, D. J., and Tanner, M. J. (2003) A band 3-based macrocomplex of integral and peripheral proteins in the RBC membrane. *Blood* 707,4180-8.
99. Gaetani, G. F., Kirkman, H. N., Mangerini, R., and Ferraris, A. M. (1994) Importance of catalase in the disposal of hydrogen peroxide within human erythrocytes. *Blood* 84, 325-30.

100. Maridonneau, I., Braquet, P., and Garay, R. P. (1983) Na<sup>+</sup> and K<sup>+</sup> transport damage induced by oxygen free radicals in human red cell membranes. *J Biol Chem* 258,3107-13.
101. Nishikimi, M., Appaji, N., and Yagi, K. (1972) The occurrence of superoxide anion in the reaction of reduced phenazine methosulfate and molecular oxygen. *Biochem Biophys Res Commun* 46, 849-54.
102. Blood components, [http://anthro.palomar.edu/blood/blood\\_components.htm](http://anthro.palomar.edu/blood/blood_components.htm).
103. Fischer, A. H., Jacobson, K. A., Rose, J., and Zeller, R. (2006) Preparation of cells and tissues for fluorescence microscopy in *Basic Methods in Microscopy*, (Spector, Goldman, Ed.), Cold Spring Harbor Laboratory Press, New York, pp 105-114.
104. Dykstra, M. J. (1993) Specimen preparation in *A Manual of Applied Techniques for Biological Electron Microscopy*, Springer, New York, pp 1-11.
105. Cai, J., Bhatnagar, A., and Pierce, W. M., Jr. (2009) Protein modification by acrolein: formation and stability of cysteine adducts. *Chem Res Toxicol* 22, 708-16.
106. Beauchamp, R. O., Jr., Andjelkovich, D. A., Kligerman, A. D., Morgan, K. T., and Heck, H. D. (1985) A critical review of the literature on acrolein toxicity. *Crit Rev Toxicol* 14, 309-80.
107. Band 3 antibody. <http://www.abcam.com/Band-3-antibody-BIII-136-abll012.html>.

108. Han, Y., Quan, G. B., Liu, X. Z., Ma, E. P., Liu, A., Jin, P., and Cao, W. (2005) Improved preservation of human red blood cells by lyophilization. *Cryobiology* 51, 152-64.
109. Goncalves, M. S. (2009) Fluorescent labeling of biomolecules with organic probes. *Chem Rev* 109, 190-212.
110. Panchuk-Voloshina, N., Haugland, R. P., Bishop-Stewart, J., Bhalgat, M. K., Millard, P. J., Mao, F., and Leung, W. Y. (1999) Alexa dyes, a series of new fluorescent dyes that yield exceptionally bright, photostable conjugates. *J Histochem Cytochem* 47, 1179-88.
111. Rosen, G. M., Pou, S., Ramos, C. L., Cohen, M. S., and Britigan, B. E. (1995) Free radicals and phagocytic cells. *Faseb J* 9, 200-9.
112. Minetti, M., and Malorni, W. (2006) Redox control of red blood cell biology: the red blood cell as a target and source of prooxidant species. *Antioxid Redox Signal* 8, 1165-9.
113. Muzyamba, M. C, Campbell, E. H., and Gibson, J. S. (2006) Effect of intracellular magnesium and oxygen tension on K<sup>+</sup>-Cl<sup>-</sup> cotransport in normal and sickle human red cells. *Cell Physiol Biochem* 17, 121-8.
114. Drew, C, Ball, V., Robinson, H., Ellory, C. J., and Gibson, J. S. (2004) Oxygen sensitivity of red cell membrane transporters revisited. *Bioelectrochemistry* 62, 153-8.
115. Messana, I., Orlando, M., Cassiano, L., Pennacchietti, L., Zuppi, C, Castagnola, M., and Giardina, B. (1996) Human erythrocyte metabolism is modulated by the O<sub>2</sub>-linked transition of hemoglobin. *FEBS Lett* 390, 25-8.

116. Chu, H., Breite, A., Ciruolo, P., Franco, R. S., and Low, P. S. (2008) Characterization of the deoxyhemoglobin binding site on human erythrocyte band 3: implications for O<sub>2</sub> regulation of erythrocyte properties. *Blood* 111, 932-8.
117. Ghio, A. J., Nozik-Grayck, E., Turi, J., Jaspers, I., Mercatante, D. R., Kole, R., and Piantadosi, C. A. (2003) Superoxide-dependent iron uptake: a new role for anion exchange protein 2. *Am J Respir Cell Mol Biol* 29, 653-60.
118. McMurtrie, H. L., Cleary, H. J., Alvarez, B. V., Loiselle, F. B., Sterling, D., Morgan, P. E., Johnson, D. E., and Casey, J. R. (2004) The bicarbonate transport metabolon. *J Enzyme Inhib MedChem* 19, 231-6.
119. Rigo, A., Stevanato, R., and Viglino, P. (1977) Competitive inhibition of Cu, Zn superoxide dismutase by monovalent anions. *Biochem Biophys Res Commun* 79, 776-83.
120. Mota de Freitas, D., and Valentine, J. S. (1984) Phosphate is an inhibitor of copper-zinc superoxide dismutase. *Biochemistry* 23, 2079-82.
121. Symonyan, M. A., and Nalbandyan, R. M. (1972) Interaction of hydrogen peroxide with superoxide dismutase from erythrocytes. *FEBS Lett* 28, 22-4.
122. Hodgson, E. K., and Fridovich, I. (1975) The interaction of bovine erythrocyte superoxide dismutase with hydrogen peroxide: inactivation of the enzyme. *Biochemistry* 14, 5294-9.
123. Fuchs, H. J., and Borders, C. L., Jr. (1983) Affinity inactivation of bovine Cu,Zn superoxide dismutase by hydroperoxide anion, HO<sub>2</sub>. *Biochem Biophys Res Commun* 116, 1107-13.

124. Elam, J. S., Malek, K., Rodriguez, J. A., Doucette, P. A., Taylor, A. B., Hayward, L. J., Cabelli, D. E., Valentine, J. S., and Hart, P. J. (2003) An alternative mechanism of bicarbonate-mediated peroxidation by copper-zinc superoxide dismutase: rates enhanced via proposed enzyme-associated peroxycarbonate intermediate. *J Biol Chem* 278, 21032-9.
125. Wildman, R. E. C, and Medeiros, D. M. (1999) Minor Minerals in *Advanced Human Nutrition*, CRC Press, Boca Raton, p 270.
126. Walder, J. A., Chatterjee, R., Steck, T. L., Low, P. S., Musso, G. F., Kaiser, E. T., Rogers, P. H., and Arnone, A. (1984) The interaction of hemoglobin with the cytoplasmic domain of band 3 of the human erythrocyte membrane. *J Biol Chem* 259, 10238-46.
127. Low, P. S. (1986) Structure and function of the cytoplasmic domain of band 3: center of erythrocyte membrane-peripheral protein interactions. *Biochim Biophys Acta* 864, 145-67.
128. Salhany, J. M., and Cassoly, R. (1989) Kinetics of p-mercuribenzoate binding to sulfhydryl groups on the isolated cytoplasmic fragment of band 3 protein. Effect of hemoglobin binding on the conformation. *J Biol Chem* 264, 1399-404.
129. Salhany, J. M., Cordes, K. A., and Gaines, E. D. (1980) Light-scattering measurements of hemoglobin binding to the erythrocyte membrane. Evidence for transmembrane effects related to a disulfonic stilbene binding to band 3. *Biochemistry* 19, 1447-54.
130. Eber, S., and Lux, S. E. (2004) Hereditary spherocytosis—defects in proteins that connect the membrane skeleton to the lipid bilayer. *Semin Hematol* 41, 118-41.

131. Mohandas, N., and Gallagher, P. G. (2008) Red cell membrane: past, present, and future. *Blood* 112, 3939-48.
132. Shikama, K. (2006) Nature of the FeO<sub>2</sub> bonding in myoglobin and hemoglobin: A new molecular paradigm. *Prog Biophys Mol Biol* 91, 83-162.
133. Wratney, A. T., and Cheifetz, I. M. (2006) Pulmonary gas exchange in *Pediatric Critical Care Medicine*, (Slonim, A. D., and Pollack, M. M., Ed.), Lippincott Williams & Wilkins, Philadelphia, p 259.
134. Giulivi, C, Hochstein, P., and Davies, K. J. (1994) Hydrogen peroxide production by red blood cells. *Free Radic Biol Med* 16, 123-9.
135. Mendiratta, S., Qu, Z., and May, J. M. (1998) Erythrocyte defenses against hydrogen peroxide: the role of ascorbic acid. *Biochim Biophys Acta* 1380, 389-95.
136. Mueller, S., Riedel, H. D., and Stremmel, W. (1997) Direct evidence for catalase as the predominant I-kC<sup>+</sup>-removing enzyme in human erythrocytes. *Blood* 90, 4973-8.
137. Nagababu, E., Chrest, F. J., and Rifkind, J. M. (2003) Hydrogen-peroxide-induced heme degradation in red blood cells: the protective roles of catalase and glutathione peroxidase. *Biochim Biophys Acta* 1620, 211-7.
138. Tacka, K. A., Dabrowiak, J. C, Goodisman, J., and Souid, A. K. (2002) Kinetic analysis of the reactions of 4-hydroperoxycyclophosphamide and acrolein with glutathione, mesna, and WR-1065. *Drug Me tab Dispos* 30, 875-82.
139. Giustarini, D., Dalle-Donne, I., Colombo, R., Petralia, S., Giampaolletti, S., Milzani, A., and Rossi, R. (2003) Protein glutathionylation in erythrocytes. *Clin Chem* 49, 327-30.

140. Hebbel, R. P., Leung, A., and Mohandas, N. (1990) Oxidation-induced changes in microrheologic properties of the red blood cell membrane. *Blood* 76, 1015-20.
141. Campanella, M. E., Chu, H., Wandersee, N. J., Peters, L. L., Mohandas, N., Gilligan, D. M., and Low, P. S. (2008) Characterization of glycolytic enzyme interactions with murine erythrocyte membranes in wild-type and membrane protein knockout mice. *Blood* 112, 3900-6.
142. Low, F. M., Hampton, M. B., and Winterbourn, C. C. (2008) Peroxiredoxin 2 and peroxide metabolism in the erythrocyte. *Antioxid Redox Signal* 10, 1621-30.

## Appendix: List of images and Z-stacks of images on DVD submitted with this thesis

### Figure 3.2

- Fig. 3.2 Images in the thesis
- Fig. 3.2 Additional images - same experimental conditions as for Fig 3.2

### Figure 3.3

- Fig. 3.3 Images in the thesis
- Fig. 3.3 Additional images - same experimental conditions as for Fig 3.3

### Figure 3.4

- Fig. 3.4 Images in the thesis
- Fig. 3.4 Z-stacks of images - same experimental conditions as for Fig 3.4

### Figure 3.5

- Fig. 3.5 Images in the thesis
- Fig. 3.5 Additional images and Z-stacks of images - same experimental conditions as for Fig 3.5

### Figure 3.6

- Fig. 3.6 Images in the thesis
- Fig. 3.6 Additional images and Z-stacks of images - same experimental conditions as for Fig 3.6

### Figure 3.7

- Fig. 3.7 Images in the thesis
- Fig. 3.7 Additional images - same experimental conditions as for Fig 3.7

Figure 3.16

- Fig. 3.16 Images in the thesis
- Fig. 3.16 Z-stacks of images - same experimental conditions as for Fig 3.16

Figure 3.17

- Fig. 3.17 Images in the thesis
- Fig. 3.17 Additional images and Z-stacks of images - same experimental conditions as for Fig 3.17